THESIS FOR THE DEGREE OF DOCTOR OF PHILOSOPHY (PHD)

System-level analyses to identify macrophage-specific mechanisms controlling skeletal muscle regeneration

by Andreas Patsalos

UNIVERSITY OF DEBRECEN

DOCTORAL SCHOOL OF MOLECULAR CELL
AND IMMUNE BIOLOGY

DEBRECEN, 2017

THESIS FOR THE DEGREE OF DOCTOR OF PHILOSOPHY (PHD)

System-level analyses to identify macrophage-specific mechanisms controlling skeletal muscle regeneration

by Andreas Patsalos

Supervisor: Professor Dr. László Nagy

UNIVERSITY OF DEBRECEN

DOCTORAL SCHOOL OF MOLECULAR CELL
AND IMMUNE BIOLOGY

DEBRECEN, 2017

Table of contents

A. Abbreviations

ATAC-seq	Assay for Transposase Accessible Chromatin with high-throughput sequencing
BM	bone marrow
BMT	bone marrow transplantation
ChIP	chromatin immunoprecipitation
CSA	cross-sectional area
CTX	cardiotoxin
DAPI	4',6-diamidino-2-phenylindole
ECM	extracellular matrix
FACS	fluorescence-activated cell sorting
FAP	fibro/adipogenic progenitor
FSC	forward scatter
FDG	fluoro- deoxyglucose
F4/80	EGF-like module-containing mucin-like hormone receptor-like 1 (EMR1)
GAST	gastrocnemius
GDF	growth differentiation factor
GO	gene ontology
GSEA	gene set enrichment analysis
Ly6C	lymphocyte antigen 6 complex, locus C
MARE	Maf recognition elements
MF	macrophage
MRI	magnetic resonance imaging
PAX7	paired box 7
PCA	principal component analysis
PET	positron emission tomography
RT-qPCR	real-time quantitative polymerase chain reaction
SSC	side scatter
TA	tibialis anterior
TF	transcription factor
TSS	transcription start site
WT	wild-type

B. Introduction

1. Inflammation

- **Overview**

The four principal signs of inflammation are known as "Celsus tetrad": calor (heat), dolor (pain), tumor (swelling) and rubor (redness). However, the past decades offered greater insights on how inflammation is initiated, sustained and resolved. Inflammation is a physiological response, initiated after infection or injury (Medzhitov 2008). Local or systemic inflammatory responses aim to eliminate threats, promote tissue repair, and healing (Wynn, Chawla et al. 2013). In the case of infection, immune memory needs to be established in order for the host to mount a faster response upon secondary encounters. In general, a controlled inflammatory response is beneficial against infection, but if dysregulated it can become harmful. Many types of inflammation-related responses are only known in pathological conditions. However, the initiation of a physiological inflammatory response is understudied. Since inflammation seemingly evolved as a response for restoring homeostasis, elucidating the mechanisms that drive physiological inflammation will help to understand the dysregulated inflammatory processes that lead to systemic chronic inflammatory states.

Through evolution, vertebrates have developed a complicated recognition system in order to effectively guard themselves. This system involves both fast acting innate, and slowly activated adaptive immune responses by delivering plasma and immune cells to the site of infection or injury. Many cell types contribute to these immune responses but in this dissertation, we will focus on the different types of macrophages and will try to dissect their roles. Innate immune cells such as monocytes and macrophages are able to detect specific molecules through their pattern recognition receptors (PRRs) and thus trigger the initiation events of inflammation (Mahla, Reddy et al. 2013). This infection recognition response has been characterized best for bacterial infections through specialized receptors called Toll-like receptors (TLRs) and NOD (nucleotide-binding oligomerization-domain protein)-like receptors (NLRs) (Kawai and Akira 2010). Tissue-resident macrophages and mast cells mediate the initiation of the inflammatory response by producing inflammatory mediators such as chemokines, cytokines, vasoactive amines, eicosanoids and products of proteolytic pathways (Turer, Tavares et al. 2008). These mediators help plasma proteins and leukocytes (mainly neutrophils) to enter the tissues at the site of infection (or injury) while at the same time prevent the exit of erythrocytes. The direct contact of neutrophils to pathogens or through cytokine secretion by tissue-resident cells, gets them activated and kill the invading pathogens by releasing the contents of their granules (reactive oxygen species, reactive nitrogen species, proteinase, cathepsin and elastase) (Nathan 2006). However, the actions of neutrophils do not distinguish between pathogen and host. Whereas sustained inflammation is essential to battling pathogens, excessive inflammation can lead to severe tissue damage. Therefore, physiological immune responses are tightly regulated and in many cases self-restricted via negative feedback signaling loops. For example, the resolution of inflammation requires a switch in lipid mediators (from prostaglandins to lipoxins) (Hansen, Keelan et al. 1999). Infiltrating macrophages produce resolvins, protectins,

transforming growth factor-β, and growth factors that have a crucial role in the resolution of inflammation and the initiation of tissue repair (Fullerton and Gilroy 2016).

As mentioned above a large number of mediators are produced during the inflammatory response. For simplicity, they are classified as inducers, which act as signals to initiate the inflammatory response, and mediators that act as effectors of inflammation. Inducers can activate specialized sensors, which in turn lead to the production of specific sets of mediators. Thus, inflammation consists of inducers, sensors, mediators and effectors, expressed and produced mainly by macrophages, thus defining the type of inflammatory response. In the following sections, these components are discussed.

- **Classical and alternative polarization of macrophages**

Macrophages are cells that are characterized by extended flexibility and plasticity (functions summarized in **Figure 1**). They undergo either classical M1 activation or alternative M2 activation depending on the signal they receive. These signals can range from microbial products to damaged cells (Mills and Ley 2014). M1 polarized macrophages *in vitro* are activated by various TLR ligands and IFN-gamma, while M2 polarized macrophages are activated by Interleukin-4 and Interleukin-13 (IL-4/IL-13) (Mantovani, Sica et al. 2004). In general, M1 macrophages express high levels of pro-inflammatory cytokines and reactive nitrogen intermediates (iNOS) and thus act strongly against microbes. On the other hand, the M2 phenotype is characterized by anti-parasitic activity, tissue remodeling, wound healing and tumor sustained progression through its immunoregulatory activity (Tumor Associated Macrophages). In addition, M2 macrophages have high expression of scavenging molecules, produce L-ornithine through the arginase pathway and are distinguished by low levels of IL-12 and high levels of IL-10. Furthermore, M1 versus M2 macrophages have different chemokine expression profiles (Mosser and Edwards 2008).

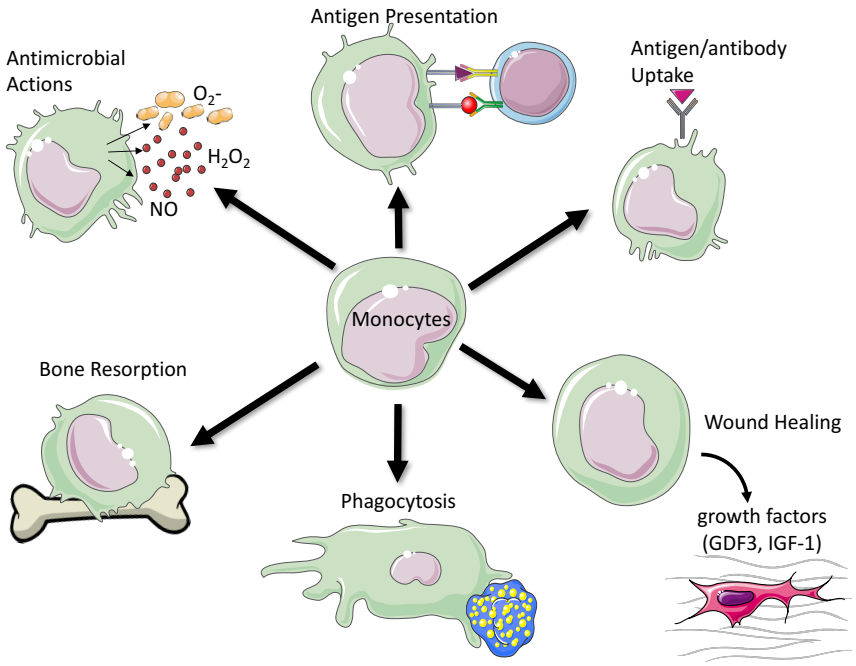

Figure 1. Schematic representation of macrophage plasticity and function.

Transcription factors, posttranscriptional regulators, sensors and signaling molecules are involved in regulating macrophage activity (Lawrence and Natoli 2011), (Roy, Schmeier et al. 2015), (Tussiwand and Gautier 2015), (Hume, Summers et al. 2016), (Lyroni, Patsalos et al. 2017). For example, the balance between activation of Signal transducer and activator of transcription-1 (STAT1) and STAT3/STAT6 fine-tunes macrophage activity and subsequently polarization (Wang, Liang et al. 2014). In this context, NF-κB and STAT1 activation promotes M1 macrophage polarization, while STAT3 and STAT6 activation results in M2 macrophage polarization, which is associated with resolution of inflammation (Wynn, Chawla et al. 2013). Similarly, the nuclear receptors PPAR-gamma and PPAR-delta regulate various aspects of M2 macrophage activation and oxidative metabolism (Bensinger and Tontonoz 2008). Krüppel-like factors such as KLF4 and KLF2 promote M2 macrophage functions through STAT6 and by suppressing the NF-κB/HIF-1α–dependent pathway (Palsson-McDermott, Curtis et al. 2015). In the same context, c-Myc gets activated by IL-4 and regulates M2-associated genes such as Scarb1, Alox15, Mrc1, STAT6 and PPARg (Stein, Keshav et al. 1992). Epigenetically IL-4 also induces the Jmjd3-IRF4 axis to inhibit M1 polarization through IRF5 and thus promote M2 polarizing conditions (Satoh, Takeuchi et al. 2010). Akt kinases and noncoding RNAs such as mir155 and mir146 have also been shown to regulate macrophage polarization (Vergadi, Ieronymaki et al. 2017).

The general dogma is that under conditions such as allergy, cancer and parasite infections the functional macrophages phenotypes *in vivo* are similar to those of canonical M1/M2 polarized states, as defined *in vitro*. Importantly, a key concept is that macrophage polarization and thus its activation status has been linked to pathology. M1 polarized macrophages have been implicated in initiating and sustaining inflammation, while the M2 polarized phenotype has been associated with the resolution of inflammation, and if dysregulated, with chronic inflammation (**Figure 2**). However, macrophage plasticity has been mainly addressed in *in vitro* systems that do not consider the complexity that the macro- and microenvironment provide within the tissue. Thus, considering the observations from recent *in vivo* studies (Varga, Mounier et al. 2016), the general dogma is currently under revision.

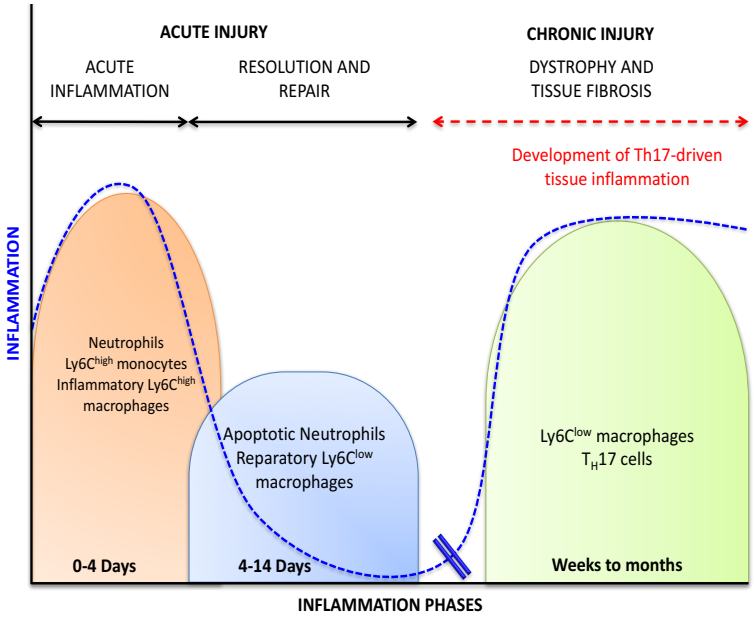

Figure 2. Inflammation phases and resolution.

- **Resolution of Inflammation**

Arising from these advances, it has been proposed that most of the chronic inflammatory diseases may be caused not only by ongoing pro-inflammatory processes, but also by dysregulated resolution, and thus therapeutic intervention might be very effective if focused in guiding inflammation towards pro-resolution. In general, resolution of inflammation involves the clearance of infiltrated inflammatory cells and restoration to homeostasis. This process is not considered passive but rather tightly regulated events need to occur. Initially, the inflammatory cues (CC-cytokines, CXC chemokines etc.), that triggered inflammation are eliminated, thus preventing further inflammatory cell infiltration and edema formation (McQuibban, Gong et al. 2000), (McQuibban, Gong et al. 2002), (Cochain, Auvynet et al. 2012), (Bunting, Comerford et al. 2013). At the same time synthesis of pro-inflammatory mediators is inhibited. Next, immune cells of the initial response such as neutrophils and eosinophils are cleared from the inflamed tissue by local apoptosis and subsequent uptake by recruited monocyte-derived macrophages in a process called efferocytosis. Once this process is complete, macrophages either undergo local apoptosis or exit the tissue by lymphatic drainage. However, it has been recently proposed that there is a third phase called post-resolution. During this phase, there is a second influx of myeloid cells (including $CD11B^{+}CD49d^{+}CD115^{+}MHCII^{+}$ myeloid-derived suppressor cells, $F4/80^{low}MHCII^{+}CD11c^{+}$ DCs, and $F4/80^{mid}CD11B^{hi}CD11c^{-}$) into the tissue and remain for weeks to regulate either the adaptive response or the degree and duration of a subsequent acute innate response (Yona, Kim et al. 2013), (Newson, Stables et al. 2014). This suggests that resolution is connecting innate and adaptive immunity, and chronic inflammation could be explained as incomplete resolution of the initial acute inflammatory response which in turn fails to initiate an appropriate adaptive immune response.

As already mentioned above, to initiate the resolution process, certain events need to take place, (1) removal of stimuli, (2) inhibiting of pro-inflammatory signaling, and (3) clearance of pro-inflammatory mediators. The importance of antigen clearance is demonstrated in immunodeficiency disorders, such as chronic granulomatous disease (Pollock, Williams et al. 1995), and autoimmune diseases, such as rheumatoid arthritis and systemic lupus erythematosus, that are driven by persistent endogenous antigens (Favas and Isenberg 2009). Following stimulus removal, receptors and their signaling pathways that initiated the release of pro-inflammatory mediators must be switched off in order to prevent excessive damage from an ongoing pro-inflammatory state. An example of a failure in dampening of pro-inflammatory signaling is sepsis. During this condition, large amounts of cytokines are still present despite negative bacterial blood cultures. A number of regulatory mechanisms of inflammation have been described (reviewed in (Stoecklin and Anderson 2006)), such as through miRNAs (i.e. miR-146, miR-21), ARE-binding proteins (tristetraprolin B-related factor 1, KH-type splicing regulatory protein and ARE RNA-binding protein 1), leucine- rich repeat-containing protein 33 or lipid mediators such as prostaglandin E2 (PGE2), that inhibit IFNg and TLR signaling and subsequently NFkB activation (Taganov, Boldin et al. 2006), (Anderson 2008), (Sheedy, Palsson-McDermott et al. 2010), (Liu, Zhang et al. 2013), (O'Brien, Fullerton et al. 2014). Following removal of the damaging agent and turning off signaling pathways, the levels of cytokines, chemokines, eicosanoids, cell adhesion molecules and other inflammatory mediators need to be catabolized and return back to their pre-inflamed state. These findings indicate that there are multiple routes

to resolution, rendering for one single intervention to be a panacea for all inflammatory diseases highly unlikely.

Pro-resolution therapeutic strategies improvement, and application to treat chronic inflammation may transform the management of some of the most frequent human illnesses. Furthermore, by approaching such disease states from the opposite perspective and asking not how to suppress the initiation of inflammation, but how to enhance the clearance of the stimulating agent, we will hopefully gain new insights into both the origins of chronic inflammation and novel therapeutics to tackle them.

2. Tissue injury and regeneration

- **Overview**

Tissue repair and regeneration are vital for survival (Das, Sinha et al. 2015). Repair, also referred to as healing, is the restoration of tissue structure and function following an injury. Infection, toxic or mechanical injury can severely impact tissue integrity. Two types of processes take place during repair of the damaged tissues: (1) proliferation of undamaged cells and (2) maturation of tissue resident stem cells. During regeneration, tissues such as liver, skeletal muscle, skin and intestine epithelia, replace damaged components and essentially help the tissue to return to homeostasis. This process occurs by proliferation of cells that survive the initial insult and retain the ability to proliferate (Cohen and Melton 2011). It is well known that mammals have a limited capacity to regenerate damaged tissues and organs. However, liver, skin, and skeletal muscle are among the few tissues with the ability to regenerate. For this reason, they have been used as reference tissues for the study of tissue regeneration.

Three types of tissues exist: labile, stable and permanent (Bryant and Mostov 2008). (1) Cells from labile tissues are constantly being lost and replenished by maturation of tissue stem cells and by proliferation of differentiated cells. Hematopoietic cells in the bone marrow (Bryder, Rossi et al. 2006), surface epithelia (skin, oral cavity, vagina, and cervix), cuboidal epithelia of the ducts, draining exocrine organs (salivary glands, pancreas, biliary tract), columnar epithelium of the gastrointestinal tract, uterus, fallopian tubes and the transitional epithelium of the urinary tract (Bryant and Mostov 2008) consist this group. As long as the pool of stem cells is preserved and provided the underlying basement membrane is intact, these tissues can readily regenerate after damage. (2) Cells from stable tissues are quiescent by remaining in the G0 stage of the cell cycle and have only minimal proliferative activity in their normal state (Sanchez Alvarado and Yamanaka 2014). These cells can proliferate in response to loss of tissue mass or due to injury. Cells of this category constitute the parenchyma of most solid tissues, such as liver, kidney, and pancreas but also endothelial cells, fibroblasts, and smooth muscle cells. Stable tissues have a limited capacity to regenerate after acute damage with the exception of the liver. The underlying mechanisms still remain elusive but likely involve interactions of cells with the ECM and local production of growth factors. (3) Cells from permanent tissues are considered to be terminally differentiated, mature and non-proliferative in postnatal life. The majority of neurons and cardiac myocytes cannot regenerate and belong to this group. Therefore, brain or heart damage is usually irreparable and results in a scar (Qian, Huang et al. 2012). However, it has been recently shown that limited stem cell proliferation and differentiation can occur in some areas of the adult brain (Gage and Temple 2013), and there is some evidence that heart myocytes may be able to proliferate following myocardial necrosis (Qian, Huang et al. 2012). Nevertheless, regardless of the proliferative capacity that may exist in these tissues, it is still insufficient to produce tissue regeneration after injury. Thus, in permanent tissues, repair is typically dominated by scar formation. Importantly, even though skeletal muscle is usually classified as a permanent tissue, satellite cells attached to the endomysium provide tremendous regenerative capacity to muscle.

The repair process consists of inflammation and proliferation of satellite and other cells (Bentzinger, Wang et al. 2013). Wounding causes the rapid activation of coagulation pathways, which results in the formation of a clot that contains fibrin, fibronectin, and complement proteins

(Henson and Hume 2006). Growth factors, cytokines, and chemokines released into the area attract migrating cells that use the clot as a scaffold. Neutrophils appear within 24 hours and they start to move toward the fibrin clot (Hotamisligil 2006). Neutrophils release proteolytic enzymes that initiate the clearance of necrotic debris and within 48 hours, satellite cells start to proliferate. By day 3, macrophages replace neutrophils. Macrophages (MFs) are the key players of tissue repair, clearing extracellular debris, fibrin, and promoting angiogenesis and ECM deposition (Fullerton and Gilroy 2016). By day 5, neovascularization reaches its peak but these new vessels are leaky, allowing the passage of plasma proteins and fluid into the extravascular space (Mounier, Chretien et al. 2011). In addition, migration of fibroblasts to the site of injury is driven by various chemokines, TNFa, PDGF, TGF-β, and FGF and their subsequent proliferation is triggered by multiple growth factors, including PDGF, EGF, TGF-β, and FGF, and the cytokines IL-1b and TNFa (Werner and Grose 2003). During the second week, the leukocyte infiltrate, edema, and increased vascularity are substantially diminished. This 2-week process is necessary to restore overall tissue homeostasis even though partial function of the tissue is being restored by the end of the first week.

- **Animal models and morphological characteristics of acute muscle injury and repair**

Muscle regeneration is a highly efficient process that if compromised can lead to several pathologies such as myopathies. Therefore, understanding the processes of tissue homeostasis, maintenance and regeneration is crucial to devise novel therapeutics. In order to study such processes, the use of reproducible and tightly controlled experimental models of muscle injury and repair are needed. The most frequently used models of acute muscle injury and repair are mechanical injury (freeze injury, irradiation, crush injury, denervation), myotoxins (notexin and cardiotoxin) and chemical agent ($BaCl_2$) (Hardy, Besnard et al. 2016). Although the regeneration process restores the muscle tissue in all these models, the pathophysiological processes involved, vary depending on the model (differences regeneration kinetics, re-vascularization, and satellite cell behavior). To begin with, CTX, NTX and $BaCl_2$ induce severe necrosis of the tissue, followed immediately by neutrophil and macrophage infiltration that leads to synchronous regeneration. Next myoblasts appear and start fusing to form larger structures (myotubes). The tissue regenerates ad integrum within a relatively short period (8 days in young adult mice) (Arnold, Henry et al. 2007). During the freeze-injury model and other mechanical injury models, asynchronous regeneration takes place instead. In these models, there are distinct regeneration foci in which all the different regeneration steps are present at the same time. In addition, although the inflammation kinetics appear to be identical for all models; differences in cytokine production exist. For example, after CTX injury, inflammatory cytokine expression returned to basal levels when the muscle was morphologically regenerated, while in the other models, the expression of cytokines was never back to basal levels (Hardy, Besnard et al. 2016). This suggest that there is still ongoing inflammation in these models despite the normal appearance of the regenerated muscles. Skeletal muscles are comprised largely of differentiated myofibers that have permanently left the cell cycle. Following injury, satellite cells which are mostly quiescent, re-enter the cell cycle and generate myoblasts that will participate in muscle restoration.

Skeletal muscle regeneration has emerged as an important paradigm to study the role of satellite and stromal cells following tissue injury. Satellite cells are vital to muscle regeneration

(Lepper, Partridge et al. 2011) (Sambasivan, Yao et al. 2011) but their function involves interactions with the macro- and micro-environment including interactions with macrophages (Chazaud, Sonnet et al. 2003) and fibroblasts (Murphy, Lawson et al. 2011). The satellite cell microenvironment changes based on the injury model. For example, after NTX or freeze injury, severe vascular lesions and granulomas (multinucleated giant cells) appear which explains the differences in regeneration kinetics. In all of the injury models, loss of satellite cells can be seen, but it also varies based on the severity of the injury. The volume of the toxins can have an impact on the area of the injured muscle. Higher volumes lead to higher satellite cell death and a delay in their division. In general, in the NTX, CTX and $BaCl_2$ models almost 60% of the satellite cells survive while with freeze injury about 95% of satellite cells are lost (Hardy, Besnard et al. 2016). However, 3-4 weeks month post-injury, a higher number of satellite cells can be seen in all models while they continue to cycle at different rates based on the model (Rocheteau, Gayraud-Morel et al. 2012). Lastly re-vascularization is an important process during skeletal muscle regeneration since it can impact both the delivery and distribution of recruited immune cells and regeneration-related factors (growth factors, cytokines, chemokines), but also the communication between endothelial and satellite cells (Mounier, Chretien et al. 2011). The mechanical injuries result in a more severe destruction of the vasculature compared to the other models prolonging the regeneration process. Since 85% of satellite cells reside near the blood vessels (Christov, Chretien et al. 2007), it can have an impact on satellite cell oxygen availability (Csete, Walikonis et al. 2001), which in turn could affect their proliferation and differentiation.

Muscle regeneration following any acute injury is a very efficient and reliable process to provide fast recovery. On the other hand, the recovery from a chronic related damage is not a very efficient process. The reason behind this is the lack of a system adapted to these types of injuries. As a result, immune responses related to muscle regeneration get dysregulated, cause muscle fibrosis and lead to impaired regeneration. Such muscle regeneration defects can be seen for example in Duchenne muscular dystrophy (DMD). In DMD the cell membrane is weak, causing chronic damage, repeated cycles of regeneration (Petrof, Shrager et al. 1993), leading to chronic inflammation that exacerbates the pathology (Wehling, Spencer et al. 2001). Importantly, it's been shown that chronic injury alters the macrophage phenotypes responsible for proper muscle regeneration following an acute injury. This in turn disrupts the normal regulation of connective tissue deposition (Lemos, Babaeijandaghi et al. 2015). Furthermore, the reparatory macrophages associated with dystrophy seem to become highly fibrogenic (by enhancing arginase 1 activity) and exacerbate the fibrosis-related pathology (Wehling-Henricks, Jordan et al. 2010). Thus, macrophages have a critical role in muscular dystrophy. However, the mechanisms that control the macrophage phenotypic transition in chronically injured muscle remain elusive.

3. Myeloid cell regulation of skeletal muscle regeneration

- **Overview**

Many cell types are taking part in the regeneration process. However, due to their plasticity, resident and recruited macrophages play a vital role in all stages of repair and fibrosis (Mosser and Edwards 2008), (Wynn and Barron 2010). In fact, a recent macrophage depletion study demonstrated that they are required for full limb regeneration in salamanders. Wound closure though, is much less dependent on macrophages following limb amputation (Godwin, Pinto et al. 2013). Similarly, a macrophage-depletion study in mice determined that macrophages provide crucial angiogenic and tissue regeneration signals following myocardial infarction in neonatal hearts (Aurora, Porrello et al. 2014). In the context of muscle regeneration macrophage depletion completely abolishes the ability of skeletal muscle to regenerate (Arnold, Henry et al. 2007), (Wang, Melton et al. 2014). Importantly, macrophages are also critical for the clearance of senescent cells (Yun, Davaapil et al. 2015) and to create a regeneration-permissive environment. Owing to their role in controlling the initiation, maintenance and resolution of wound-healing responses in different organ systems, they are considered major therapeutic targets (Aurora and Olson 2014).

Different macrophage populations reside in many tissues and usually derived from the yolk sac during the early stages of embryogenesis. However, some derive from later stages of embryogenesis such as from fetal liver and hematopoietic stem cells (Epelman, Lavine et al. 2014), (Epelman, Lavine et al. 2014), (Gomez Perdiguero, Klapproth et al. 2015). The tissue resident macrophages are important during development but also for normal tissue homeostasis by producing growth and trophic factors to support neighboring tissues (Wynn, Chawla et al. 2013). Following acute injury, a large number of inflammatory Ly6C^{high} monocytes are recruited from the bone marrow and circulation. The recruitment takes place via gradients of chemokines and adhesion molecules. These macrophage precursors far exceed the number of tissue resident macrophages (Davies, Jenkins et al. 2013), (Galli, Borregaard et al. 2011), but both proliferate and undergo distinct phenotypic changes in response to the local tissue microenvironment milieu (Jenkins, Ruckerl et al. 2011), (Jenkins, Ruckerl et al. 2013). Early studies on macrophage contribution to tissue repair was focused on their role as scavenger cells that uptake cellular debris, pathogens, neutrophils and other apoptotic cells following tissue injury (Peiser, Mukhopadhyay et al. 2002). However, a number of recent studies have demonstrated a more complex, specialized and critically timed states of monocytes and macrophages during repair, regeneration and fibrosis (Anders and Lech 2013), (Munoz-Canoves and Serrano 2015), (Murray and Wynn 2011), (Novak, Weinheimer-Haus et al. 2014), (Sica and Mantovani 2012), (Gundra, Girgis et al. 2014), (Vannella, Barron et al. 2014), (Varga, Mounier et al. 2016). According to these studies the different macrophage phenotypes could be tissue-, stimulus- and phase-specific. A tissue such as skeletal muscle can cause distinct populations of immune cells to appear depending on disease etiology. For example, in a skeletal muscle regeneration paradigm, inflammatory monocytes infiltrating the injured muscle switch to a repair macrophage phenotype to support myogenesis in an AMPKa1 (5'-AMP-activated protein kinase catalytic subunit α1) dependent manner (Mounier, Théret et al. 2013). On the other hand, dystrophic

muscle and increased pathological fibrosis has also been associated with distinct macrophage populations (Vidal, Serrano et al. 2008).

During the initial cellular response following the injury, chemokines, matrix metalloproteinases and various inflammatory molecules are produced by the infiltrating macrophages (Wynn and Barron 2010). This is supported by the fact that depletion of macrophages early after the injury, will result in a diminished inflammatory response (Duffield, Forbes et al. 2005). However, as mentioned above, depletion of macrophages will lead to impaired clearance of necrotic debris and subsequently to less efficient regeneration (Zhang, Rowe et al. 2012). Following the initial inflammatory phase, macrophages acquire a pro-resolution and tissue repair phenotype (Ramachandran, Pellicoro et al. 2012) which is characterized by the production of several growth factors, such as members of the TGF- β superfamily including transforming growth factor β1 (TGF-β1) and other growth factors such as platelet-derived growth factor (PDGF), insulin-like growth factor 1 (IGF-1), and vascular endothelial growth factor α (VEGF-α). These secreted factors seem to promote satellite and fibroblast cell proliferation, differentiation and neovasculature development (Berse, Brown et al. 1992), (Chujo, Shirasaki et al. 2009), (Rappolee, Patel et al. 1998), (Shimokado, Raines et al. 1985), (Willenborg, Lucas et al. 2012). This macrophage subtype can also facilitate the synthesis of extracellular-matrix components (Murray and Wynn 2011), respond and secrete interleukin-10 (IL-10) and other inflammation inhibitory mediators, such as programmed cell death ligands 1 and 2 (Khalil, Bereznay et al. 1989), (Said, Dupuy et al. 2010), (Shouval, Biswas et al. 2014), (Zigmond, Bernshtein et al. 2014)). The current notion is that monocytes and macrophages respond differently to similar inflammatory signals and depend on the inflammation phase. This suggests that the diverse phenotypes observed during regeneration are neither M1 (pro-inflammatory) nor M2 (anti-inflammatory). In conclusion, different macrophage phenotypes seem to play crucial and unique roles at each stage of the regeneration process. Identifying the regulators of the phenotypic shift is critical to devise targeted muscle-inflammation related therapeutics.

- **Inflammatory monocyte to repair macrophage transition**

The mechanisms of infection-induced inflammation are far better understood than those of other inflammatory processes such as the ones related to injury. The infection-induced inflammation is vital for survival but might be a special case. It is clear now that the physiological inflammation induced by injury does not seem to fit the classic pattern of inflammation. The reason behind this is that a cell state is distinct while tissue states are graded. For example, tissues might contain cells that are dead, malfunctioned or healthy, all at the same time. Thus, at normal conditions, the tissues remain at homeostatic state, usually by the help of tissue-resident macrophages (Wynn, Chawla et al. 2013). However, when tissues undergo stress due to an acute injury for example, they can malfunction if the insult is excessive. In this case additional recruited macrophages are needed to help the tissue overcome these issues. A particularly interesting and important aspect of regeneration is the invasion and conversion of circulating inflammatory monocytes into inflammatory macrophages and then conversion into repair-type ones (Arnold, Henry et al. 2007), (Varga, Mounier et al. 2013), (Varga, Mounier et al. 2016). Acute muscle injury causes the recruitment of monocytes/macrophages into the damaged area of the muscle and

this invasion peaks within the first 2 days after the injury (Tidball 2004). In the absence of macrophages, muscle regeneration is severely impaired (Arnold, Henry et al. 2007), (Tidball and Wehling-Henricks 2007), (Mirza, DiPietro et al. 2009), (Wang, Melton et al. 2014), highlighting the importance of these cells in the regeneration process. The roles of these immune cells in response to injury are to (1) confine the damage, (2) clear the necrotic debris through phagocytosis, and (3) repair the damage. There are multiple lines of evidence to suggest that macrophages instruct satellite cells to proliferate and differentiate. They do that by secreting cytokines, growth factors and other molecules that regulate the satellite cell pool (Tidball and Villalta 2010), (Mounier, Théret et al. 2013), (Saclier, Yacoub-Youssef et al. 2013), (Tonkin, Temmerman et al. 2015). This highly dynamic process is characterized by an in-situ transition of infiltrating monocytes from an inflammatory ($Ly6C^{high}F4/80^{low}$) to a repair ($Ly6C^{low}F4/80^{high}$) macrophage phenotype (Varga, Mounier et al. 2013), which appears to be indispensable for proper muscle regeneration (Wang, Liang et al. 2014).

Distinct inflammatory and repair macrophage phenotypes have also been reported in spinal-cord injury models. In these models, inflammatory monocytes ($Ly6C^{high}CX3CR1^{low}$) enter the injury sites in a CCL2-dependent manner. The movement of repair macrophages ($Ly6C^{low}CX3CR1^{high}$) is controlled by adhesion proteins (VCAM-1, VLA-4) and endothelial-cell-surface enzymes that are implicated in leukocyte extravasation (Shechter, London et al. 2013), (Shechter, Miller et al. 2013), (Evans, Barkauskas et al. 2014). Thus, it appears that the guided trafficking of infiltrating monocytes and macrophages towards the injury site provides crucial signals to shape their unique functions. Similar studies in cardiac muscles, revealed regulators (such as regenerating islet-derived 3β and C19orf10) of macrophage migration to the injury sites (Lorchner, Poling et al. 2015). These factors are involved in removal of neutrophils by repair macrophages, thus protecting these tissues from extensive damage and cardiac rupture following myocardial infarction (Korf-Klingebiel, Reboll et al. 2015). Recent studies also highlight that a single population of monocytes can acquire both pro-inflammatory and pro-repair phenotypes, suggesting that an *in situ* phenotypic transition, rather than recruitment of a different pro-reparative Ly6C subset, takes place. For example, removing the $Ly6C^{-}$ monocytes populations from the circulation does not affect the presence of repair macrophages or the outcome of muscle regeneration (Varga, Mounier et al. 2013). In addition, activin-a has been identified as a repair macrophage-derived mediator participating in the phenotypic shift of microglia from a pro-inflammatory to a repair phenotype (Miron, Boyd et al. 2013). Similar findings in liver injury models suggest that cytokines such as IL-4, IL-10, and the uptake of dead cells through phagocytosis regulate the conversion of inflammatory monocytes into repair macrophages (Dal-Secco, Wang et al. 2015), (Ramachandran, Pellicoro et al. 2012). In addition, in these models Wnt signaling appears to be an important pathway in macrophages, which regulates regeneration by driving the differentiation of progenitor cells to hepatocytes (Boulter, Govaere et al. 2012). In a lung injury model (acute pathogen-induced injury), it has been shown that IL-17, IL-4, IL-10 and IGF-1 drive the conversion to an anti-inflammatory macrophage phenotype to promote lung healing (Chen, Liu et al. 2012). In the context of muscle regeneration, IL-10 also seems to play a key role in the phenotypic switching of muscle macrophages (Deng, Wehling-Henricks et al. 2012) through CCAAT/enhancer binding protein beta (C/EBPb) (Ruffell, Mourkioti et al. 2009). Macrophage invasion is not altered in the C/EBPb null mice but M2-specific genes are altered leading to impaired regeneration. It is important to note that recent studies have questioned the

importance of alternative macrophage polarization (M2-like) and IL-4 in muscle regeneration (Goh, Henderson et al. 2013), (Heredia, Mukundan et al. 2013). Muscle repair macrophages directly target satellite cells by secreting cytokines and growth factors to promote their differentiation into mature myotubes (Saclier, Yacoub-Youssef et al. 2013). On the other hand, inflammatory macrophages inhibit myogenic precursor fusion demonstrating again that different macrophage states can have various effects on satellite cell fate and subsequently muscle regeneration. Collectively, these studies demonstrate how the timely transition of inflammatory monocytes to reparative macrophages is critical for tissue regeneration.

The macrophage phenotype switch involves many other molecular and cellular processes. It has been suggested that phagocytosis of neutrophils controls the conversion to the repair phenotype. In case phagocytosis is impaired then macrophages cannot acquire this phenotype (Fadok, Bratton et al. 1998), (Arnold, Henry et al. 2007). Similar to acute injury models in other tissues, cytokines orchestrate the conversion in muscle macrophages. IFN-g promotes the inflammatory phenotype while at the same time inhibits the repair type. In support of this observation an increase in repair macrophage activation and a decrease in muscle damage have been observed in IFN-g null mice (Villalta, Deng et al. 2011). At the cellular level mitogen-activated protein kinase phosphatase-1 (MKP-1), controls the phenotypic shift of muscle macrophages through regulating mitogen-activated protein kinase (MAPK) p38 and Akt kinases. In MKP-1 null mice the transition occurs faster which results in dysregulated regeneration (Perdiguero, Sousa-Victor et al. 2011). In the same context, AMPK-a1 has been implicated in the macrophage phenotypic transition. AMPK-a1 null mice express inflammatory cytokines at higher levels while the AMPK-a1 overexpression model reveals a significant decrease in their expression (Sag, Carling et al. 2008), (Mounier, Théret et al. 2013). These studies show that the conversion of muscle macrophages from inflammatory to repair ones are finely regulated with multiple targets and pathways being involved (summarized in **Figure 3**). How all these elements are regulated and coordinated is still unclear.

- **Effector molecules and secreted growth factors in the regulation of muscle regeneration.**

Interest in deciphering the pathways and the diverse macrophage subsets that sustain tissue-damaging inflammatory responses has increased lately, given that delineating the mechanisms would lead to developing novel therapeutics for various types of inflammatory diseases (Han, Jung et al. 2013), (Xu, Zhu et al. 2012), (Xu, Liu et al. 2015). Following acute sterile muscle injury, macrophages secrete cytokines to activate and enhance satellite cell proliferation and differentiation. At the same time, the tissue itself produces mediators and factors (myokines) that act on an autocrine or endocrine manner and influence the regeneration process (Pedersen 2011), (Pedersen and Febbraio 2008). Most of the studies identifying these myokines where performed in the context of physical activity. More recently, some of these factors have been implicated in muscle regeneration in which they seem to heavily impact this process. For example, human myoblasts secrete IL-6 in response to IL-1, TNF-a or LPS treatment *in vitro* (Gallucci, Provenzano et al. 1998) and in IL-6 null mice migration and proliferation of satellite cells is greatly diminished (Serrano, Baeza-Raja et al. 2008). In addition, since infiltrating macrophages also secrete IL-6 they further stimulate proliferation of satellite cells. In C2C12 myocyte cell

cultures, IL-6 has been shown to be involved in the myocyte differentiation program as well. Inhibiting IL-6, decreased differentiation while overexpression increased myotube formation (Baeza-Raja and Munoz-Canoves 2004), (Hoene, Runge et al. 2013). Overall, these results highlight IL-6 as a myokine secreted by multiple sources including macrophages and impact satellite cell migration to the injury site, proliferation and differentiation into myotubes (Kurek, Nouri et al. 1996), (Zhang, Li et al. 2013).

Leukemia inhibitory factor (LIF) is another myokine secreted in the muscle during exercise (Broholm and Pedersen 2010) and regeneration (Barnard, Bower et al. 1994), (Kurek, Nouri et al. 1996). Interestingly, *in vivo* infusion of LIF enhances regeneration by directly acting on proliferation and differentiation of satellite cells (Barnard, Bower et al. 1994). *In vitro*, LIF activates C2C12 maturation through the JAK2/STAT2 pathway (Yang, Liu et al. 2009), while targeting of the LIF receptor with siRNA markedly decreases human myoblast proliferation (Broholm, Laye et al. 2011). In human skeletal muscle interleukin 7 (IL-7) seems to have similar function on satellite cell differentiation and similarly targeting the IL-7 receptor decreases their maturation to myotubes *in vitro* (Haugen, Norheim et al. 2010). In addition, recombinant IL-7 treatment activates satellite cell migration but inhibits their maturation (Haugen, Norheim et al. 2010). In the context of muscle injury and regeneration, IL-7 is involved in guiding satellite cells to the injury site and keeps them from differentiating until the proper signals overcome this inhibition. Interleukin 4 is another cytokine proposed to affect satellite cell differentiation and myotube formation through fusion (Horsley, Jansen et al. 2003). CXC ligand 1 (CXCL-1) and interleukin 8 impact regeneration by attracting neutrophils to the injury site (Lira, Zalamea et al. 1994), (Pedersen and Febbraio 2012). Their exact mode of action in skeletal muscle regeneration is still not clear. During aging, production of these cytokines/myokines is either diminished or altered, leading to declining muscle function. Thus, it will be interesting for future studies to address the potential effect these molecules could have in restoring the age-related muscle repair inefficiency.

- **Muscle resident-immune cell cross-talk during regeneration**

Skeletal muscle regeneration is a collection of highly synchronized processes involving several cellular, molecular and signaling responses. Coordinating inflammation and regeneration is particularly important for efficient repair (ad integrum) following acute injury (Bentzinger, Wang et al. 2013). A chief reason for the lack of better understanding of muscle repair is that skeletal muscle tissue comprises many different cell types, such as satellite cells, fibroblasts, fibro/adipogenic progenitors (FAPs), endothelial and periendothelial cells, mast cells, macrophages (resident and patrolling circulatory monocytes) and T cells, which can all affect the myofiber environment (reviewed in (Wynn 2008) and (Bentzinger, Wang et al. 2013)). Any disturbance of these cells' interactions could disrupt tissue homeostasis and consequently repair. Satellite cells are known to be key regulators of the skeletal muscle compartment (Lepper, Partridge et al. 2011), (Murphy, Lawson et al. 2011), (Sambasivan, Yao et al. 2011). These cells are undifferentiated myogenic cells that are found between the sarcolemma and basal lamina, and can fuse to establish new myofibres (Hawke and Garry 2001). These quiescent cells mature into post mitotic myofibres through specific extracellular signals. Initially these paracrine or autocrine signals result in myoblast expansion followed by pro-differentiation signals that are

required to induce their maturation. The exact nature of such signals is still not clearly defined. Many candidate molecules have been proposed to mediate myoblast differentiation such as IL-6 (Serrano, Baeza-Raja et al. 2008), insulin growth factors (Tonkin, Temmerman et al. 2015), and more recently growth differentiation factors (Varga, Mounier et al. 2016), supporting the notion that a range of factors are involved in this differentiation process. Only recently we started to understand which cell types (FAPs and macrophages) are responsible for producing these factors (Arnold, Henry et al. 2007), (Joe, Yi et al. 2010). During muscle regeneration satellite cells interact primarily with inflammatory and stromal cells, i.e. fibroblasts, pericytes and FAPs (Bentzinger, Wang et al. 2013). Importantly, it has been suggested that the cross-talk between these tissue compartments is crucial both in regulating myoblast expansion and differentiation but also regarding the outcome of skeletal muscle regeneration. How the cross-talk between satellite cells and other tissue compartments contributes to synchronized repair is not known. At the same time, the field lacks adequate methodology to study and thoroughly delineate the exact nature of such interactions.

It is known that repair macrophages activate angiogenesis (Ochoa et al., 2007) and induce satellite cell differentiation (Chazaud, Brigitte et al. 2009). A model of repair macrophage depletion (CCR2 −/− mice), shows the importance of this subtype in regeneration (Tidball and Wehling-Henricks 2007), while *in vitro* studies demonstrate that these cells enhance the expression of myogenin (muscle differentiation marker), and myocyte fusion (Arnold, Henry et al. 2007). In human muscle biopsies after exercise, repair macrophages co-localize with differentiating satellite cells (Saclier, Yacoub-Youssef et al. 2013). Insulin-like growth factor-1 (IGF-1) is an important hormone secreted by the repair macrophages acting on satellite cells and seems to restore proper regeneration dynamics when administered exogenously (Lu, Huang et al. 2011).

Skeletal muscle mass, function, and ability to repair, all progressively decline with aging resulting in restrictions to mobility, voluntary function and eventually quality of life. With aging satellite cell proliferation and differentiation capacity declines (Shefer, Van de Mark et al. 2006), as well as macrophage cytokine production (Hearps, Martin et al. 2012), (Nyugen, Agrawal et al. 2010), (Qian, Luo et al. 2012), (van Duin, Mohanty et al. 2007), (van Duin, Mohanty et al. 2007). As a consequence their ability to repair injured muscle markedly declines with aging, following a progressive loss of muscle tissue homeostasis (Cheung and Rando 2013). In addition, the deprivation of the reserve pool of satellite cells also contributes to this disruption of homeostasis (Welle 2002). *In vitro*, it has been shown that aged satellite cells delay entering the differentiation program compared to satellite cells from young mice. This seems to be a follow up consequence to their reduced capacity to proliferate (Shefer, Van de Mark et al. 2006). Moreover, the number of differentiating satellite cells is decreased in aged mice, as shown by downregulation of differentiation markers such as desmin and myogenin (Charge, Brack et al. 2002), (Collins, Zammit et al. 2007). Of note, the loss of muscle regeneration capacity with age appears to be reversible. Altered immune responses with aging, usually referred to as immunosenescence, can also contribute to impaired muscle regeneration due to their role in activating satellite cell expansion and maturation (Shaw, Goldstein et al. 2013). Immunosenescence also contributes to the development of chronic low-grade inflammation. Knowing the key role of macrophages in regulating satellite cell function, one can assume that changes in the macrophage function due to aging would affect muscle regeneration (Ehrhardt and Morgan 2005). However, it's still

unclear how aging affects satellite cell function and macrophage phenotypic transition, and their subsequent immune/muscle cell cross-talk. Such work will help us to develop approaches to preserve the muscle regenerative capacity in aged individuals.

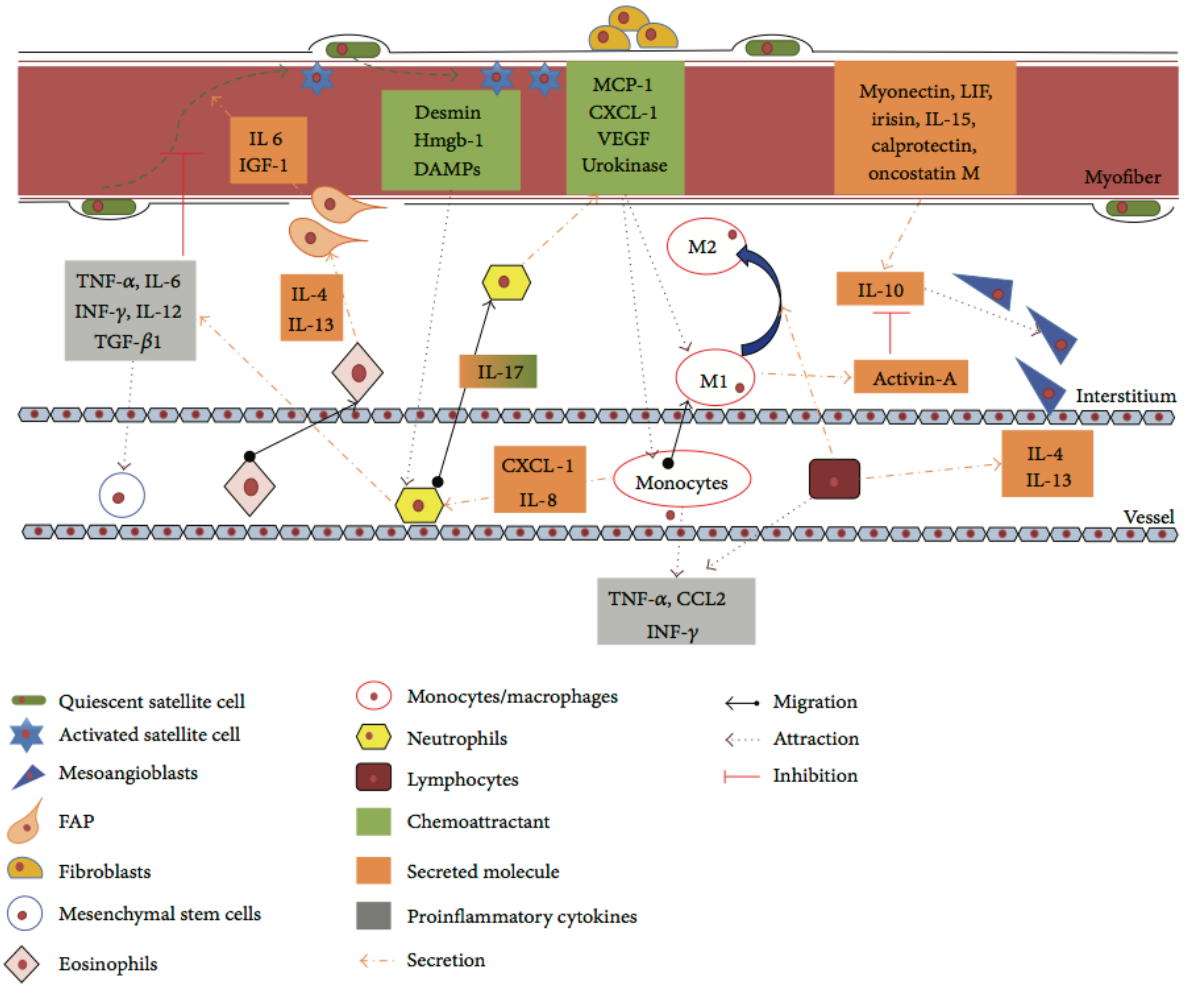

Figure 3. Secreted molecules and paracrine effects from resident and circulating cells involved in skeletal muscle inflammation (Costamagna, Costelli et al. 2015).

C. Hypothesis and Research Questions

Macrophages are considered major therapeutic targets due to their role in controlling the initiation, maintenance, and resolution of wound-healing responses in different tissues and organs. However, our knowledge is fragmented on how MFs change their phenotype, employ sensory and regulatory mechanisms and use effector functions to serve such reparatory roles. This is particularly important because the proper signaling between the participating cell types can ensure precise progression of repair, while avoiding asynchrony which can lead to regeneration delay, fibrosis and/or chronic inflammation (Dadgar, Wang et al. 2014). We sought to identify such integrated sensory, regulatory and effector mechanisms equipping a macrophage with the capacity to repair damaged tissues. In addition, it is likely that the microenvironment is driving the inflammatory to repair phenotypic switch, but it still remains to be determined how macrophages make this *in situ* phenotypic shift. Thus, we hypothesized that there is likely to be reciprocal communication between local muscle cell populations and macrophages. For example, the presence and signals from the satellite cells might be required for the invasion and phenotypic shift of macrophages, which is crucial for the outcome of muscle regeneration.

Here, the cardiotoxin (CTX)-induced skeletal muscle injury model was applied, as an established and highly reproducible *in vivo* model of acute muscle injury and sterile physiological inflammation (Hardy, Besnard et al. 2016). Unbiased transcriptomic analysis of the *in vivo* isolated MF populations involved in regeneration was carried out. Based on preliminary data from the system-level analyses we hypothesized that the nuclear hormone receptor, PPARg regulates muscle macrophage function and via this muscle regeneration. Furthermore, we asked whether growth factors secreted from muscle macrophages are required for proper regeneration and interaction of macrophages with skeletal muscle cells. The identified factors will be subsequently tested for their ability to restore muscle regeneration in geriatric models of impaired regeneration.

During the next phase of our studies we were interested in what kind of epigenomic changes are taking place during macrophage subtype specification following CTX injury. We hypothesized that by using an unbiased genomic approach called “assay for transposase accessible chromatin” (ATAC-seq), we could study the chromatin structure and accessibility during the transition of inflammatory macrophages to repair type ones, and thus identify novel regulators of this process.

Lastly, we wanted to identify what are the cell interactions within the injured tissue cell milieu that contribute or potentially control the macrophage phenotypic switch. We hypothesized that altering the muscle tissue integrity and cell composition by ablating local muscle satellite cells prior to the injury, would affect the *in situ* macrophage phenotypic shift and subsequently impact muscle regeneration.

D. Aims

Our work focused on identifying multi-level interactions between inflammatory and repair macrophages and skeletal muscle cells during regeneration and repair. Our long-term goal has been to identify and characterize sensory, regulatory and effector functions ascribable to macrophages during muscle regeneration and tissue repair. We have used unbiased genomic approaches (RNA-seq and ATAC-seq) combined with advanced cell separation from injured and regenerating tissues to identify molecules likely to be required as sensors of the environment, regulators of transcription during the macrophage phenotypic switch, and effector molecules contributing to myoblast proliferation, differentiation and myofiber formation.

Specific aims:

1. Assessing the role of newly identified sensors and regulators in a model of skeletal muscle regeneration (CTX):
    i. Lipid activated transcription factor PPARg:
        - *In vivo* molecular analysis of macrophage PPARg function in inflammation and tissue injury (fiber size distribution, necrotic clearance).
        - Identification of PPARg target genes using gene expression profiling and characterization of the contribution of these genes to muscle regeneration.
    ii. Heme sensor and transcriptional repressor BACH1:
        - *In vivo* molecular analysis of macrophage BACH1 function in macrophage dynamic phenotype switch, cell invasion, gene expression, inflammation and tissue injury (fiber size distribution, necrotic clearance).
        - Identification of BACH1 target genes using gene expression profiling and characterization of the contribution of these genes to muscle regeneration.

2. Assessing the role of newly identified effector molecules in an acute sterile muscle injury model (CTX):
    i. Growth differentiation factor GDF3:
        - *In vivo* molecular analysis of macrophage secreted GDF3 in muscle injury (fiber size distribution).
        - GDF3 role in primary myoblasts and aged muscles (*in vivo* administration of recombinant protein).
    ii. Growth differentiation factor GDF15:
        - *In vivo* molecular analysis of macrophage GDF15 function in macrophage dynamic phenotype switch, cell invasion and tissue injury (fiber size distribution).
    iii. Heme catabolizing enzyme HMOX1:

- *In vivo* molecular analysis of macrophage HMOX1 in macrophage dynamic phenotype switch, cell invasion, and tissue injury (fiber size distribution, necrotic clearance).

3. Explore the potential existence of a reciprocal cross-talk between the skeletal muscle tissue and myeloid cells recruited following acute injury:
    i. Use two *in vivo* models as a mean to alter cellular composition prior to muscle injury:
        - Irradiation.
        - Genetic ablation of a specific muscle cell population ($PAX7^+$ cells).
    ii. Use bone marrow transplantation to replenish myeloid cells.
    iii. Use PET-MRI *in vivo* imaging to monitor the myeloid cell phenotypic switch *in situ*.

E. Materials and Methods

Ethical approval:
All animal experiments were carried out in accordance with guidelines prescribed by the Institutional Animal Care and Use Committee at Sanford Burnham Prebys Medical Discovery Institute and University of Debrecen, School of Medicine following Hungarian (license no.: 21/2011/DEMÁB) and European regulations.

Mice:
Wild type BoyJ (B6.SJL-Ptprca Pepcb /BoyJ, stock number 002014) and C57BL/6J male control mice were obtained from the Jackson Laboratories and bred under specific-pathogen free (SPF) conditions. $Pparg^{fl/fl}$LysMCre+ (refered to as PPARg MacKO), Gdf15 KO (provided by Dr. Se-Jin Lee at John Hopkins University), Bach1 KO (obtained by Dr. Kazuhiko Igarashi at Tohoku University), $Hmox1^{fl/fl}$ LysMCre (obtained by Dr. George Kollias at BSRC-Athens), Gdf3 KO (provided by Dr. Chester Brown at Baylor College of Medicine), and littermate C57BL/6 albino controls were used in the experiments. Mice of 23-28-month-old were obtained by GlaxoSmithKline. Experiments were conducted on adult (2-6-month-old) male mice unless otherwise noted. For *in vivo* heme treatments mice were treated with either 30 mg/kg hemin (Sigma) or saline daily. All irradiation experiments were performed under anesthesia in cohorts of 12 animals per experiment. Briefly, mice were anaesthetized with a single intraperitoneal dose of ketamine/xylazine (ketamine 80-100 mg/kg, xylazine 10-12.5 mg/kg). Irradiated and bone marrow transplanted mice were maintained in an SPF status (autoclaved top filter cages) for the entire course of experimentation and antibiotics (amoxicillin antibiotic, clavulanic acid [500 mg/ 125 mg/ liter of drinking water]) were administered in the drinking water for 4 weeks after transplantation to minimize bacterial contamination within the water source and potentially decrease the burden of gastrointestinal bacteria. Irradiated mice were also fed autoclaved rodent chow ad libitum. Animals that undergo irradiation for BMT typically lose a considerable amount of weight, only to gain it back relatively quickly after successful transplantation. Weight loss of 20%, or greater was used as a rationale for euthanasia before the intended experimental endpoint according to the IACUC guidelines. The Pax7CreER/+, Rosa26DTA/+ strain, designated Pax7-DTA, was generated by crossing Pax7CreER/CreER and Rosa26DTA/DTA strains. Pax7-DTA pups were genotyped by PCR (Nishijo, Hosoyama et al. 2009), (Wu 2006). The tamoxifen-treated mice were kindly provided by Dr. John McCarthy and Dr. Charlotte Peterson. For tissue collection mice were euthanized by either isoflurane overdose (adjusted flow rate or concentration to 5% or greater) or CO_2 exposure (adjusted flow rate 3 L/min) in accordance to the University of Debrecen and Sanford Burnham Prebys Medical Discovery Institute's IACUC guidelines.

Bone Marrow Transplantation (BMT):
Recipient congenic BoyJ mice (7 weeks old) are irradiated with 9.5 or 11 Gy using a Theratron 780C cobalt unit for the ablation of the recipient bone marrow. The animals to be irradiated were immobilized using a circular cage (mouse pie cage) that can hold up to 11 mice (alert mice). Following the irradiation, isolated bone marrow cells (in sterile RPMI-1640 medium) flushed out from the femur, tibia and humerus were transplanted into the recipient mice by retro-orbital injection ($20x10^6$ BM cells per mice). This experimental BMT CD45 congenic model allows us to

detect donor, competitor and host contribution in hematopoiesis and repopulation efficiency of donor cells (congenic mice with CD45.1 versus CD45.2). The CD45.1 and CD45.2 contribution is detected by flow cytometry at 8-12 weeks following the BMT. In short, a cut at the tail tip of the mice provided a drop of blood that was placed into 0.5 ml PBS + 1% FBS + 10 U/ml Heparin buffer (samples kept on ice). The cells were directly stained by 2 µl (1/50 dilution) mouse anti-mouse CD45.2-FITC (clone 104) and 2 µl (1/50 dilution) rat anti-mouse GR1-PE (clone RB6-8C5) antibodies (BD Pharmingen) and incubated on ice for 30 min. After 2 washes with ice-cold PBS/FBS/Heparin buffer, cells were resuspended in 0.5-1 ml FACS Lysing solution (BD Cat #349202). Cells where then incubated for 5 min at RT and centrifuged (400g, 5 min, 4°C). The double stained samples were run on BD FACS Calibur and determined the ratio of donor cells. The repopulation is always gated on the granulocyte fraction based on FSC, SSC and Gr1 staining.

Bone Marrow Transplantation (BMT) including local radioprotection:
A modification of the above protocol was used by introducing hindlimb lead shielding. The animals to be irradiated were anesthetized via intraperitoneal injection of ketamine (80 mg/kg) and xylazine (10 mg/kg), and placed into a plastic box, with double wall. Water was used between the walls, as scattering medium, in order to get homogeneous dose distribution. Two 5 cm high led blocks were used for protection one of the legs of the mouse. The blocks were on the PMMA shadow tray of the cobalt unit, more than 20 cm distance to the surface of the plastic box, so the air absorbs the Compton electrons from the blocks. In order to account for the buildup region of cobalt energy, 5 mm thickness top box plate was used. The source surface distance (SSD) and source axis distance (SAD) was 80 cm and the beam size covered 21 x 21 cm. The activity of the Cobalt-60 isotope was about 50 TBq (1350 Ci). Animals were generally irradiated for short periods of time (20-30 min as a function of the given date) depending on the radioisotope decay charts, amount of irradiation needed, and source of ionizing energy. Following the irradiation, isolated bone marrow cells from donor C57BL/6J mice were transplanted into the recipient mice by retro-orbital injection.

Lower body irradiation:
For this method 5 cm thick lead blocks were used during irradiation, to protect one of the back legs of lightly sedated mice. We focused the radiation field (14.4 x 4.8 cm) only in the lower part of their bodies just below the hip thus minimizing radiation exposure to the rest of the body. The source surface distance (SSD) and source axis distance (SAD) was kept the same and mice were irradiated with a dose of 11 Gy. The animals left to recover for 8 weeks after the radiation exposure.

Acute sterile muscle injury:
Mice were anaesthetized with isoflurane (adjusted flow rate or concentration to 1.5 %) and 50 µl of cardiotoxin ($12X10^{-6}$ M in PBS) (from Latoxan) was injected in the tibialis anterior (TA) muscle. Muscles were isolated for flow cytometry analysis at day 1 to day 8 post-injury or for muscle histology at day 8 to day 20 post-injury.

Histological analysis of muscle regeneration:
Muscles were removed and snap frozen in nitrogen-chilled isopentane (–160°C). 8 µm thick cryosections were cut and stained with hematoxylin-eosin (H&E). For each histological analysis, at least 5 slides (per condition) were selected in which the total regenerative region within the CTX injured TA muscle was at least 70%. For each TA, myofibers in the entire injured area were counted and measured. H&E muscle sections were scanned with Mirax digital slide scanner and the Cross Sectional Area (CSA) was measured with HALO software (Indica Labs). CSAs for these samples are reported in μm^2. Quantitative analysis of necrotic/phagocytic vs. centrally nucleated myofibers was performed using the Panoramic Viewer software and was expressed as a percentage of the total number of myofibers. Necrotic/phagocyted myofibers were defined as pink pale patchy fibers invaded by basophil single cells (macrophages).

Immunohistochemistry (Frozen sections):
Tissue sections were fixed and permeabilized in ice cold acetone for 5 min and blocked for 30 minutes at 20 °C (room temperature) in PBS containing 2 % bovine serum albumin (BSA). Tissues were stained for 1 h at room temperature using a primary antibody diluted in 2 % BSA. The primary antibodies used for immunofluorescence were rabbit anti-laminin (L9393 SIGMA) at a dilution of 1/200, chicken anti-PAX7 (DSHB) at a dilution of 1/20, rabbit anti-Desmin (Abcam 32362) at a dilution of 1/200 and rat anti-F4/80 (Abcam 6640) at a dilution of 1/200. In all cases, the primary antibody was detected using secondary antibodies (dilution 1/200) conjugated to FITC (JIR 703-095-155) or Cy3 JIR (711-165-152). The nuclei were counter stained with 0.1-1 µg/ml Hoechst. Fluorescent microscopy was performed using Carl Zeiss Axio Imager Z2 microscope equipped with lasers at 488, 568 and 633 nm. Figures were analyzed and assembled using Fiji (image processing package based on ImageJ) and Illustrator CS5 (Adobe).

***In vivo* Isolation of macrophages from muscle:**
Fascia of the TA was removed. Muscles were dissociated in RPMI containing 0.2% collagenase B (Roche Diagnostics GmbH) at 37°C for 1 hour and filtered through a 100 µm and a 40 µm filter. CD45+ cells were isolated using magnetic sorting (Miltenyi Biotec). For FACS, macrophages were treated with 5% Fcγ receptor blocking antibodies and with 10% normal rat serum: normal mouse serum 1:1 mix, then stained with a combination of PE-conjugated anti-Ly6C antibody at a dilution of 1/200 (HK1.4, eBioscience), APC-conjugated F4/80 antibody at a dilution of 1/50 (BM8, eBioscience) and FITC-conjugated Ly6G antibody at a dilution 1/100 (1A8, Biolegend). $Ly6C^{high}$ $F4/80^{low}$ macrophages, $Ly6C^{low}$ $F4/80^{high}$ macrophages and $Ly6G^{high}$ $Ly6C^{med}$ $F4/80^{-}$ neutrophils were quantified. In each experiment, control samples were processed in parallel to minimize experimental variation. Cells were analyzed on a BD FACSAria III sorter and data analysis was performed using BD FACSDIVA (BD Biosciences) and FlowJo V10 (FlowJo, LLC) software.

RNA isolation:
Total RNA was isolated with TRIZOL reagent according to the manufacturer's recommendation. 20 µg glycogen (Ambion) was added as carrier for RNA precipitation.

RT-qPCR:

Transcript quantification was performed by quantitative real-time RT (reverse transcriptase) PCR (polymerase chain reaction) using SYBR Green assays. RT-qPCR results were analyzed with the standard delta Ct method and results were normalized to the expression of Rps26 or Ppia. Primer sequences used in transcript quantification are as follows:

Pax7	F: 5’ GGCACAGAGGACCAAGCTC 3’
	R: 5’ GCACGCCGGTTACTGAAC 3’
Il10:	F: 5’ CAGAGCCACATGCTCCTAGA 3’
	R: 5’ TGTCCAGCTGGTCCTTTGTT 3’
Igf1:	F: 5’ AGCAGCCTTCCAACTCAATTAT 3’
	R: 5’ TGAAGACGACATGATGTGTATCTTTAT 3’
Dusp1:	F: 5’ TGGTTCAACGAGGCTATTGAC 3’
	R: 5’ GGCAATGAACAAACACTCTCC 3’
Slc40a1:	F: 5’ ACCCATCCCCATAGTCTCTGT 3’
	R: 5’ CCGATTCTAGCAGCAATGACT 3’
Ftl1:	F: 5’ AGTTTCAGAACGATCGCGGG 3’
	R: 5’ GGAAGTCACAGAGATGAGGGTC 3’
Tnfsf12:	F: 5’GAGCCCCCTGAACTGAATC 3’
	R: 5’ AGGCCGGACTAGTTGTTCC 3’
Cebpb:	R: 5’ TGATGCAATCCGGATCAA 3’
	R: 5’ CACGTGTGTTGCGTCAGTC 3’
Spp1:	F: 5’ TCCCTCGATGTCATCCCTGT 3’
	R: 5’ TTGACTCATGGCTGCCCTTT 3’
Hmox1:	F: 5’ CTGCTAGCCTGGTGCAAGATACT 3’
	R: 5’ GTCTGGGATGAGCTAGTGCTGAT 3’
Il6:	F: 5' CAAAGCCAGAGTCCTTCA 3'
	R: 5' GGTCCTTAGCCACTCCTT 3'
Arg1:	F: 5'TTTTAGGGTTACGGCCGGTG 3'
	R: 5' CCTCGAGGCTGTCCTTTTGA 3'
Socs3:	F: 5' ATTTCGCTTCGGGACTAGC 3'
	R: 5' AACTTGCTGTGGGTGACCAT 3'
Pparg:	F: 5' TCCATTCACAAGAGCTGACCC 3'
	R: 5' GGTGGAGATGCAGGTTCTACT 3'
Gdf3:	F: 5' GGGTGTTCGTGGGAACCT 3'
	R: 5' CCATCTTGGAAAGGTTTCTGTG 3'

Small animal PET-MRI imaging using ^{18}F-FDG:
PET-MRI experiments were conducted during the light cycle to minimize muscle activity. C57BL/6 or BoyJ mice were injected with 8.0 ± 0.2 MBq of ^{18}F-FDG via the lateral tail vein in 200 µl volume. 50 min after ^{18}F-FDG injection animals were anaesthetized by 3% isoflurane with a dedicated small animal anesthesia device and whole body PET scans (10 min static PET scans) were acquired using the preclinical nanoScan PET/MRI system (Mediso Ltd., Hungary). To prevent movement, the animals were fixed to a mouse chamber (MultiCell Imaging Chamber, Mediso Ltd., Hungary) and positioned in the center of field of view (FOV). For the determination of the anatomical localization of the organs and tissues, T1-weighted MRI scans were performed (3D GRE EXT multi-FOV; TR/TE 15/2 ms; FOV 70 mm; NEX 2). PET volumes were reconstructed using a three-dimensional Ordered Subsets Expectation Maximization (3D-OSEM) algorithm (Tera-Tomo, Mediso Ltd., Hungary). PET and MRI video and images were automatically co-registered by the PET/MRI instrument's acquisition software (Nucline). Reconstructed, reoriented and co-registered images were further analyzed with InterView™ FUSION (Mediso Ltd., Hungary) dedicated image analysis software.

PET data analysis:
Radiotracer uptake was expressed in standardized uptake values (SUVs). Ellipsoidal 3-dimensional Volumes of Interest (VOI) were manually drawn around the edge of the TA and GAST muscle activity using InterView™ FUSION multi-modal visualization and evaluation software (Mediso Ltd., Hungary). The standardized uptake value (SUV) was calculated as follows: SUV = [VOI activity (Bq/mL)]/[injected activity (Bq)/animal weight (g)], assuming a density of 1 g/mL

Ex vivo radiotracer uptake studies:
Cells were isolated from injured muscles as described above. Live cells for both myeloid CD45^{+} and non-myeloid CD45- fractions were selected using FACS-sorting based on FSC/SSC gating and then washed and resuspended in PBS containing 1 mM glucose. The samples were pre-incubated at 36 °C for 10 min at a cell concentration of 1 × 10^6 /ml in PBS and 0.37 MBq/ml ^{18}F-FDG was then added to each sample. After the addition of the radioligand, cells were further incubated at 36 °C for 50 min and the uptake was terminated by the addition of ice-cold PBS. The cells were then washed three times with cold PBS and resuspended in 1 ml of cold PBS, and the radioactivity was measured. The tubes were measured in a Canberra Packard gamma-counter for 1 min within the ^{18}F-sensitive energy window. Decay-corrected radiotracer uptake was expressed as counts min^{-1} $(10^6$ cells$)^{-1}$ (cpm). The displayed data are the means ± SD of the results of at least three independent experiments, each performed in triplicate.

Expression data processing and analysis:
GSE71155 data sets were loaded into the Genespring GX software, and multiarray average summarization was carried out. Next, the lowest 5% of the entities with detectable signals were filtered out as not expressed. Duplicate entities, not/poorly annotated transcripts and transcripts reporting inconsistent expression values were also discarded. Further analysis was carried out on the filtered data set based on the RAW expression values. Heatmap was generated based on log_{10}-transformed raw values with R software package pheatmap. Hierarchical clustering analysis

was then applied by Euclidean distance measure and Ward's clustering algorithm, to find correlated genes.

Myogenic precursor cell (MPC) culture:
Murine MPCs were obtained from TA muscles and cultured using standard conditions in DMEM/ F12 (Gibco Life Technologies) containing 20% FBS and 2% G/Ultroser (Pall Inc). For proliferation studies, MPCs were incubated for 1 day with conditioned medium + 2.5% FBS or with 2.5% FBS medium containing 100-600 ng of GDF3 or GDF15 mouse recombinant protein. Cells were then incubated with anti-Ki67 antibodies at a dilution of 1/200 (15580 Abcam), which were subsequently visualized using Cy3-conjugated secondary antibodies at a dilution of 1/200 (Jackson Immunoresearch Inc). For differentiation studies, MPCs were incubated for 3 days with conditioned medium containing 2% horse serum or with 2% horse serum medium containing 300 ng/ml recombinant GDF3. Cells were then incubated with anti-Desmin antibodies at a dilution of 1/200 (32362 Abcam), and in combination with a Cy3-conjugated secondary antibody at a dilution of 1/200 (Jackson Immunoresearch Inc).

Image capture and analysis for myoblast cultures:
Fusion index (for myogenic cells) was calculated as the number of nuclei within myotubes divided by the total number of nuclei. The nuclei number was estimated based on DAPI staining and using the Image J software. Desmin staining was used for detecting the myotubes.

Microarray analysis of muscle macrophages:
Global expression pattern was analyzed on Affymetrix GeneChip Mouse Gene 1.0 ST arrays. The microarray data are publicly available (Data access: GSE71155).

Western Blotting:
GDF3 and GDF15 protein expression was measured using Western Blot analysis. Samples from CTX injected TA muscles were lysed in RIPA buffer. GDF3 was targeted using rabbit monoclonal Anti-GDF3 primary antibody (ab109617, Abcam, Cambridge, MA) at 1:1000 dilution in 5% BSA/TBS-T overnight at 4°C. GDF15 was targeted using rabbit polyclonal (ab105738, Abcam) at 1:1000 dilution in 5% BSA/TBS-T overnight at 4°C. Anti-GAPDH mouse monoclonal primary antibody (AM4300, Ambion, Carlsbad, CA) was used as a protein loading control at 1:10000 – 1:20000 dilution in 5% BSA/TBST overnight at 4°C.

RNA sequencing (RNA-Seq) library preparation:
cDNA library for RNA-Seq was generated from 100-400 ng total RNA using TruSeq RNA Sample Preparation Kit (Illumina, San Diego, CA, USA) according to the manufacturer's protocol. Briefly poly-A tailed RNA molecules were pulled down with poly-T oligo attached magnetic beads. Following purification, mRNA was fragmented with divalent cations at 85^{o}C, and then cDNA was generated by random primers and SuperScript II enzyme (Life Technologies). Second strand synthesis was performed followed by end repair, single `A` base addition and ligation of barcode indexed adaptors to the DNA fragments. Adapter specific PCRs were performed to generate sequencing libraries. Libraries were size selected with E-Gel EX 2% agarose gels (Life

Technologies) and purified by QIAquick Gel Extraction Kit (Qiagen). Libraries were sequenced on HiSeq 2500 instrument. Three biological replicates were sequenced for each population.

RNA-seq analysis:

RNA-seq samples were analyzed according to the pipeline described in Barta et al. 2011. Briefly, the 50 bp raw single reads were aligned using TopHat (Kim et al. 2013) to the mm10 genome assembly (GRCm38) and only the uniquely mapped reads were kept using '--max- multihits 1' option, otherwise the default parameters were used. SAMtools (Li et al. 2009) was used for indexing the alignment files. Coverage density tracks (wig files) for RNA-seq data were generated by igvtools with 'count' command and then converted into tdf files using 'toTDF' option. Genes with CPM (counts per million) >= 10 (at least in one sample) were considered to be expressed. Statistically significant difference was considered as p value < 0.05 from GLM test using R package edgeR (Robinson, McCarthy et al. 2010). Data analysis was also performed using Strand NGS software, Version 2.8, Build 230243 (Strand Life Sciences). Aligned reads were loaded into Strand NGS before performing DESeq normalization for hierarchical clustering analysis (Euclidean similarity measure and Ward's linkage rule used), and data visualization using Principal Component Analysis (PCA). When comparing data across three or more groups, the obvious option is to use the One-way ANOVA statistical test. The One-Way ANOVA takes a comprehensive approach in analyzing data and attempts to extend the logic of t-tests to handle three or more groups concurrently. It uses the mean of the sum of squared deviates (SSD) as an aggregate measure of variability between and within groups. It assumes independent and random samples drawn from a normally distributed source. Additionally, it also assumes that the groups have approximately equal variances, which can be practically enforced by requiring the ratio of the largest to the smallest group variance to fall below a factor of 1.5. These assumptions are especially important in case of unequal group-sizes. When group-sizes are equal (samples are independent and random) like in the CTX model, the test is amazingly robust, and holds well even when the underlying source distribution is not normal. The significant ANOVA result suggests rejecting the null hypothesis H0 = ''means are the same''. It does not tell which means are significantly different. For a given gene, if any of the group pair is significantly different, then in ANOVA test the null hypothesis will be rejected. Post hoc tests are multiple comparison procedures commonly used on only those genes that are significant in ANOVA F-test. The most common post hoc test is Tukey's Honestly Significant Difference or HSD test. Tukey's test calculates a new critical value that can be used to evaluate whether differences between any two pairs of means are significant. One simply calculates one critical value and then the difference between all possible pairs of means. Each difference is then compared to the Tukey critical value. If the difference is larger than the Tukey value, the comparison is significant. Next multiple testing correction using Bonferroni and Benjamini Hochberg methods (replicate analysis) were used for identifying differentially expressed genes under different experimental conditions. $\log_{10}$ adjusted p-values and $\log_2$ fold changes generated by these analyses were plotted using R package pheatmap (version 3.2.1) to create heatmaps. Genes with normalized expression lower than 6 across all samples were not expressed and thus removed from the analysis. Pathway analysis was performed with the DAVID (Database for Annotation, Visualization and Integrated Discovery) online tool (https://david.ncifcrf.gov/).

Gene ontology analysis:
Lists of genes were analyzed using Panther tool (http://www.geneontology.org/) and the GO Enrichment Analysis to create a gene ontology (GO). GOs with p values < 0.0001 and fold enrichment > 2 were selected and results were presented according to their $-\log_{10}$(p value).

Differentiation of bone marrow-derived macrophages:
Isolation and differentiation of BMDMs were performed as described earlier (Daniel, Balint et al. 2014). Briefly, isolated bone marrow- derived cells were differentiated for 6 days in the presence of L929 supernatant.

ChIP (Chromatin immunoprecipitation):
ChIP-qPCR was performed essentially as previously described (Daniel, Balint et al. 2014), (Daniel, Nagy et al. 2014). Bach1 antibody was a gift from Dr Spilianakis (IMBB-FORTH, Greece). We used the following primers for qPCR:

IL10 +13kb:	F: 5' TCCCTGAGCCACCAGATAGAT 3'
	R: 5' ATTTAGTAGGGCTTCCCCAGC 3'
Dusp1 -25kb:	F: 5' AGATGACCCAAAGGGAAGCTG 3'
	R: 5' GCCTCCCCCACCTGACTAAT 3'
Spp1 -9kb:	F: 5' ACACGAACAAAGGCGAAACTC 3'
	R: 5' AGCTTCTGTGTGACTCGGC 3'
Ftl1 -1kb:	F: 5' GGCCCTTAGTGGAAGGGGTA 3'
	R: 5' GGAAAACAGACCACAAGCCC 3'
Cebpb +76kb:	F: 5' CCCAAGCTTCCCAGAACTCG 3'
	R: 5' TGCCTTGCACCCAAAAATGC 3'
Slc40a1 +43kb:	F: 5' GGCAGGGTCCAGGGAAACTA 3'
	R: 5' GTGACAGAGGGACACATCGG 3'
Gdf3 -47kb:	F: 5' ATGCTCACGCAGACTTGACT 3'
	R: 5' ACGAGAAAATGTTGGCACAGC 3'
Socs3 +22kb:	F: 5' TTTGGTTCCCCAGTGGTGTTC 3'
	R: 5' CGGATCATAGCTTTCCCCCA 3'
Pparg -17kb:	F: 5' CTCCTCTTTCGTCTGAGGTTTGA 3'
	R: 5' AGCTGACAGAGAATCTGGGGA 3'
Tnfsf12 +3,7kb:	F: 5' CTGTCCATGTCATGTGGCCT 3'
	R: 5' ACTCCCCGTGAATGAAGCTG 3'
Igf1 -15kb:	F: 5' CTTCCTTAGTAGCTGCACCAGT 3'
	R: 5' GCAAGCCATAGGGAAGAGGAA 3'
Arg1 -4kb:	F: 5' CCAAAGTGGCACAACTCACG 3'
	R: 5' CATAAGGTCACGGAGGGTGG 3'

Hmox1 Eα:	F: 5’ TGGGAGGGGTGATTAGCAGA 3’
	R: 5’ TAGCTGAGGCTGAGGGAACA 3’
Hmox1 Eβ:	F: 5’ CCGGATACTAGTGACTGCCC 3’
	R: 5’ CCACTTAAGGGCATGTGGGG 3’

Real-Time Quantitative PCR for enhancer RNA (eRNAs):
RNA was isolated with Trizol reagent (Ambion). RNA was DNase-treated and reverse transcribed with High- Capacity cDNA Reverse Transcription Kit (Applied Biosystems) according to the manufacturer’s protocol. Transcript quantification was performed by qPCR reactions using SYBR green master mix (BioRad). Transcript levels were normalized to Ppia or Actb. We used the following eRNA primers:

Hmox1 Eα (E1 neg.strand):	F: 5’ TTGTCCTACGTGTGTGGCAG 3’
	R: 5’ GAAGGCAGGAGACTCCAGTG 3’
Hmox1 Eβ (E2p neg.strand):	F: 5’ AAGGGACAGAAGGAAGCTGAT 3’
	R: 5’ GTGGGGCAGTCACTAGTATCC 3’
Hmox1 Eγ (gamma) (used also for ChIP):	F: 5’ CTGTGAGTTCTGGTCCGTGG 3’
	R: 5′ ACAGGAACATCTTGGAGCCAG 3’
Hmox1 Eδ (E2 pos.strand):	F: 5’ GCCCTTAAAGGCAGGGAACT 3’
	R: 5’ AAGGCATACTTGGGGATGGT 3’
Hmox1 Eδ (E2 neg.strand):	F: 5’ GCTAGCATGCGAAGTGAGCA 3’
	R: 5’ GCACAGCTCCGGATTCCTAAT 3’
Hmox1 Eε (used also for ChIP):	F: 5’ TGCTCAGTCTCCGTGTATGT 3’
	R: 5’ CCTGGCTTTGAGTCCATTCAT 3’
Cebpb +76kb:	F: 5’ CCAACTCCAACAAACTGCCC 3’
	R: 5’ GTCCAGGCACGACAGATGAG 3’
Slc40a1 +43kb:	F: 5’ TCACCTATGAAGCCTCCCTCA 3’
	R: 5’ AGGCATTGGCAGAAATAGGC 3’
Gdf3 -47kb:	F: 5’ TTGGGTAGAGGTGGTGTATGC 3’
	R: 5’ AGCCTCATGACCTGACTGAGA 3’
Socs3 +22kb:	F: 5’ ATGAAACCAGCCTGTGGAGAT 3’
	R: 5’ AACCTGAGAAGCTGATGGGTC 3’
Pparg -17kb:	F: 5’ ACAAATTATCTCAGGGGTTGGGA 3’
	R: 5’ GACAAGTTGGAGTTTGGCTCC 3’
Igf1 -15kb:	F: 5’ GCCTTTCTGAGTCTGGGTGA 3’
	R: 5’ CAAGGAGATGGAGCCAACCT 3’
Ftl1 -1kb:	F: 5’ GCTGTACGGCTCTGGAGTG 3’
	R: 5’ CCCAAATCAACAGACCACCG 3’
Spp1 -9kb:	F: 5’ ACCCCTCAGCCAACTTCTGA 3’
	R: 5’ GGTTGGGAGCTGGAGAATGC 3’

Arg1 -4kb:	F: 5' ATGAGCTGGTCTCTCGTCGG 3'
	R: 5' GGCCATGGTATGTGTTTCCC 3'
Dusp1 -25kb:	F: 5' AGCCAGAGCAGTGAAAAGGA 3'
	R: 5' TCCCTTGAGGCCATTTTGCT 3'
Il10 (used also for ChIP) +13kb:	F: 5' TCCCTGAGCCACCAGATAGAT 3'
	R: 5' ATTTAGTAGGGCTTCCCCAGC 3'

ATAC-seq:

ATAC-seq was carried out as described earlier with minor modification (Buenrostro, Giresi et al. 2013). 20 000 cells were sorted in ice-cold PBS. Nuclei were isolated with ATAC-Lysis Buffer (10 mM Tris-HCl pH 7.4, 10 mM NaCl, 3 mM $MgCl_2$, 0.1% IGEPAL) and were used for tagmentation using Nextera DNA Library Preparation Kit (Illumina) from 2-3 biological replicates. After tagmentation DNA was purified with MinElute PCR Purification Kit (Qiagen). Tagmented DNA was amplified with Kapa Hifi Hot Start Kit (Kapa Biosystems) using 9 PCR cycles. Amplified libraries were purified again with MinElute PCR Purification Kit. Fragment distribution of libraries was assessed with Agilent Bioanalyzer and libraries were sequenced on a HiSeq 2500 platform.

ATAC-seq analysis:

Two replicates of Ly6Chigh and low blood monocytes, muscle-derived Ly6Chigh macrophages 1 day and Ly6Chigh and low macrophages 2 and 4 days upon muscle injury were used for the ATAC-seq experiments (20 000 sorted cells per sample). The primary analysis of ATAC-seq-derived raw sequence reads has been carried out using our newest version of ChIP-seq analysis command line pipeline (Barta, 2011) including the following steps: Alignment to the mm10 mouse genome assembly was done by the BWA tool (Li and Durbin 2009), and BAM files were created by SAMTools (Li, Handsaker et al. 2009). Signals (peaks) were predicted by MACS2 (Zhang, Liu et al. 2008), and artifacts were removed according to the blacklist of ENCODE (ENCODE Project Consortium, 2012). All regions derived from at least any two samples were united within 0.5 kb and those summits having the highest MACS2 peak score in any sample were assigned to each region. Promoter-distal regions were selected excluding the TSS ± 0.5kb regions according to the mouse GRCm38.p1 (mm10) annotation version. Tag directories used by HOMER in the following steps were generated with a 120 bp nucleotide fragment length with makeTagDirectory (Heinz, Benner et al. 2010). Genome coverage (bedgraph and tdf) files were generated by makeUCSCfile.pl (HOMER) and igvtools, respectively, and used for visualization with IGV2 (Thorvaldsdottir, Robinson et al. 2013). Read distribution (RD) heat maps were created by annotatePeaks.pl (HOMER), went through an upper decile normalization and were visualized by Java TreeView (Saldanha 2004). 10 clusters of promoter-distal open chromatin regions were discriminated by K-means clustering based on the RD of all samples used. Dynamically changing clusters with similar profile but different density, were united. Motif enrichments for all 10 clusters were determined by findMotifsGenome.pl (HOMER). Top PU.1 and TRE motif hits as well as the MARE (mafa, mafk and bach1) motifs of HOMER's motif collection were used to map the putative regulatory elements to each region around the chosen summits plotted in 30-nucleotide windows using annotatePeaks.pl (HOMER) and other command line programs including

intersectBed (BEDtools) (Quinlan and Hall 2010). TRE motif matches overlapping with MAREs were excluded from the analysis. Motif distribution plots were visualized by Java TreeView.

Statistics:

ANOVA with Bonferroni correction for multiple testing was used to determine statistical significance using GraphPad Prism 6. Adjusted p values (P<0.05=*, P<0.01=**, P<0.001=***, P<0.0001=****) are stated within figure legends and all means are displayed ± SEM. For qRT-PCR analysis, three biological samples were used for each condition. For FACS marker analysis, four independent samples were analyzed. At least 10^5 cells were counted for FACS cell populations. For the histology experiments, at least 10 biological samples were used (each animal provides 2 biological samples). For the CSA distribution, two-way ANOVA was used to mark significance for each size class.

F. Results

Part 1. Transcriptional regulation of macrophages during skeletal muscle regeneration

We sought to understand the role and contribution of myeloid cells, primarily macrophages and also their interactions during skeletal muscle regeneration. We chose the CTX induced skeletal muscle injury model since this model proved to be instrumental for the identification of exogenous mechanisms of muscle regeneration (Chazaud 2014), (Varga, Mounier et al. 2016). This model is also suitable to study the effect of the regenerating muscle upon myeloid cell activity. The model works as follows: by injecting cardiotoxin (snake venom peptide that acts as protein kinase C-specific inhibitor) intramuscularly, homogenous skeletal muscle damage in the *Tibialis anterior* (TA) muscles is induced. Identical morphological changes can be observed during the course of regeneration.

Cardiotoxin induced skeletal muscle damage is a robust model of immune cell assisted regeneration

Histological analysis by hematoxylin and eosin (H&E) staining demonstrated global myofiber destruction and edema at days 1 and 2 post injury (**Figure 4A**). By day 8 after the injury the overall architecture of the muscle is restored although most regenerated myofibers were smaller and display central myonuclei, a known hallmark of recent muscle regeneration (**Figure 4A**). Thus, any change in the cellular composition or altered histological features at day 8 post injury, indicates perturbations in intracellular communications.

Upon CTX injury a large number of circulating immune cells infiltrate and accumulate in a rapid and highly ordered manner inside the injured tissue. This pool of invading cells consists primarily of neutrophils, monocytes and macrophages. $Ly6C^{high}$ $F4/80^{low}$ monocytes infiltrate early at day 1 to promote the clearance of necrotic debris, whereas $Ly6C^{low}$ $F4/80^{high}$ macrophages emerge later through a phenotypic shift (Varga, Mounier et al. 2013) starting at day 2 and completed by day 4, to assist tissue healing (**Figures 4B-C**). Complementary to these results, $F4/80^{high}$ expressing macrophage's localization was assessed using immunohistochemistry from injured muscles at Day 4 and 8 after CTX (**Figure 4D**). Furthermore, it was shown that $Ly6C^{high}$ macrophages express tumor necrosis factor α (TNFα) and interleukin (IL)-1β at higher levels and transforming growth factor β (TGF-β) and IL-10 at lower levels compared to $Ly6C^{low}$ macrophages (Perdiguero, Sousa-Victor et al. 2011), (Wang, Melton et al. 2014). Therefore, they were considered as pro-inflammatory and anti-inflammatory macrophages, respectively. However, we recently reported (Varga, Mounier et al. 2016) that $Gr1^{+}$ and $Gr1^{-}$ muscle derived macrophages do not display, in general, high differential expression levels of pro-inflammatory (M1) or anti-inflammatory (M2) markers. In line with our previous report, re-analyzing more recent publicly available microarray data sets (Varga, Mounier et al. 2016), that was obtained using our FACS gating strategy (**Figure 4B**), and by performing hierarchical clustering on a large number of known macrophage marker genes, we report expression patterns with modest differences (**Figure 4E**). Out of 69 markers we looked at, only 14 followed the expected pattern based on the M1/M2 axes, among them CD80, CD86, Nlrp3, Ccr2, Irf4, Emr1, Igf1, Pparg, Clec10a (**Figure 4E**).

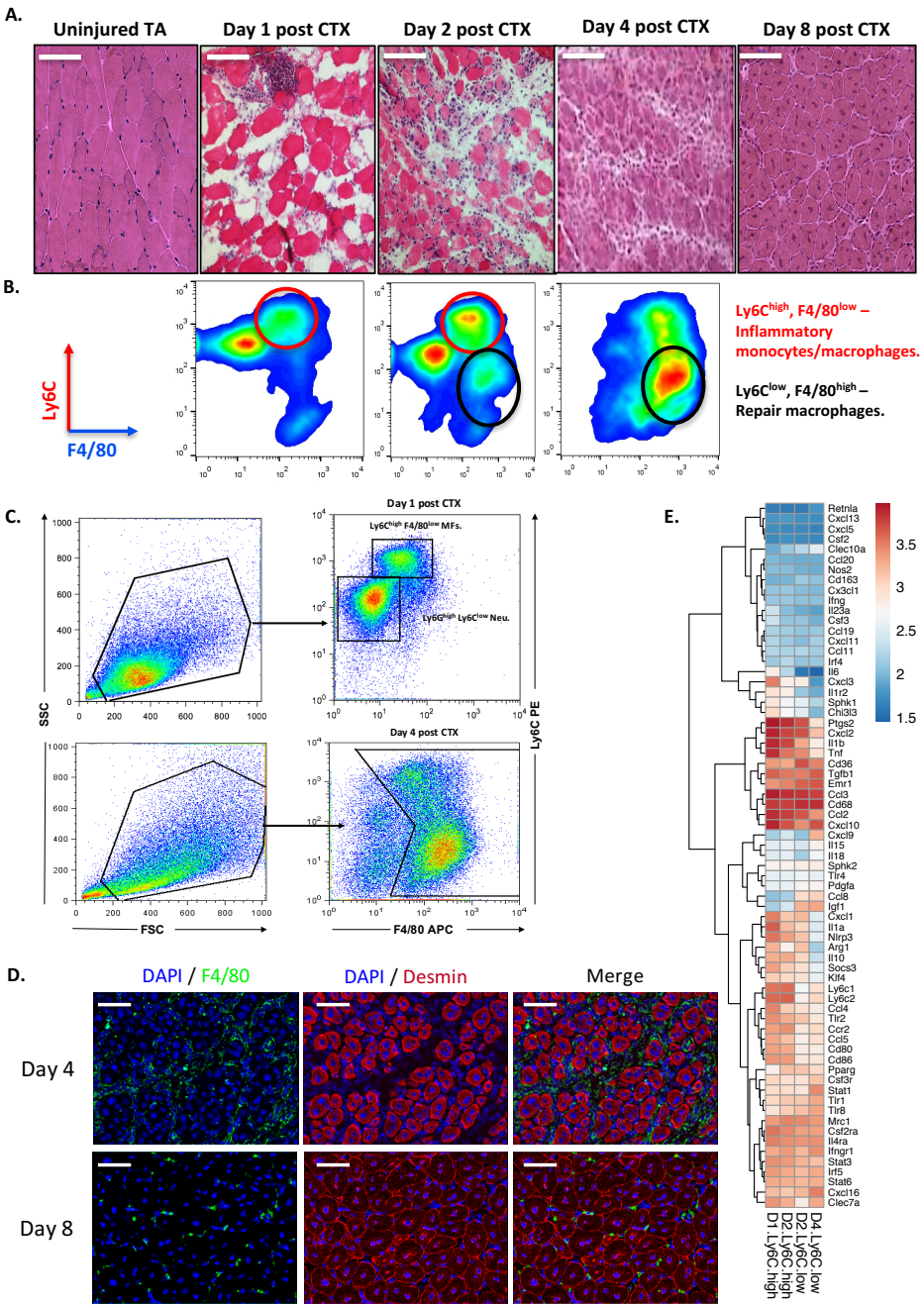

Figure 4. Cardiotoxin induced injury model and dynamic phenotype shift of muscle infiltrating macrophages.

A. *Tibialis anterior* muscles from C57BL/6J mice were injected with CTX and were isolated at various days after injury. Representative H&E stained muscle are shown. Scale bars represent 100µm.

B. $CD45^{+}$ cells isolated from regenerating muscle according to their Ly6C, Ly6G and F4/80 expression. Red circles labels inflammatory ($Ly6C^{high}$ $F4/80^{low}$) and black circles label repair ($Ly6C^{low}$ $F4/80^{high}$).

C. FACS gating strategy to enumerate muscle infiltrative macrophages at day 1 and 4 post CTX injury. $CD45^{+}$ cells were gated for an FSC/SSC pattern consistent with monocytic cells, and then percentage of $Ly6C^{high}$ $F4/80^{low}$ and $Ly6C^{low}$ $F4/80^{high}$ MF subsets of all FSC/SSC-gated cells was calculated.

D. Immunofluorescence images of regenerating tibialis anterior muscle from a 9-wk-old wild-type mouse at Day 4 and Day 8 after cardiotoxin-induced injury. The tissue was stained with antibodies directed against the macrophage marker F4/80 (green), the intermediate filament protein desmin (red) and with DAPI (blue) to visualize the cell nuclei. Scale bars represent 100 µm.

E. Heatmap representation of the expression pattern of pro-inflammatory and anti-inflammatory markers by muscle derived $Ly6C^{high}$ and $Ly6C^{low}$ macrophages at day 1, 2 and 4 post CTX injury (GEO: GSE71155). Hierarchical clustering was performed to find correlate genes.

In addition, the repair macrophages (Ly6C^{low}) exhibited minimal expression of the well-established M2 marker CD163 (**Figure 4E**). Other markers such as MRC1 and CD68 where highly expressed but remained unchanged between the different muscle macrophage subtypes (**Figure 4E**). The expression pattern of Ly6C, Ly6G and F4/80 genes reported the expected patterns in the sorted populations and therefore validated the sorting strategy (**Figures 4B-C**). These results show that Ly6C^{high} and Ly6C^{low} macrophages in regenerating muscle display distinct inflammatory profiles than those described in the literature *in vitro* or from the M1/M2 macrophage subtype classification and thus cannot be defined as canonical M1 or M2 macrophages. These findings support the notion that surface markers for macrophage subsets vary depending on the injury model and tissue they are extracted from.

Global gene expression profile of muscle macrophages

To extent the gene expression profiles of the muscle macrophages obtained through microarrays RNA-seq analysis was performed on the selected macrophage populations. Principal component analysis (PCA) analysis (**Figure 5A**) of muscle macrophages versus circulating monocytes and other tissue macrophages (Kuppfer cells, Bone Marrow Derived Macrophages) identified by the Immunological Genome Consortium revealed that muscle macrophages formed a well distinct group (**Figure 5C**), likely due to origin from a regenerating and not a steady-state tissue, as previously shown (Varga, Mounier et al. 2013). These results also showed that macrophage populations segregated by day, more than Ly6C status (Ly6C^{high} vs Ly6C^{low}). Moreover, the analysis showed the presence of 2 groups of macrophages: cells isolated during the first phases of muscle regeneration (day 1 and day 2) clustered together while those extracted at later time point (day 4) clustered together apart. This corresponds to the two main phases of inflammation in regenerating muscle that are the pro-inflammatory phase (day 1-2), followed by the resolving/regenerative phase (day 4). These results were confirmed using hierarchical clustering method on all samples showing high clustering of biological replicate samples belonging to each condition (**Figures 5A-C**).

To compare the gene expression changes between macrophage subsets at each time point, the expression values for each gene were normalized across all conditions. Next the normalized expression values were plotted in both the Ly6C^{high} and Ly6C^{low} subsets measured at each time points. **Figure 5D** shows a simplified scheme of the comparisons made, with the number of genes showing significant differences between any 2 analyzed conditions. First, for each time point, Ly6C^{high} macrophages were compared to corresponding Ly6C^{low} cells to reveal genetic events associated with the inflammatory status of macrophages (**Figure 5D**). Confirming the above analyses, the highest number of differentially expressed genes was observed at day 2 of regeneration. Second, each macrophage subset was compared to its closest neighboring time points to analyze variation of gene expression longitudinally along the regeneration process. The number of genes whose expression significantly changed was equally or slight higher than the changes seen in the Ly6C^{high} vs. Ly6C^{low} comparison. This observation confirmed the above clustering and PCA analyses (**Figures 5A-C**) and showed that while Ly6C^{high} macrophages were different from Ly6C^{low} cells, both populations underwent further transcriptomic changes during the time course of muscle regeneration (**Figure 5D**) (Varga, Mounier et al. 2016).

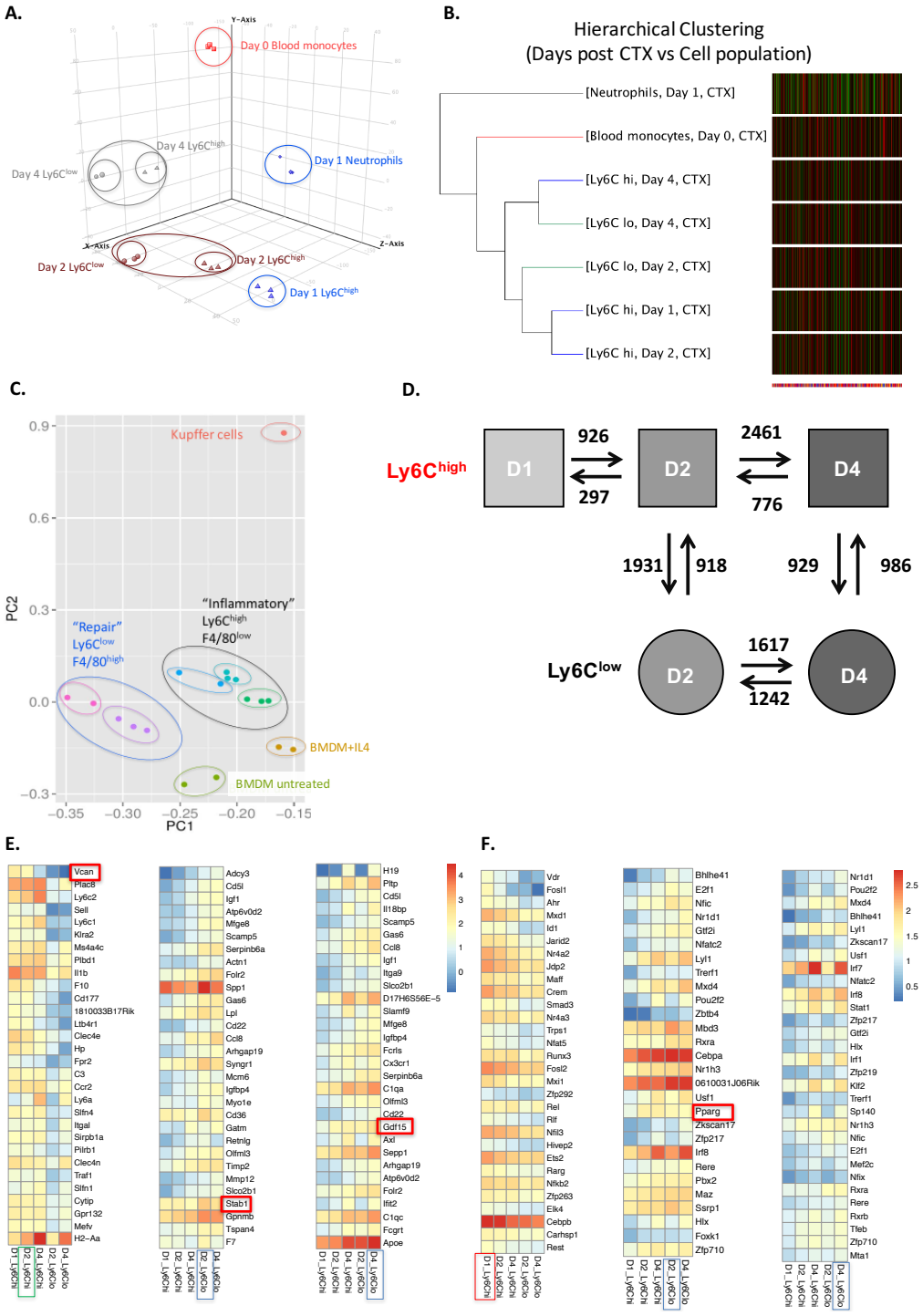

Figure 5. Global molecular signature of muscle macrophage subsets.

A. Relative distance between different subsets of muscle-derived macrophages was assessed using 3D principal component analysis.

B. Hierarchical clustering of muscle-derived macrophages based on all expressed genes.

C. PCA comparison of muscle-derived macrophage subsets with various tissue resident macrophages (biological replicates are shown).

D. Schematic of macrophage subset comparisons. Analysis of differential gene expression involved two-way ANOVA analysis followed by Tukey post-hoc tests to find genes whose expression showed significant differences between the MF subsets (p value < 0.05). Numbers represent upregulated and downregulated genes between the compared conditions. Arrows point toward inductions.

E. Heat map and gene lists showing the expression pattern of effector genes by regenerating Ly6C^{high} and Ly6C^{low} muscle-derived macrophages. Expression values are visualized as $-\log_{10}$(normalized expression).

F. Heat map and gene lists showing the expression pattern of transcription factors by regenerating Ly6C^{high} and Ly6C^{low} muscle-derived

In addition, a series of molecules secreted by macrophages that have been involved in myogenesis, such as IGFs, follow the expected expression pattern with increased expression as regeneration proceeds, and particularly in Ly6C^{low} macrophages (**Figure 5E**). Thus, gene expression data showed good overlap with anticipated expression patterns of known regulators and effectors of muscle regeneration (**Figures 5E-F**). This indicated that an unbiased analysis of the gene expression patterns using RNA-seq (with higher sensitivity than microarrays) might report yet unidentified molecular mechanisms that are relevant to the acute and resolution phases of the inflammation within the injured muscle.

Comparison of Ly6C^{high} and Ly6C^{low} macrophage subsets during muscle regeneration

Several strategies were tested to analyze the kinetics of gene expression by macrophage subsets during the time course of muscle regeneration. We found that the "vertical" comparison between Ly6C^{high} and Ly6C^{low} macrophage subsets at each time point provided the most robust results. Interestingly, the top genes that were upregulated at day 2 in the Ly6C^{high}F4/80^{low} vs Ly6C^{low}F4/80^{high} populations (**Figure 5D**), were associated with inflammation such as Il1b, Clec4e, Ccr2, Nfkb2, Cebpb (**Figures 5E-F left panel heatmaps**). This observation is in accordance with the role of Ly6C^{high} macrophages in the initiation of the inflammatory response following injury. To identify other inflammatory markers with a similarly strong predictive power for Ly6C^{high}F4/80^{low} cells, the "find similar entity" algorithm of the StrandNGS software was used to find genes that were regulated similarly as Ly6C on the first 2 days of muscle regeneration. At the top of the list, an extracellular matrix proteoglycan named versican was exclusively expressed in Ly6C^{high}F4/80^{low} macrophages, notably at the first stages of muscle regeneration (**Figure 5E left panel heatmap**). These results indicated that macrophages could be active contributors of ECM reorganization during the initial phase of muscle regeneration.

Similarly, many of the top-ranking genes that were upregulated at day 2 and day 4 in the Ly6C^{low}F4/80^{high} vs Ly6C^{high}F4/80^{low} populations (**Figure 5D**) were associated with mature macrophages and tissue repair, such as Igf1, Myo1e, CD36, Cx3cr1, Pparg, Stat1, Rxra, Cebpa (**Figures 5E-F center and right panel heatmaps**). Among these genes, the growth differentiation factor 15 was upregulated in Ly6C^{low}F4/80^{high} macrophages at the later stages of muscle regeneration at Day 2 and Day 4 respectively (**Figures 5E-F center and right panel heatmaps**).

Based on these unbiased findings, we hypothesized that Gdf15 could potentially influence the outcome of skeletal muscle regeneration either as regulators of macrophage function or as effectors acting on the muscle tissue itself. To test this hypothesis, we used the Gdf15 full body knock out mice (Gdf15 KO).

Macrophage GDF15 regulates skeletal muscle regeneration by activating myoblast proliferation

WT and Gdf15 KO animals were injected with CTX to induce TA muscle injury and then regeneration was analyzed by morphometric analysis. The Gdf15 KO animals showed a pronounced delay in their TA muscle regeneration at day 8 and 16 post CTX (**Figure 6A**). Firstly, the mean cross-sectional area (CSA) of the regenerating muscle fibers was significantly smaller compared to control WT mice at day 8 (**Figure 6C**), and 16 (**Figure 6D**) following injury. Second,

regenerative areas with increased inflammatory infiltrations persisted in Gdf15 KO muscles at day 8 (**Figure 6A**), suggesting that the resolution of inflammation was delayed. Since GDF15 is a growth factor we also checked for any pre-existing developmental musculature problems at day 0 (uninjured) (**Figures 6A and 3B**). No difference in the mean CSA was observed in the uninjured muscles of Gdf15 KO mice (**Figure 6B**). To ascertain whether GDF15 deficiency in the hematopoietic compartment was indeed the major contributor to the observed phenotype we used a second genetic model, in which bone marrow from the total body KO were used to reconstitute the hematopoietic compartment in irradiated WT animals. When compared with animals that received WT bone marrow, mice that received bone marrow deficient in GDF15 exhibited a profound impairment in regeneration (**Figures 6E and 6F**). Altogether, the results from the 2 distinct genetic models clearly indicated that that GDF15 critically contributes to muscle regeneration.

Next, we analyzed the GDF15 protein expression in whole muscle lysates of CTX injured WT mice, which provided a snapshot of GDF15 protein levels during the time course of regeneration. The protein expression closely followed the induction seen at the mRNA level in MFs and showed a pronounced induction, which peaked at day 4 (**Figure 6G left panel**), at the time when inflammation subsides and regenerative processes start to dominate within the injured muscle. It is important to note that the GDF15 protein induction during CTX injury was undetectable in muscle samples from Gdf15 KO animals (**Figure 6G right panel**). To characterize the GDF15 effector function, cultured primary myoblasts were treated with recombinant GDF15. Addition of rGDF15 to the culture medium increased myoblast proliferation (**Figures 6H and 6I**). These results suggested that GDF15, once released from MFs within the injured/regenerating tissues, could regulate molecular pathways relevant to the proliferation of satellite cells.

The dynamics and composition of immune infiltration in injured muscle in WT and Gdf15 KO animals was also examined. The numbers of $CD45^+$ cells isolated from injured muscle at day 1-4 was determined. More myeloid cells infiltrated the injured muscle in Gdf15 KO animals at day 2 and 4 post CTX (**Figure 6J**). This result is suggestive of delay regeneration dynamics. By following the differentiation dynamics of MFs from day 2 onward we detected significant differences in the subset composition of infiltrating MFs at day 2 and 4 after CTX injury (**Figures 6K-M**). Collectively, these results show that Gdf15 deficiency affects both myeloid cells infiltration and differentiation within the regenerating muscle.

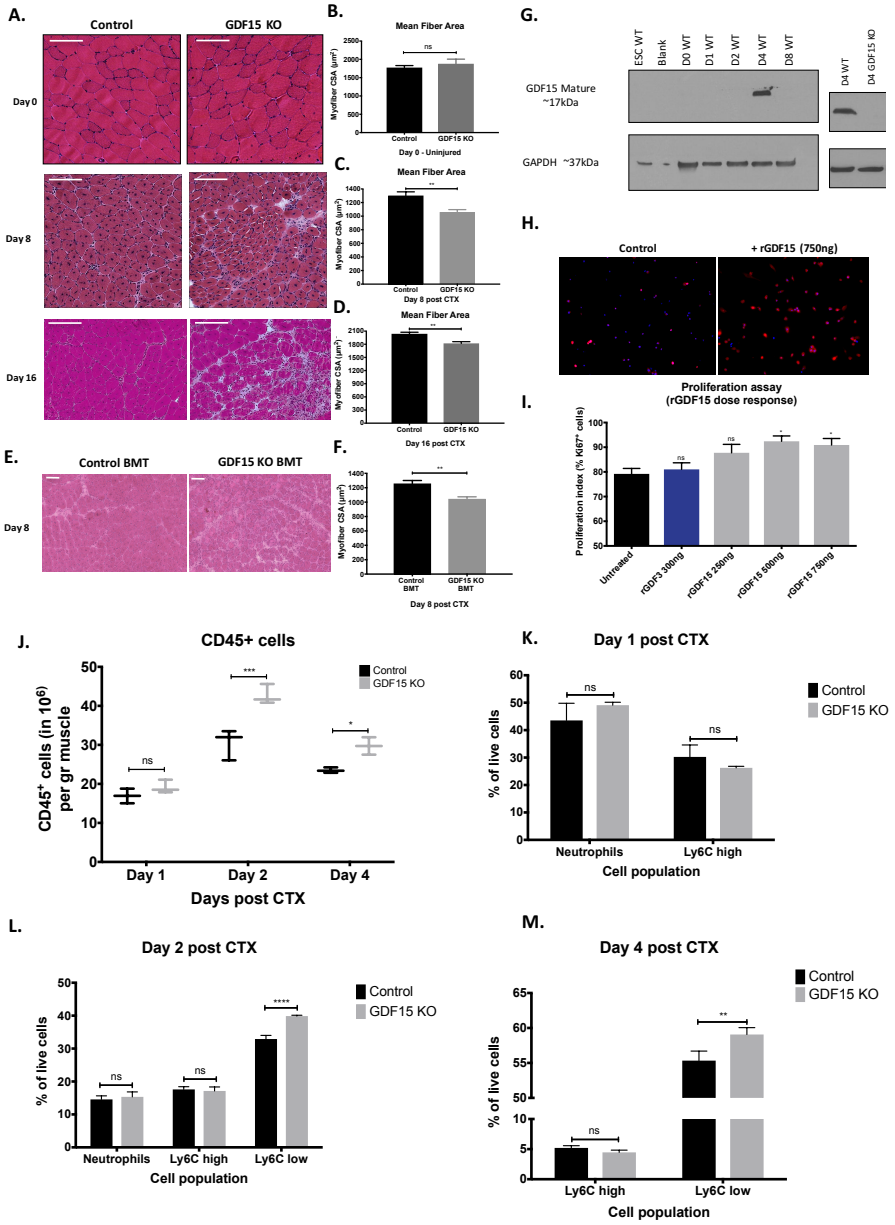

Figure 6. Impaired regeneration of skeletal muscle in Gdf15-deficient animals.

A. Representative images of H&E stained skeletal muscle from WT control and Gdf15 KO mice prior (day 0) or post CTX induced injury (day 8, and day 16) are shown. Scale bars in the lower left corner represent 200 µm.

B. C., D. Average fiber cross section area (CSA) of regenerating muscle at indicated timepoints post CTX injury in WT control and Gdf15 KO animals.

E. Representative images of H&E stained skeletal muscle from Control BMT and Gdf15 KO BMT mice at day 8 post CTX induced injury are shown. Scale bars in the lower left corner represent 100 µm.

F. Average fiber cross section area (CSA) of regenerating muscle at indicated timepoint post CTX injury in Control BMT and Gdf15 KO BMT animals.

G. GDF15 protein expression in whole-muscle lysates of regenerating muscles from WT mice at indicated timepoints (D, day). Right blot shows negative control for GDF15.

H. Immunofluorescence (IF) against Ki67 (red) and DAPI (blue) shows a drastic enhancement of proliferation in the presence of recombinant (r) GDF15 in the *in vitro* primary myoblast proliferation assay (n = 3).

I. *In vitro* proliferation assay on primary myoblasts in the presence of recombinant GDF15 (% of Ki67+ cells) (n = 4).

J. Number of infiltrating myeloid ($CD45^+$) cells in regenerating muscle from WT control and Gdf15 KO muscles at indicated timepoints post CTX injury (n = 8 muscles per group).

K. L., M. Percentage of inflammatory ($Ly6C^{high}$ $F4/80^{low}$) and repair ($Ly6C^{low}$ $F4/80^{high}$) MFs from WT control and Gdf15 KO muscles at indicated timepoints following CTX injury (n = 8 mice per group).

In all bar graphs, bars represent mean ± SEM.

Macrophage PPARg regulates skeletal muscle regeneration

Recent reports suggested cell metabolism as a defining factor in MFs identity and functional status (Lavin, Winter et al. 2014), (Odegaard and Chawla 2011), (Okabe and Medzhitov 2014), (Vats, Mukundan et al. 2006). When analyzing the RNA-seq expression data (**Figure 5**) for metabolic regulators that could account for such a preference for metabolic genes, we found that a master regulator of metabolism, Pparg, was expressed at a high level in the Ly6C^{low} repair subset (**Figure 5F**). Based on this finding, we hypothesized that MF PPARg is a metabolic sensor and regulator of skeletal muscle regeneration. To test this hypothesis, we used the Pparg$^{fl/fl}$ LysM-Cre mouse strain, which is deficient in PPARg specifically in myeloid lineages (herein referred to as PPARg MacKO) (Clausen, Burkhardt et al. 1999).

WT and PPARg MacKO animals were injected with CTX to induce TA muscle injury and then regeneration was analyzed by a combination of morphometric and FACS analysis. We found that PPARg MacKO animals showed a pronounced delay in their TA muscle regeneration (**Figure 7A**). CSA of the regenerating muscle fibers was significantly smaller in the PPARg MacKO than in WT mice at day 8 and day 21 following CTX injury (**Figure 7E**). The distribution of CSA in the PPARg MacKO animals was shifted to the left both at day 8 (**Figures 7C**) and day 21 (**Figures 7D**) post CTX. In addition, a significantly higher number of necrotic/phagocytic fibers were present at day 8 post CTX in PPARg MacKO mice (**Figures 7A-B**), indicating either a delayed clearance of dying myofibers or an altered dynamics of muscle fiber death in KO animals. As PPARg is expressed in muscle at a low but detectable level, we wanted to ascertain whether PPARg deficiency in the hematopoietic compartment was indeed the major contributor to the observed phenotype. To prove this, we used a second genetic model, in which bone marrow from the total epiblastic conditional KO of PPARg (Pparg$^{fl/-}$ Sox2Cre) (Nadra et al., 2010) was used to reconstitute the hematopoietic compartment in irradiated WT animals (bone marrow transplanted or BMT animals). TA muscles of recipient BMT animals were injected with CTX 12 weeks after BMT and histological analysis of muscle regeneration was carried out 22 days post injury. When compared with animals that received WT bone marrow (WT BMT), mice that received bone marrow deficient in PPARg (PPARg KO BMT) exhibited a profound deficit in regeneration (**Figures 7F-G**). Altogether, the results from these two distinct genetic models clearly indicated that PPARg activity in muscle infiltrative MFs critically contributed to the timely resolution of inflammation and to regeneration.

PPARg regulates cell type specific genes in muscle infiltrating MFs

As only few paracrine signaling pathways between MFs and tissue progenitors have been described, we decided to pursue the identification of the putative regulatory circuit that might connect muscle infiltrating MFs to myotube differentiation in a PPARg dependent manner. As PPARg is a transcription factor, we presumed that a relevant change in the gene expression in muscle MFs must shed light on the regulatory circuit that is abrogated in PPARg KO MFs. To identify PPARg dependent gene expression changes in muscle infiltrating MFs, we isolated representative populations of MFs from regenerating muscle (Day 1, 2 and 4 post CTX) from WT and PPARg MacKO animals and analyzed their gene expression profiles by microarrays (**Figure 8A**). The central objective of our analyses was to identify the cell type in which PPARg was active

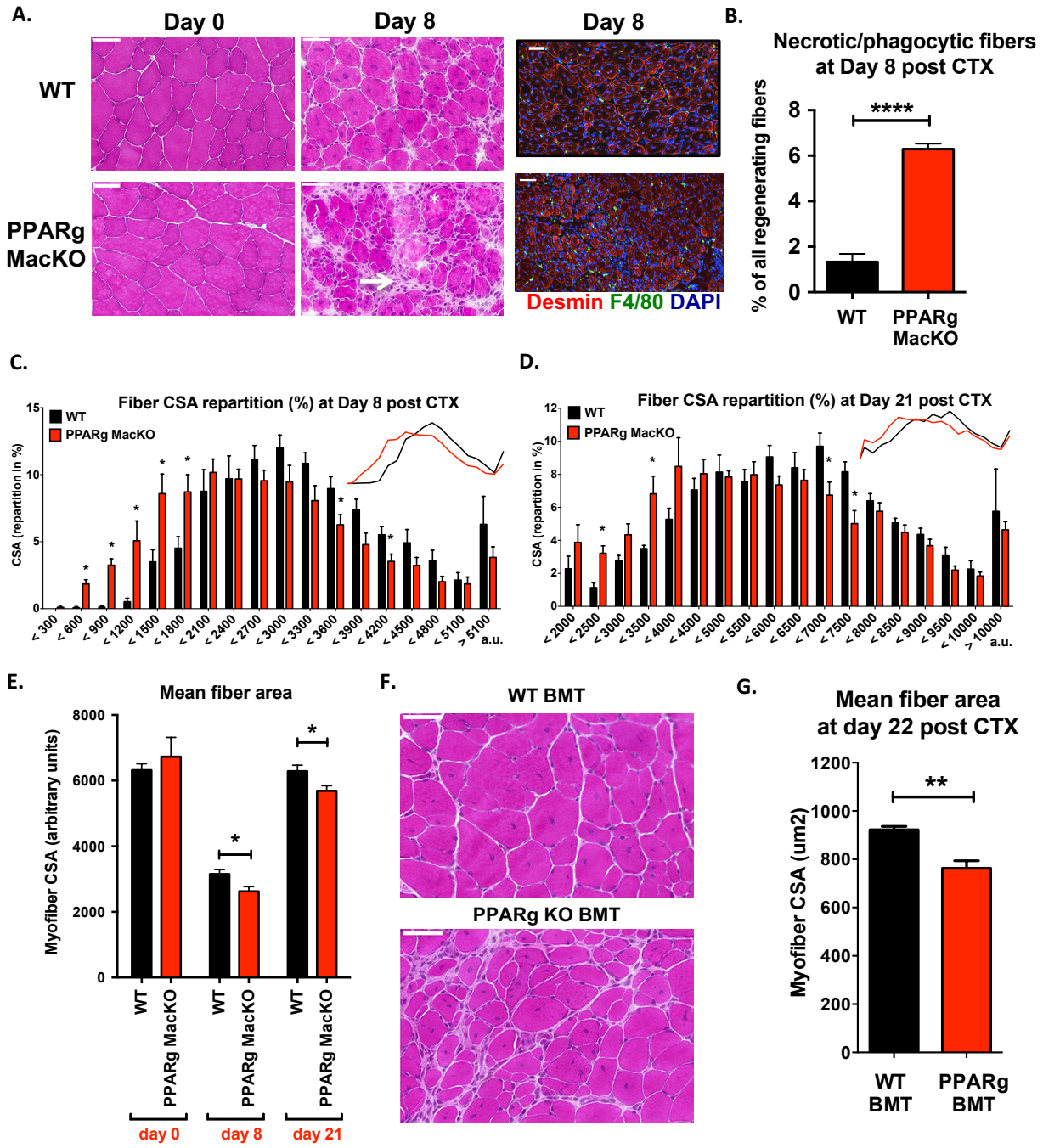

Figure 7. Impaired regeneration of skeletal muscle in PPARg-deficient animals.

A. Representative images of H&E stained skeletal muscle from WT and Pparg$^{fl/fl}$ LysM-Cre mice prior (day 0) or post CTX induced injury (day 8) are shown. Asterisk labels phagocytic and/or necrotic fibers and arrow points to foci of inflammatory infiltrations. IHC detection of desmin (red), F4/80 (green), and nuclei (blue) at day 8 post CTX injury is also shown. Scale bars in the upper left represent 50 µm.

B. The ratio of phagocytic and/or necrotic fibers relative to all regenerative fibers at day 8 of regeneration in WT and Pparg$^{fl/fl}$ LysM-Cre muscle sections is shown.

C. D. Fiber size repartition of regenerating muscle in WT or Pparg$^{fl/fl}$ LysM-Cre animals at day 8 and day 21 post CTX injury, respectively.

E. Mean fiber cross section area (CSA) of regenerating muscle at indicated timepoints post CTX injury in WT and Pparg$^{fl/fl}$ LysM-Cre animals.

F. Representative images of H&E stained skeletal muscle 22 days after CTX injury from bone marrow transplanted (BMT) animals that received either WT or Pparg$^{fl/fl}$ Sox2-Cre bone marrow.

G. Muscle fiber CSA of WT or Pparg$^{fl/fl}$ Sox2-Cre BMT animals 22 days post CTX injury (n = 8 muscles for both genotypes).

In all bar graphs, mean values ± SEM are shown.

and the genes that were regulated by PPARg. We created heat maps for all 4 examined macrophage subsets (**Figure 8A**). These heatmaps show all genes that were differentially expressed in one relevant subset and also show the expression pattern of these genes in all the other MF subsets. Next, we analyzed the gene sets that were downregulated in PPARg MacKO MFs. The top 5 genes that were most differentially downregulated in PPARg MacKO cells are shown in **Figure 8B**. Strikingly, there was 1 gene, namely Growth differentiation factor 3 (Gdf3), that was consistently downregulated in all 4 investigated MF populations (**Figures 8A-B**). Thus, we identified several putative PPARg target genes that showed consistent PPARg dependency in more than one muscle MF subsets. Interestingly, the genes we identified as PPARg dependent in muscle MFs did not belong to the group of canonical PPARg regulated genes described in various myeloid cells in earlier studies (such as Plin2 (Adrp), Cd36, Angptl4 or Fabp4) (Szanto, Balint et al. 2010), (Welch, Ricote et al. 2003). One possible reason for this discrepancy could be that most *in vitro* studies apply synthetic or natural ligands of PPARg to study the transcriptional activity of the receptor upon ligand activation.

Macrophage secreted GDF3 regulates myoblast differentiation and muscle regeneration

To focus on putative PPARg regulated genes whose activity could promote muscle regeneration, we pursued a biased screening approach where we interrogated the list of differently expressed genes based on a set of criteria designed to maximize our chance to find such factors. We were looking for genes that (1) were PPARg dependent in more than one MF subset, (2) coded a secreted factor and (3) whose activity might be linked to muscle differentiation based on existing data. Strikingly, one gene, Gdf3 (Levine and Brivanlou 2006), (Levine, Levine et al. 2009), (Shen, Huang et al. 2009), fit all these criteria. Gdf3 was statistically significantly downregulated in PPARg MacKO MFs in all four investigated MF subsets. In fact, Gdf3 was the top ranked gene (ranked by fold change difference) in 3 out of 4 MF subsets (**Figure 8B**). Second, GDF3 belongs to the TGFβ family, whose members are secreted factors acting in a paracrine manner. Finally, several members of the TGFβ family are known regulators of muscle regeneration, including GDF8 (also known as Myostatin) (Massague, Cheifetz et al. 1986), (McPherron, Lawler et al. 1997). Therefore, we selected Gdf3 as the most likely PPARg dependent gene that contributes to muscle regeneration for further analysis. Next, we analyzed the GDF3 protein expression in whole muscle lysates of CTX injured WT mice, which provided a snapshot of GDF3 protein levels during the time course of regeneration. The protein expression closely followed the induction seen at the mRNA level in MFs and showed a pronounced induction, which peaked at day 4 (**Figure 8C**), at the time when inflammation subsides and regenerative processes start to dominate within the injured muscle.

According to our model, the regeneration delay in MF PPARg deficient animals was, at least partly, attributable to a diminished MF derived GDF3 secretion within regenerating muscles. This model posits that GDF3 deficiency in MFs should yield impairment in regeneration comparable to PPARg MacKOs. Indeed, muscle regeneration after CTX injury was altered in full body Gdf3 KO animals at day 8 as shown by the mean fiber size (**Figure 8E**) and distribution of CSA (**Figure 8D**). It was reported that the full body deletion of Gdf3 showed incomplete penetrance as it resulted in early embryonic lethality in approximately 35% of Gfd3 KO embryos (Shen, Huang et al. 2009), which suggested possible compensatory mechanisms that rescued the

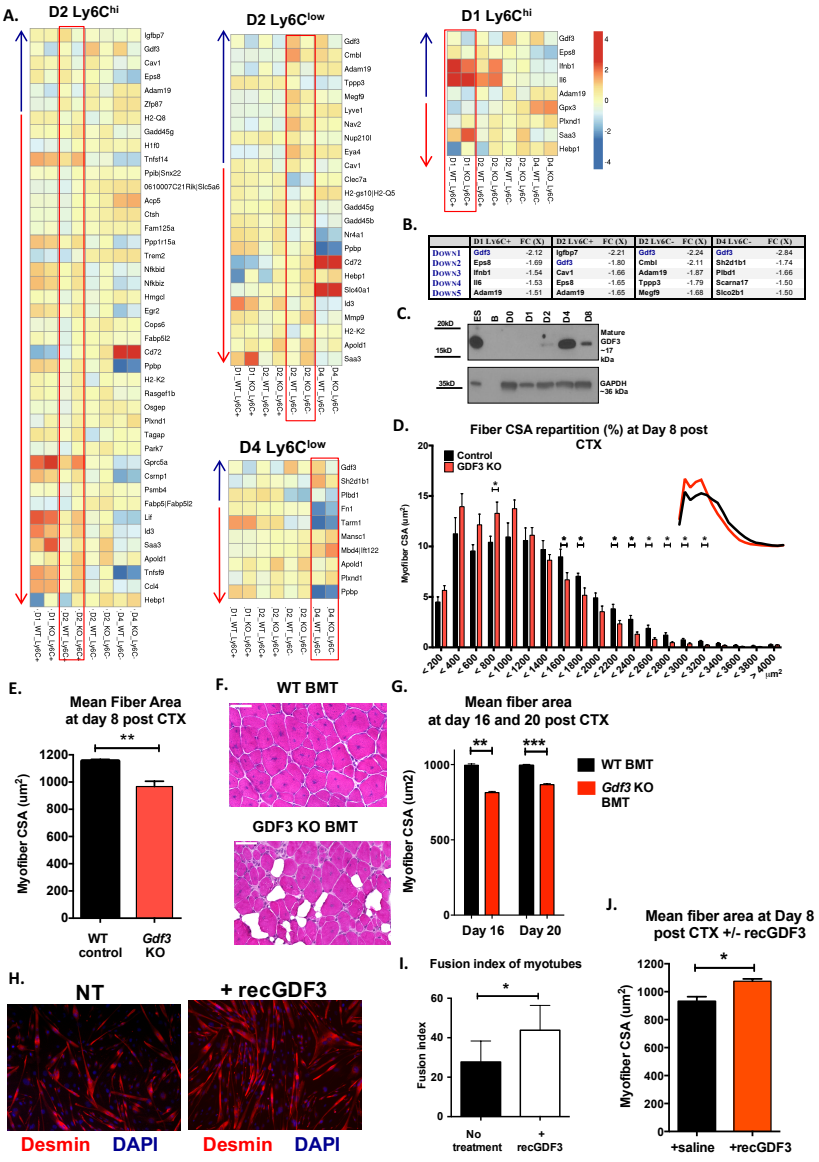

Figure 8. PPARg regulates macrophage GDF3 and GDF3 deficiency impairs muscle regeneration.

A. Transcriptional analysis of the Ly6C^{high} and Ly6C^{low} macrophage populations derived from WT and Pparg$^{fl/fl}$ LysM-Cre animals. Heatmap representation of genes that show the highest differential ($p < 0.05$, FC >= 1.5) expression in the four sorted WT vs. Pparg$^{fl/fl}$ LysM-Cre macrophages at day 1 Ly6C^{high}, day 2 Ly6C^{high} and day 2 Ly6C^{low}, and day 4 Ly6C^{low} cells (labeled as D1 Ly6C+ etc). In each heatmap, the differentially expressed genes are highlighted within a red square and the expression pattern of these genes in the other macrophage subtypes is also shown for reference. Blue and red arrows label genes that are downregulated or upregulated in WT vs. Pparg$^{fl/fl}$ LysM-Cre cells, respectively. The blue and red arrows point to the direction of increasing fold change difference.

B. Top 5 downregulated genes in the four sorted macrophage populations in Pparg$^{fl/fl}$ LysM-Cre macrophages. Table lists gene symbols and fold change differences (FC). Gdf3 that are downregulated in Pparg$^{fl/fl}$ LysM-Cre in all four subtypes, is highlighted in blue color.

C. GDF3 protein expression in whole-muscle lysates of regenerating muscles from WT mice at different timepoints (D, day).

D. Myofiber CSA repartition in CTX injured WT or Gdf3 KO muscles at day 8 (n = 7).

E. Mean Myofiber CSA in CTX injured WT or Gdf3 KO muscles at day 8 (n = 7).

F. Representative H&E-stained muscle sections of WT BMT and Gdf3 KO BMT animals, 16 days post CTX injury (n = 4). Scale bars represent 50 µm.

G. Myofiber CSA measurement in WT BMT and Gdf3 KO BMT animals, 16 and 20 days post CTX injury.

H. IF against Desmin (red) and DAPI (blue) shows a drastic enhancement of myotube formation in the presence of recombinant (r) GDF3 in the *in vitro* primary myoblast myogenesis assay (n = 3).

I. *In vitro* differentiation assay on primary myoblasts in the presence of recombinant GDF3 (n = 4).

J. Improvement in regeneration by administration of either saline or recombinant GDF3 in Pparg$^{fl/fl}$ LysM-Cre animals. CSA measurements are shown.

In all bar graphs, bars represent mean ± SEM.

potentially lethal phenotype. To limit the involvement of such compensatory mechanisms and to ascertain the hematopoietic source of GDF3 during muscle regeneration, we decided to generate BMT animals reconstituted with Gfd3 KO bone marrow. When the GDF3 chimeric animals were challenged with CTX induced muscle injury, they exhibited an impairment in regeneration at day 16 and 20 (**Figures 8F-G**). When compared with WT BMT animals, GDF3 KO chimeras contained more regenerating myofibers with smaller CSA and the regenerating muscle was replete with lipid accumulations, which are hallmarks of defective muscle regeneration (**Figure 8F**). To further prove the requirement for GDF3 in muscle regeneration, we injected 300 ng of recombinant GDF3 into CTX injured muscles of PPARg MacKO mice at day 4 post CTX. We found that the exogenously added GDF3 rescued the regeneration deficit seen in these animals (**Figure 8J**). The above observations underlined the importance of MF derived GDF3 in skeletal muscle regeneration and validated our model regarding the existence of a PPARg-GDF3 axis responsible for the regulation of tissue regeneration. Therefore, GDF3 appears to be an effector in regeneration. To characterize this effector function, primary myoblasts were treated with recombinant GDF3. Addition of GDF3 to the culture medium induced a robust effect of GDF3 on myotube formation (**Figure 8H**). Myoblast cultures showed a pronounced increase in their fusion index in the presence of GDF3 (**Figures 8I**). These results suggested that GDF3, once released from MFs within the injured/regenerating tissues, could regulate molecular pathways relevant to the fusion of differentiating muscle cells.

GDF3 restores muscle regeneration in aged mice

The PPARg-GDF3 regulatory axis described in our studies identifies a sensory-regulatory-effector mechanism, by which MFs are regulators of the tissue progenitor compartment. This axis orchestrates tissue regeneration, possibly in unison with other members of the TGFβ family, leading to synchronous regeneration. This let us to hypothesize that GDF3 expression might be impaired in geriatric mice (23-28 month-old) and by infusing rGDF3 intramuscularly, we can potentially restore the muscle ability to regenerate, through proper activation of satellite cells.

Initially, we wanted to validate that aged mice have an impairment in muscle regeneration following CTX injury. Indeed, muscle regeneration after CTX injury was altered in geriatric animals at day 8 and day 12 (**Figure 9A**) as shown by the distribution of CSA (**Figure 9C-D**) and the increase in necrotic fiber content at day 8 post CTX (**Figure 9E**). Surprisingly, we observed that old mice (23-month old) have larger fibers in the uninjured state (**Figure 9A upper panel**), a skew to the right on the size distribution of myofiber CSA (**Figure 9B**) and no histological signs of atrophy when compared to younger (2-month old) mice. However, this “hypertrophy” might be an adaptation to the loss of muscle function which is obvious in older mice and has been described previously (Amthor, Macharia et al. 2007).

Next, we hypothesize that immunosenescence, in addition to the age-related changes of resident muscle cells function, could disrupt the cross-talk between immune and muscle cells, likely contributing to age-related impairment in muscle regeneration. Indeed, altered myeloid cell number infiltration (**Figure 9F**) and phenotypic switching from $Ly6C^{high}$ to $Ly6C^{low}$ macrophages is impaired (**Figure 9G-J**) in aged mice. In addition, decreased protein expression of GDF3 can be observed at day 4 post CTX in the aged mice compared to young controls validating our initial hypothesis (**Figure 9K**). Next, we wanted to check whether introducing recombinant

GDF3 back into the animals will restore regeneration. Indeed, a single intramuscular dose of 300 ng rGDF3 at day 4 post CTX restores the morphological features of the muscle by day 8 (**Figures 9L-M**). Importantly treating young mice with rGDF3 had no obvious enhancing effect (myofiber size increase or faster regeneration) (**Figure 9M**), suggesting that the physiological endogenous levels of GDF3 are sufficient for proper regeneration and an impairment needs to precede in order for the rGDF3 treatment to have an effect. Taken together, these results highlight that GDF3 is able to modulate muscle-resident cells, and possibly immune and muscle cell cross-talk during muscle repair in a geriatric model of impaired regeneration.

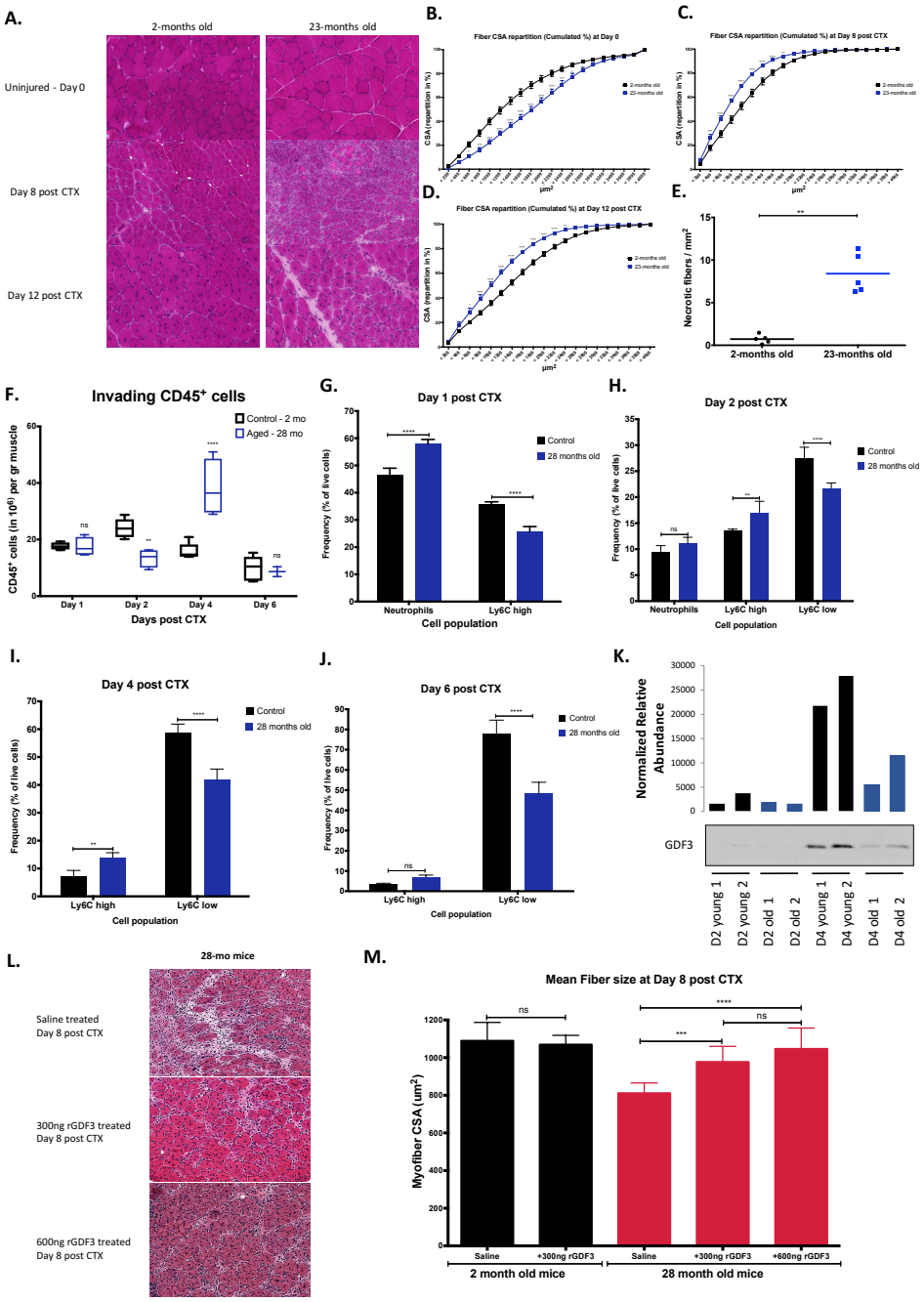

Figure 9. Effects of recombinant GDF3 on aged muscle.

A. Representative images of H&E stained skeletal muscle from young adult (2-month old) and geriatric (23-month old) mice prior (day 0) or post CTX induced injury (day 8 and 12) are shown. Scale bars in the upper left represent 100µm.

B. C., D. Fiber size repartition of regenerating muscle in young or geriatric animals at indicated timepoints post CTX injury.

E. The ratio of necrotic fibers relative to regeneration area at day 8 of regeneration in young adult and geriatric muscle sections is shown.

F. Number of infiltrating myeloid (CD45+) cells in regenerating muscle from young or geriatric muscles at indicated timepoints post CTX injury (n = 8 muscles per group).

G. H., I., J. Percentage of inflammatory (Ly6C^{high} F4/80^{low}) and repair (Ly6C^{low} F4/80^{high}) MFs from young or geriatric muscles at indicated timepoints following CTX injury (n = 8 mice per group).

K. GDF3 protein expression in whole-muscle lysates of regenerating muscles from young or geriatric at different timepoints (D, day). Two biological replicates are shown for each condition with normalized values to total protein of each sample.

L. M. Improvement in regeneration by administration of recombinant GDF3 in young (2-month old) or geriatric (28-month old) animals. (L) H&E stained images and (M) CSA measurements are shown.

In all bar graphs, bars represent mean ± SEM.

<u>Part 2.</u> Chromatin determinants of macrophage phenotypic transition during skeletal muscle regeneration

During the next phase of our studies we were interested in what kind of epigenomic changes are taking place during macrophage subtype specification following acute sterile injury by CTX. We hypothesized that by using an unbiased genomic approach called "assay for transposase accessible chromatin" (ATAC-seq), we could study the chromatin structure and accessibility during the transition of inflammatory macrophages to repair type ones, and thus identify novel regulators of this process. ATAC-seq experiments revealed a dynamic and dramatically reorganized chromatin structure, affecting both inflammatory and repair related marker gene loci (Arg1, Il1b, Klf4, Cd68, Slc40a1, Il1r2, Tgfbr1, Cd80, Nfkb1, Mcl1, Il10, Igf1, Ptges) (**Figure 10A**). Global genomic analysis of ATAC-seq data helped to pinpoint the dynamic changes at each time point and for each population, allowing the identification of opening and closing genomic loci. We discriminated 2 clusters (namely Class I and Class II) based on their opening/closing patterns during time (**Figure 10B**). Remarkably, 9191 sites became accessible (Class II) at day 1 after injury; compared to circulating monocytes (sorting strategy shown on **Figure 11A**); while 18404 became less accessible (Class I). Surprisingly, by day 4 post CTX most of the detected sites had reversed their accessibility having now either less accessible (Class II) or more accessible (Class I) sites (**Figure 10B**). GO analysis on the 2 clusters validated that the gene loci taking part in this dynamic chromatin changes belong to terms such as "regulation of cytokine production", "cell adhesion", "myeloid cell differentiation", "wound healing", "immune response activation" which are all functionally related to the response following CTX injury (**Figures 10C, 11C-G**). Therefore, it appears that the transcriptional changes (**Figure 11B**) were accompanied and probably underpinned by major changes in the chromatin structure (**Figures 10A-B**). Altogether, these results show that macrophages extremely remodel their open chromatin profile upon CTX injury and following resolution of inflammation, leading to timely chromatin opening at different stages of the regeneration process.

MARE binding TFs remodel the muscle related macrophage genome

In light of these data, a more thorough and detailed evaluation of immune cells is warranted. Applying our bioinformatics pipeline, (Daniel, Balint et al. 2014), (Nagy, Daniel et al. 2013) we could detect and identify sequence motifs associated with the unique chromatin regions changing during the phenotypic transition. The potential finding will inform us about the binding sites of potential transcriptional regulators. Using *de novo* motif analysis, TF motifs that are significantly enriched under the changing sites in the two clusters were identified (**Figures 10D-E**). Surprisingly, regions that close showed more enrichment for PU.1 motifs while on the other hand we found that the TRE (12-O-Tetradecanoylphorbol-13-acetate (TPA)- response element) and MARE (Maf recognition element) motifs were enriched at the sites opening at day 1 (**Figure 10E**). MARE binding TFs have never been described or implicated in such dynamic chromatin changes. Evaluation of RNA-seq and microarray data from the *in vivo* isolated macrophages following CTX injury revealed that only 4 members of the MARE binding TF family are expressed, including BACH1, NFE2L2, MAF, and MAFB but only 2 are differentially expressed

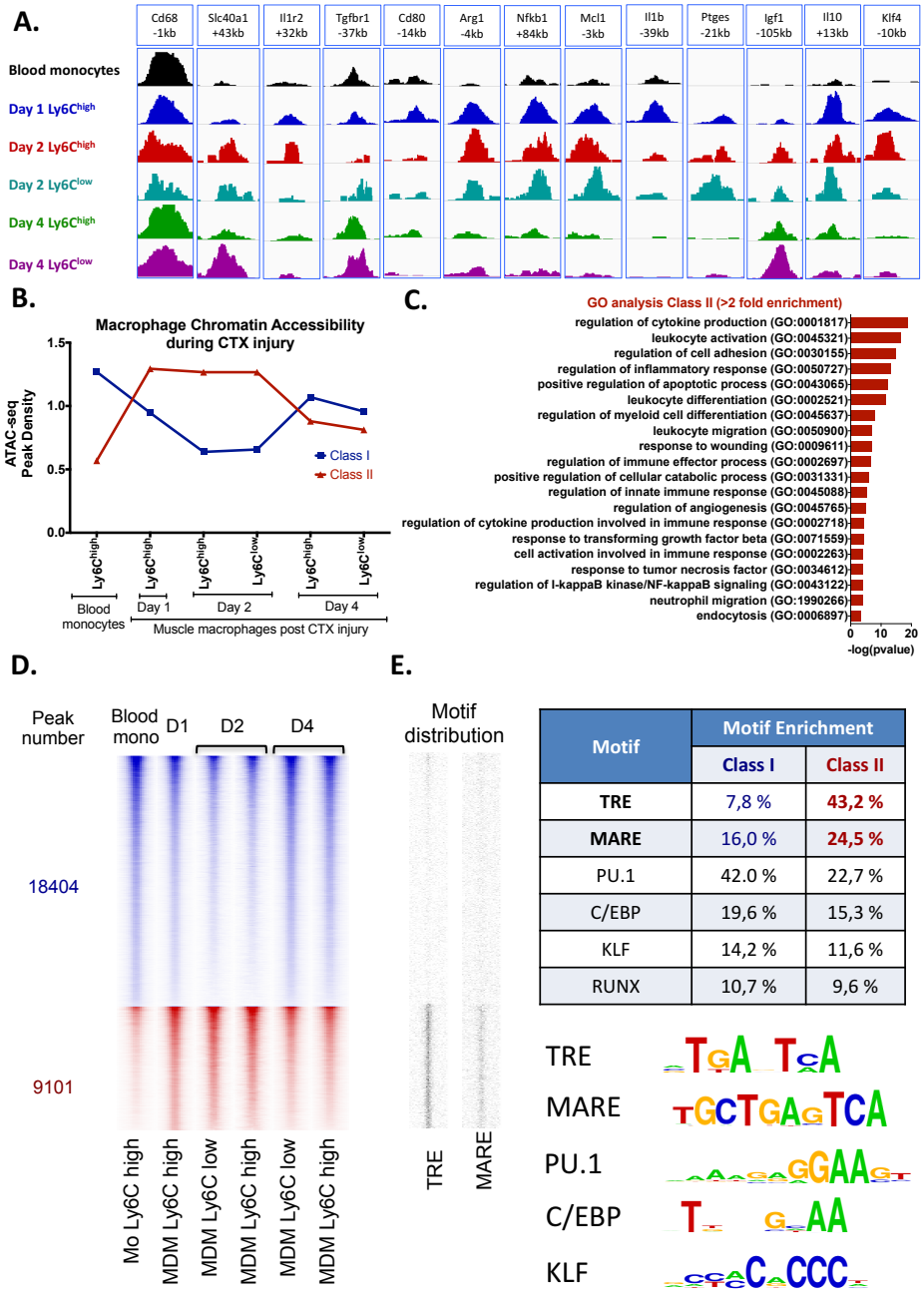

Motif	Motif Enrichment	
	Class I	Class II
TRE	7,8 %	43,2 %
MARE	16,0 %	24,5 %
PU.1	42.0 %	22,7 %
C/EBP	19,6 %	15,3 %
KLF	14,2 %	11,6 %
RUNX	10,7 %	9,6 %

Figure 10. Clustering and motif analysis of accessible chromatin sites in blood and muscle infiltrating muscle monocytes.

A. IGV genome browser view of promoter distal regions of known inflammatory and regeneration related genes according to ATAC-seq data derived from blood monocytes and Ly6C^{high} and Ly6C^{low} muscle-derived macrophages recovered and sorted from regenerating muscle upon CTX injury.

B. Chromatin openness clustering around promoter-distal regions following opposite patterns according to the ATAC-seq data. Clustered genomic regions depicted in red (Class II) become *de novo* accessible upon muscle infiltration. Blue color corresponds to Class I cluster of closing regions.

C. GO analysis of the genes associated with distal ATAC-seq signals following the Class II cluster during the full course of regeneration from blood monocytes to day 4 macrophages.

D. RD plot represents 750 nucleotides around the top summits of ATAC-seq enrichments for each sample. Blue and red colors represent opposite chromatin dynamics (Mo: monocytes, MDM: muscle-derived macrophages).

E. Motif distribution heat map shows the enrichment of the indicated motifs identified in the same regions as shown on the RD plot. Table shows the motifs frequency near the summits for both Classes of dynamics and below the motif matrices sequence logo.

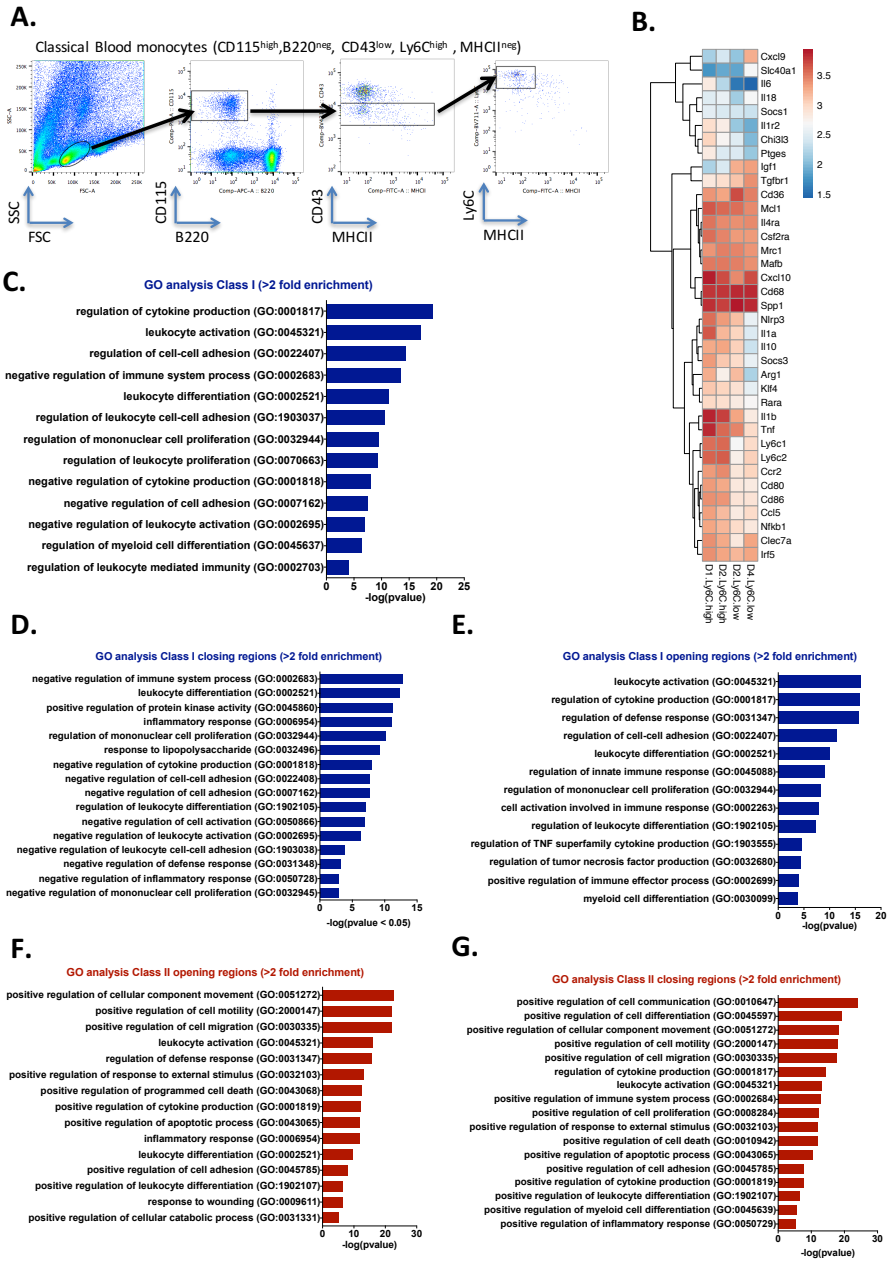

Figure 11. GO analysis of clusters of genes associated with ATAC-seq signal in muscle-derived macrophages.

A. FACS gating strategy to sort circulating monocytes. Leukocytes were gated on a FSC/SSC pattern consistent with monocytic cells, and then markers for CD115, B220, CD43, MHCII and Ly6C were used to isolate classical blood monocytes.

B. Heat map showing the expression pattern of inflammation and regeneration related genes by regenerating Ly6C^{high} and Ly6C^{low} muscle-derived macrophages. Expression values are visualized as –log10(normalized expression).

C. GO analysis of the genes associated with distal ATAC-seq signals following the Class I cluster during the full course of regeneration from blood monocytes to day 4 macrophages.

D. GO analysis of the genes associated with distal ATAC-seq signals downregulated in Class I cluster during the transition from blood monocytes to day 2 macrophages.

E. GO analysis of the genes associated with distal ATAC-seq signals upregulated in Class I cluster during the transition from day 2 to day 4 macrophages.

F. GO analysis of the genes associated with distal ATAC-seq signals upregulated in Class II cluster during the transition from blood monocytes to day 2 macrophages.

G. GO analysis of the genes associated with distal ATAC-seq signals downregulated in Class II cluster during the transition from day 2 to day 4 macrophages.

(BACH1 and NFE2L2), in inflammatory Ly6C^{high} vs repair Ly6C^{low} macrophages, suggesting that these two TFs are activated in macrophages as part of the injury response (**Figure 12A**).

In summary, our unbiased approach using ATAC-seq identified the presumed TFs who might be relevant in macrophage phenotypic transition, and showed the dynamic nature of the regeneration process with regards to changes at the chromatin level.

Hmox1 is a direct target gene of Bach1, driven by a damage response specific enhancer cluster

Transcription factors can be categorized on the basis of their effect on gene expression. Transcriptional activators like NFE2L2 (Nuclear Factor, Erythroid 2 Like 2) promote gene expression and have signal-dependent activity. Transcriptional repressors like BACH1 (BTB Domain And CNC Homolog 1) inhibit gene expression driven by transcriptional activators and therefore function to oppose or shape their functional outcome (**Figure 12B**). Therefore, to understand the function of transcriptional activators, it is essential to consider the transcriptional repressors that they antagonize. Moreover, as the process of cellular differentiation requires both activation of lineage-specific gene expression programs and suppression of alternative lineage gene expression programs, it is important to consider the functions of transcriptional repressors in the context of the alternative lineage programs that they antagonize.

As an example of data integration, the MARE binding transcriptional repressor BACH1 is highly expressed and overrepresented in Ly6C^{high} inflammatory macrophages (**Figure 12A**) while its binding motif is unexpectedly enriched specifically in the open chromatin regions forming the class II cluster (**Figure 10E**). BACH1 is a basic leucine zipper (bZIP) protein that is released from the chromatin in response to cell injury and inflammation, and as an end result a significant increase in the expression of antioxidant proteins, such as heme oxygenase 1 (HMOX1), that protect against oxidative damage (Ogawa, Sun et al. 2001), (Sun, Hoshino et al. 2002) can be observed. Importantly, BACH1 has an interesting feature in that itself is regulated by an acute damage response ligand (heme) which directly binds to BACH1 and removes its suppressive activity (**Figure 12B**). Gene expression measurements in heme treated bone marrow derived macrophages verified the BACH1 signal dependent activity and that Hmox1, an enzyme crucial for toxic heme clearance, is a direct BACH1 target gene (**Figure 12C**). Further analysis of the Hmox1 locus using ATAC-seq data visualization (**Figure 12D**) and BACH1 chromatin immunoprecipitation (ChIP) identified the regulatory elements (**Figure 12E**), showing extensively transcribed enhancer regions (**Figure 12F**), forming an enhancer cluster (**Figure 12D**) spanning 12 kb upstream of Hmox1 transcription start site (TSS). Among the 5 enhancers (Eα-Eε) identified, only 2 (Eα and Eδ) where previously described in the literature (Sun, Hoshino et al. 2002). Based on silico motif analysis score, those two enhancers (Eα and Eδ) are indeed the ones with the strongest MARE binding motifs (**Figure 12D lower panel**) but their enhancer RNA transcriptional activity is not as robust compared to the rest, and especially in the case of Eδ (**Figure 12E**). Last but not least re-analyzing publicly available datasets from various models of muscle injury such glycerol-induced, contraction-induced and freeze-induced, we observed Bach1 and Hmox1 gene expression induction in all the models at various time-points compared to uninjured controls (**Supplementary Figures 1A-B**) suggesting the involvement of these genes in acute type of injuries.

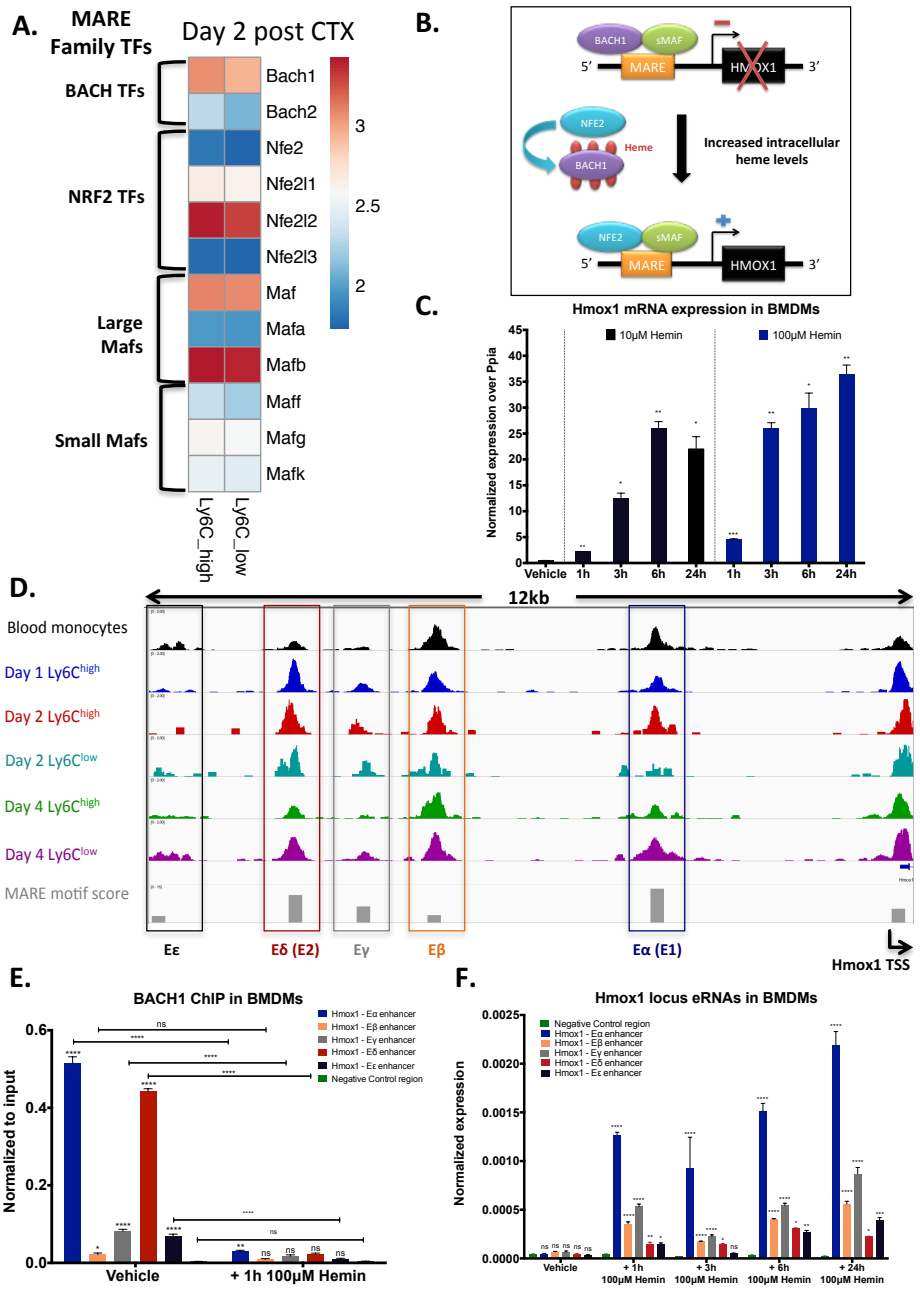

Figure 12. BACH1 genomic binding sites are overrepresented in the open chromatin of inflammatory macrophages

A. Heat map showing the expression pattern of MARE binding TFs in regenerating Ly6C^{high} and Ly6C^{low} muscle-derived macrophages. Expression values are visualized as $-\log_{10}$(normalized expression).

B. Model describing the regulation of Hmox1 or other target genes by Bach1 and heme. Maf-related factors may serve as partners for Bach1. Bach1 occupies MARE enhancers to repress transcription of Hmox1 gene under normal conditions. An increase in heme levels alleviates Bach1-mediated repression through inhibition of its DNA-binding activity and subsequent nuclear export, making MAREs available for activating Maf complexes including Nrf2.

C. Hmox1 mRNA expression in WT BMDMs treated with various doses of hemin for the indicated timepoints.

D. Identification of possible enhancers around the Hmox1 locus using ATAC-seq data. Putative enhancers are labeled by boxes and in the lower panel the motif score prediction for MARE binding for each enhancer.

E. BACH1-ChIP on the putative enhancer regions in BMDMs reveal Bach1 binding in all marked enhancers around the Hmox1 locus with Eα and Eδ being the strongest ones. Heme treatment for 1 h alleviates Bach1 binding validating our results.

F. Hmox1 enhancer RNA measurements in BMDMs upon heme treatment at various timepoints.

In all bar graphs, bars represent mean ± SEM.

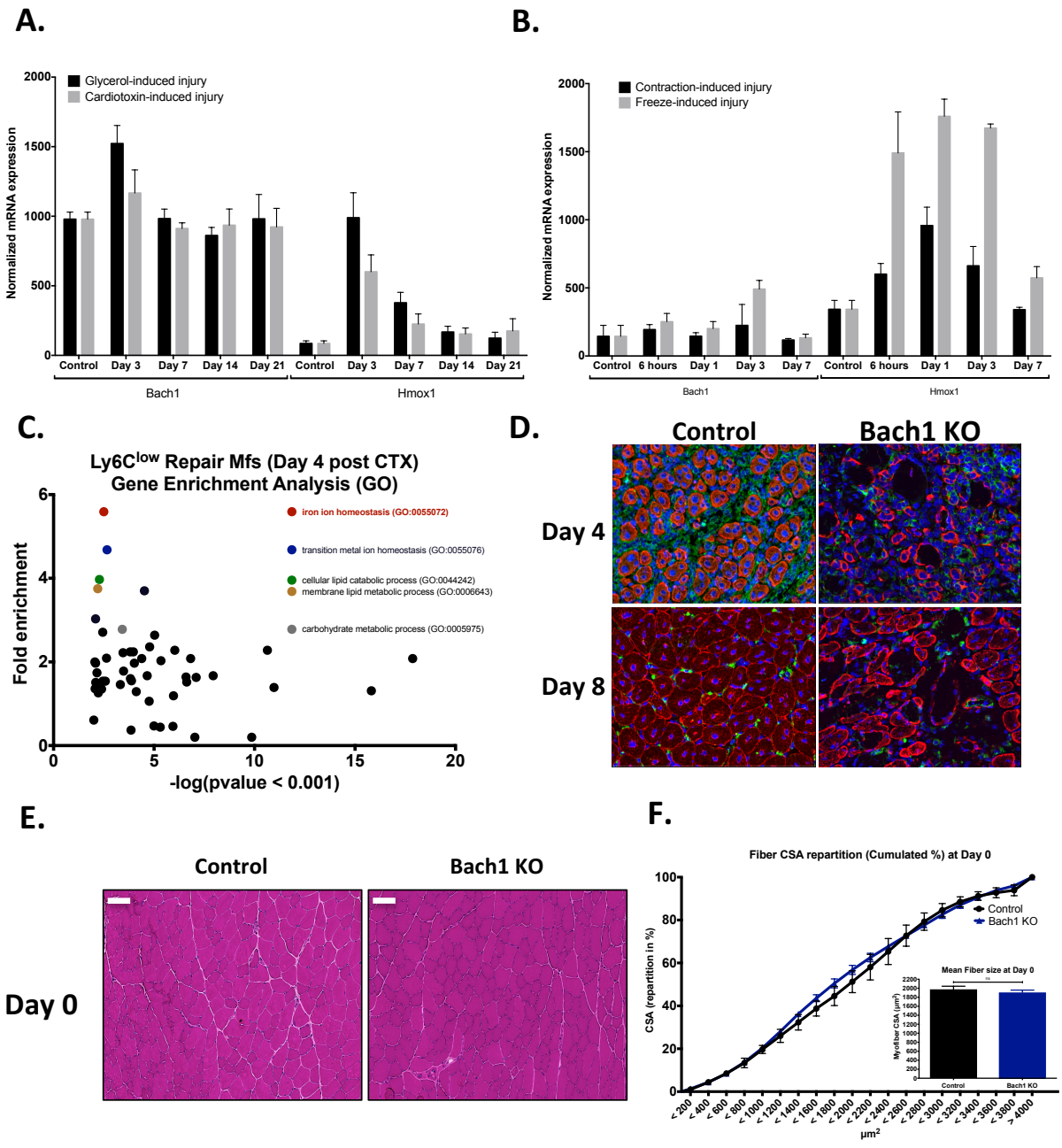

Supplementary Figure 1. Heme-BACH1-Hmox1 axis in acute injury models

A. mRNA expression of Bach1 and Hmox1 in glycerol and cardiotoxin-induced injury at timepoints indicated.

B. mRNA expression of Bach1 and Hmox1 in contraction and freeze-induced injury at timepoints indicated.

C. GO analysis of the genes that are differentially expressed as inflammatory Ly6C^{high} macrophages differentiate into regenerative Ly6C^{low} macrophages during muscle regeneration at day 4 post CTX injury.

D. IHC detection of desmin (red), F4/80 (green), and nuclei (blue) in WT control and Bach1 KO at day 4 and 8 post CTX injury is also shown.

E. Representative images of H&E stained skeletal muscle from WT and Bach1 KO mice prior any injury (day 0) are shown. Scale bars in the upper left represent 100 µm.

F. Fiber size repartition of uninjured muscle from WT or Bach1 KO animals. Mean fiber CSA is shown in the inset.

In all bar graphs, bars represent mean ± SEM.

The homeostatic response to injury comprises the modulated expression of genes involved in heme and iron handling (Corna, Caserta et al. 2016). A gene enrichment analysis on our RNA-seq data from CTX injured muscle infiltrating macrophages, revealed that iron and heme related pathways are being enriched in the Ly6C^{low} repair macrophages (**Supplementary Figure 1C**), further suggesting that the heme-BACH1-HMOX1 axis could have a crucial role in the inflammatory response and muscle regeneration outcome after CTX injury.

Heme-Bach1-Hmox1 axis is required for efficient muscle regeneration

Searching for the functional role of Bach1, Hmox1 and heme during muscle regeneration we used our CTX injury model and utilized *in vivo* heme treatments (i.p 30mg/kg heme daily), Bach1 KO animals and myeloid specific Hmox1 KO mice (Hmox1$^{fl/fl}$ LysMCre). Notably, Bach1 KO serves also as genetic model of Hmox1 overexpression, while *in vivo* heme treatments serves both as a transient BACH1 knock-down model and consequently a HMOX1 overexpression model. In all 3 experimental setups (heme treatments, Bach1 KO, and Hmox1$^{fl/fl}$ LysMCre), muscle regeneration was severely impaired at day 8 post CTX, in comparison to control muscles as shown by histological analysis (**Figure 13A, 13C, 13E**). These impairments can also be illustrated by a significant shift to the left of the distribution of the myofiber Cross Sectional Area (**Figure 13B, 13D and 13F**), a decrease in the mean CSA of regenerating myofibers (**Figure 13B, 13D and 13F right panels**), and a dramatic increase in necrotic fibers (**Figure 13G**). Necrosis in the BACH1 KO was so severe that we decided to validate this observation by desmin (a major intermediate filament protein) staining at day 4 and 8 post CTX (**Supplementary Figure 1D**), but also by an independent *in vivo* assay utilizing Evans Blue dye (EBD) uptake. Indeed, EBD uptake was significantly increased and can be observed both macroscopically (**Figure 13H**), and by quantifying the dye uptake inside the Bach1 KO muscles at day 8 post CTX (**Figure 13I**).

Next, we wanted to check whether regeneration will still be impaired at later stages of the regeneration process in the Bach1 KO. Intriguingly, both at day 21 and day 70 post CTX the Bach1 KO failed to recover to physiological levels compared to controls, as illustrated by histological analysis (**Figures 14A and 14C**), a shift to the left of the distribution of the myofiber Cross Sectional Area (**Figure 14B, 14D**) and a decrease in the mean CSA of regenerating myofibers (**Figures 14B and 14D right panels**). It's important to note that no developmental impairment was observed in Bach1 KO uninjured muscles (**Supplementary Figures 1E and 1F**) suggesting that the muscle regeneration/growth impairment is only evident after an acute injury. To limit the involvement of compensatory mechanisms in other tissue compartments and to ascertain the hemapoietic involvement during muscle regeneration, we decided to generate BMT animals reconstituted with Bach1 KO bone marrow. When the BACH1 KO chimeric animals were challenged with CTX induced muscle injury, they exhibited an impairment in regeneration at day 8 (**Figures 14E**). When compared with WT BMT animals, BACH1 KO chimeras contained more regenerating myofibers with smaller CSA (**Figure 14F**) and the regenerating muscle was replete with necrotic fibers (**Figure 14I**), which are hallmarks of defective muscle regeneration. To further validate our results, we also performed the gain of function BMT in which WT bone marrow was transplanted into BACH1 KO mice. According to the histological assessment (**Figure 14G**), the CSA distribution (**Figure 14H**) and the necrotic content (**Figure 14I**) the Bach1 KO mice that received the WT BM were able to recover to physiological levels at day 8 following CTX with no signs of

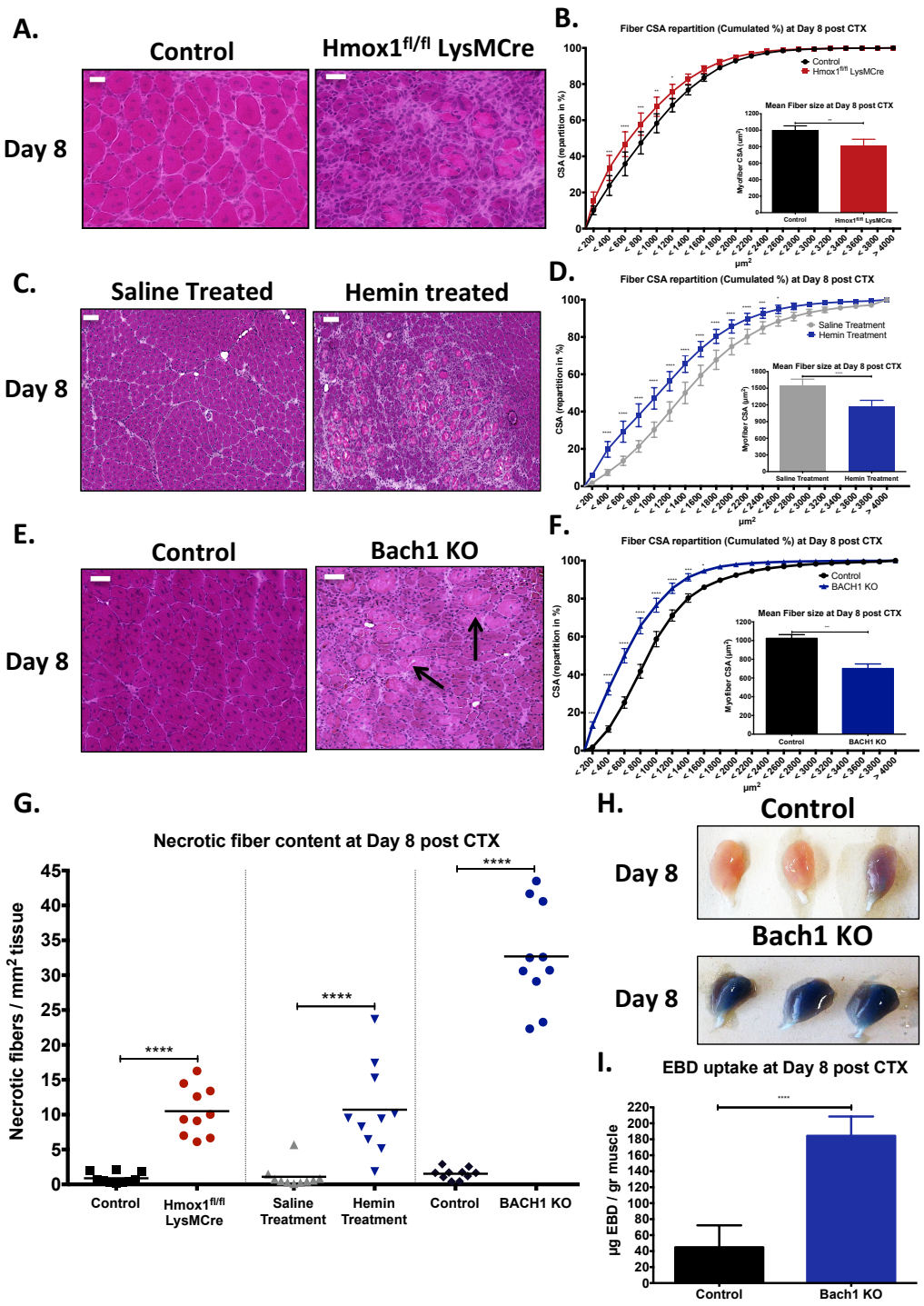

Figure 13. Impaired regeneration of skeletal muscle in Bach1-deficient, Hmox1-deficient and *in vivo* heme treated animals

A. C., E. Representative images of H&E stained skeletal muscle from WT control, Hmox1 $^{fl/fl}$ LysM-Cre, hemin treated or Bach1 KO animals at day 8 post CTX induced injury are shown. Scale bars in the upper left corner represent 100 µm.

B. D., F. Fiber size repartition of regenerating muscle in WT control, Hmox1 $^{fl/fl}$ LysM-Cre, hemin treated or Bach1 KO animals at day 8 post CTX injury. Inset shows average fiber CSA of regenerating muscle at day 8 post CTX injury.

G. The ratio of necrotic fibers relative to regeneration area at day 8 of regeneration in WT control, Hmox1 $^{fl/fl}$ LysM-Cre, hemin treated or Bach1 KO muscle sections is shown.

H. Representative macroscopical images of WT control and Bach1 KO TA muscles at day 8 following CTX injury. Mice were administrated systemically with Evan Blue Dye (EBD) 24 hours before muscle harvest.

I. *In vivo* EBD uptake assay from Bach1 KO TA muscles at day 8 post CTX.

In all graphs, bars represent mean ± SEM.

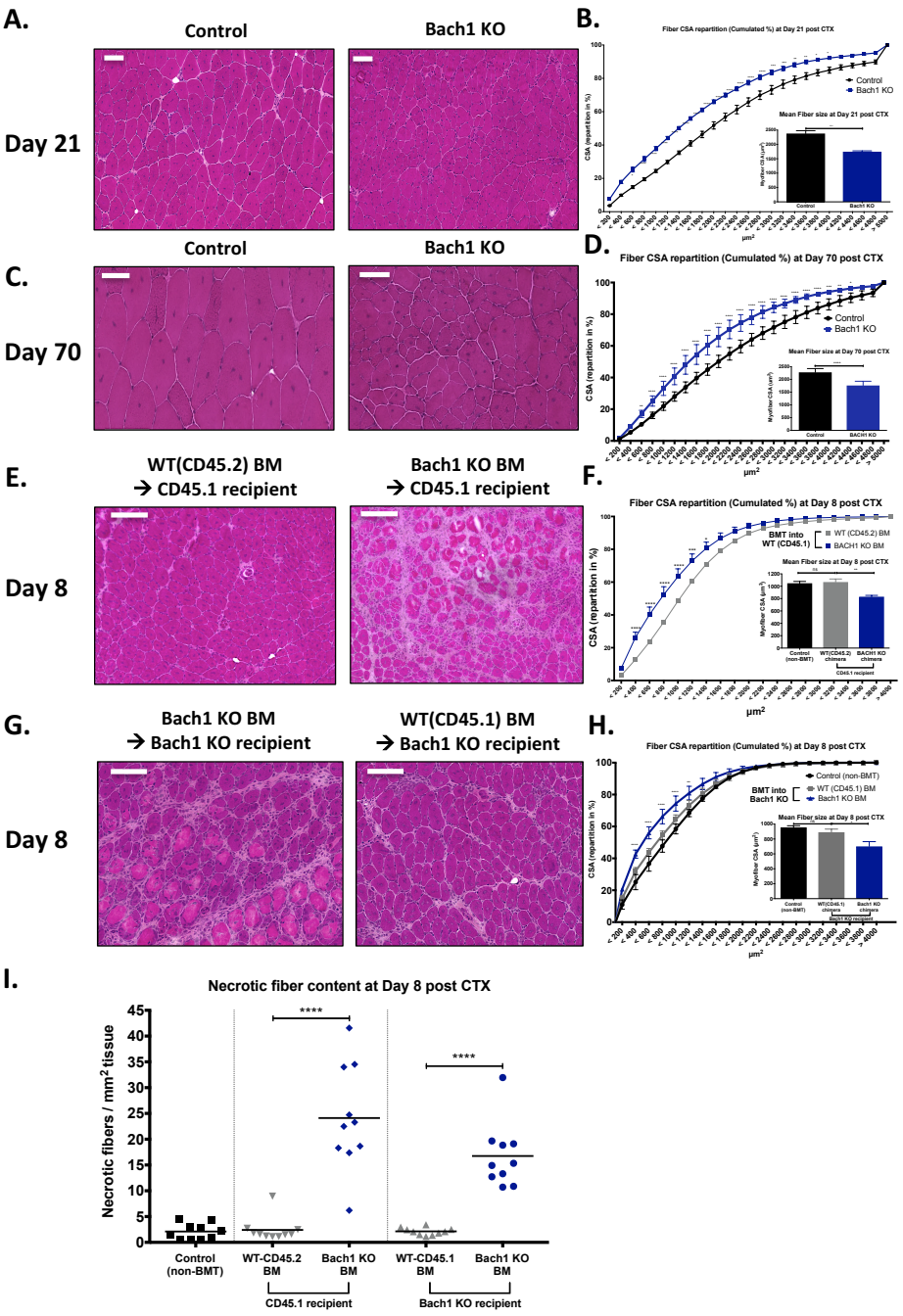

Figure 14. BACH1 hematopoietic involvement and prolonged muscle recovery of Bach1-deficient mice following injury

A. C. Representative images of H&E stained skeletal muscle from WT control and Bach1 KO animals at day 21 and 70 post CTX induced injury are shown. Scale bars in the upper left corner represent 100µm.

B. D. Fiber size repartition of regenerating muscle in WT control and Bach1 KO animals at day 21 and 70 post CTX injury. Inset shows average fiber CSA of regenerating muscle at day 21 and 70 post CTX injury.

E. Representative images of H&E stained skeletal muscle 8 days after CTX injury from WT BoyJ bone marrow transplanted animals (CD45.1 recipients) that received either WT (CD45.2) or Bach1 KO bone marrow.

F. Myofiber cross sectional area repartition (cumulated) and mean CSA (right panel) at day 8 post CTX injury from WT BMT animals transplanted with either WT (CD45.2) or Bach1 KO bone marrow.

G. Representative images of H&E stained skeletal muscle 8 days after CTX injury from Bach1 KO bone marrow transplanted animals that received either WT (CD45.1) or Bach1 KO bone marrow.

H. Myofiber cross sectional area repartition (cumulated) and mean CSA (right panel) at day 8 post CTX injury from Bach1 KO BMT animals transplanted with either WT (CD45.1) or Bach1 KO bone marrow.

I. The ratio of phagocytic and/or necrotic fiber area relative to the regeneration area at day 8 in control and BMT muscle sections are shown.

In all graphs, bars represent mean ± SEM.

any muscle regeneration impairment. These data further illustrate the involvement of BACH1 in the muscle regeneration process through the direct regulation of the immune response.

Heme-Bach1-Hmox1 axis controls the phenotypic transition of myeloid cells following CTX injury

Next, we asked whether the impaired muscle regeneration was caused by a defect in the cellular dynamics of the myeloid cell infiltrate during muscle regeneration. Hence, we injected both TA muscles of Bach1 KO, Hmox1$^{fl/fl}$ LysMCre, and heme treated mice with CTX and isolated the myeloid cells at Day 1, 2 and 4 after the injury using CD45^{+} magnetic bead selection. Interestingly, we did not find any difference in the numbers of invading myeloid cells (CD45^{+}) at any of timepoints we examined (**Figure 15A**), thus excluding the possibility of a massively diminished myeloid cell invasion contributing to the muscle regeneration impairment we observed previously (**Figure 13)**.

However, this finding did not exclude the possibility of a change in the cellular composition and differentiation of the infiltrating myeloid cells. Therefore, we examined the dynamics of the infiltrating myeloid cell populations during the course of the regeneration period under the same conditions (**Figures 15B-E**). The most obvious differences could be seen at day 4 post CTX, when the ratio of Ly6C^{high} F4/80^{low} and Ly6C^{low} F4/80^{high} macrophages in injured muscle between Hmox1$^{fl/fl}$ LysMCre, Bach1 KO and heme treated versus controls show remarkable differences (**Figures 15D**). Normally, in an uncompromised tissue, by day 4 after CTX injury, Ly6C^{high} inflammatory macrophages were progressively differentiating into Ly6C^{low} repair macrophages (**Figure 4B**). Surprisingly, in the case of Hmox1$^{fl/fl}$ LysMCre muscles, the phenotypic shift is severely delayed (**Figure 15E lower panel**). In contrast, in the case of Bach1 KO and heme treated muscles, the ratio of Ly6C^{low} is higher (**Figure 15D and 15E lower panel**). In summary, we observe significant differences in the ratios of inflammatory and repair macrophages, during their phenotypic transition. These data suggest a critical role for heme, BACH1 and HMOX1 in response to the acute sterile injury, showing that they function as a switch between inflammatory (Ly6C^{high}) to repair macrophages (Ly6C^{low}).

Muscle regeneration related genes are novel Bach1 targets and contribute to the impaired muscle repair phenotype

Evaluation of gene expression data from Bach1 KO muscle infiltrating macrophages revealed dysregulation of numerous genes (Il6, Il10, Dusp1, Slc40a1, Cebpb, Gdf3, Igf1, Pparg) involved in muscle regeneration and macrophage phenotype switching pathways (Serrano, Baeza-Raja et al. 2008), (Ruffell, Mourkioti et al. 2009), (Deng, Wehling-Henricks et al. 2012), (Perdiguero, Sousa-Victor et al. 2011), (Tonkin, Temmerman et al. 2015), (Corna, Caserta et al. 2016), (Varga, Mounier et al. 2016), suggesting that Bach1 potentially controls the expression of these important genes (**Figure 16A**) by regulating their enhancers. Initially we wanted to identify whether distal differentially accessible chromatin regions around these gene loci, detected by ATAC-seq (**Figures 10A and 16D**), are indeed differentially changing during the course of regeneration in the muscle infiltrating macrophages but also compare their enhancer RNAs (eRNAs) expression in WT vs Bach1 KO macrophages extracted from the injured muscles.

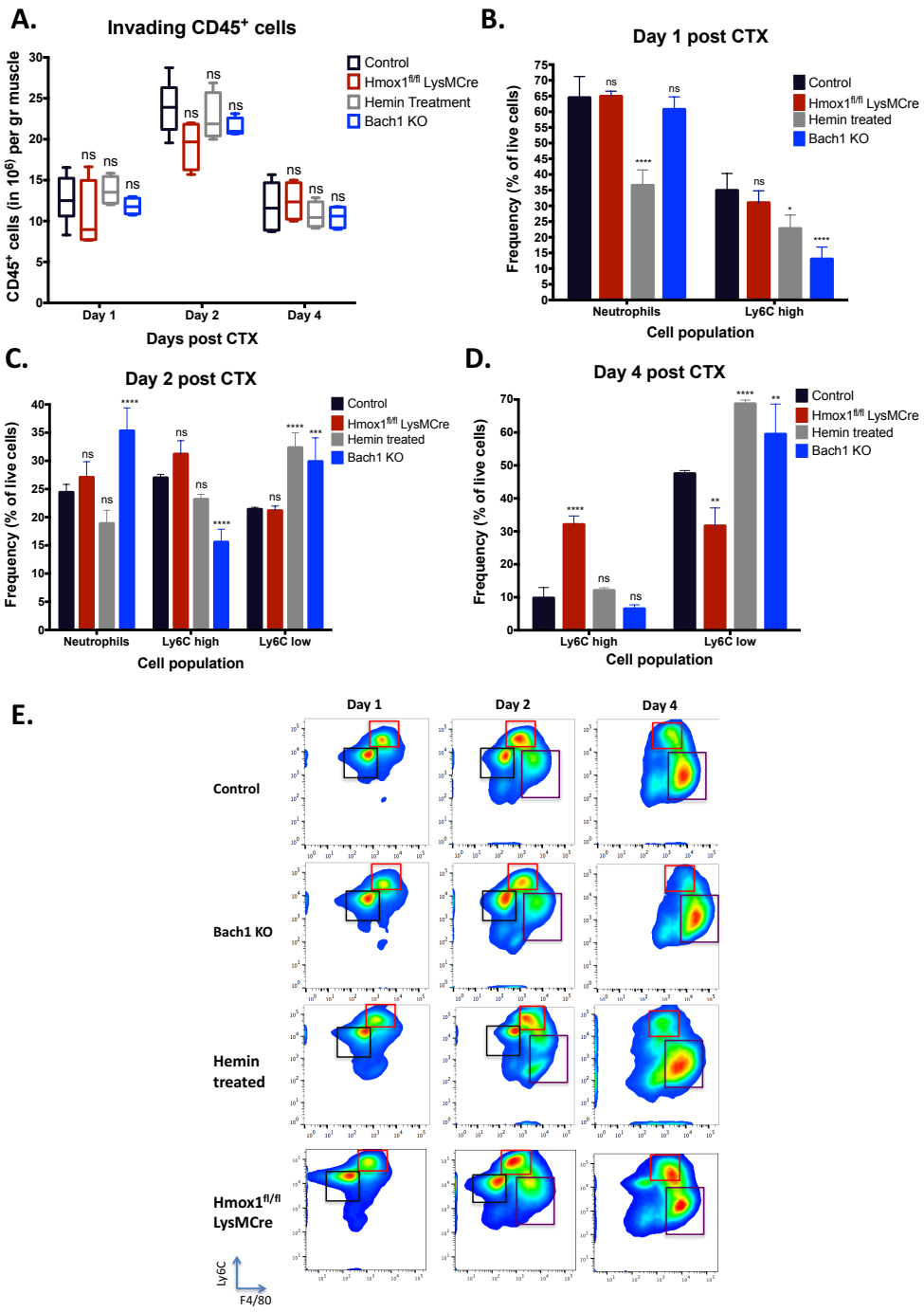

Figure 15. Altered phenotypic transition of infiltrating myeloid cells in Bach1-deficient, Hmox1-deficient and *in vivo* heme treated animals following CTX injury

A. Number of infiltrating myeloid ($CD45^+$) cells in regenerating muscle from WT control, Hmox1 $^{fl/fl}$ LysM-Cre, hemin treated or Bach1 KO muscles at indicated timepoints post CTX injury (n = 8 muscles per group).

B. C., D. Percentage of inflammatory ($Ly6C^{high}$ $F4/80^{low}$) and repair ($Ly6C^{low}$ $F4/80^{high}$) MFs from WT control, Hmox1 $^{fl/fl}$ LysM-Cre, hemin treated or Bach1 KO muscles at indicated timepoints following CTX injury (n = 8 mice per group).

E. Representative FACS images of inflammatory and repair macrophages from WT control, Hmox1 $^{fl/fl}$ LysM-Cre, hemin treated or Bach1 KO muscles at indicated timepoints post CTX injury.

In all bar graphs, bars represent mean ± SEM.

As expected many of the enhancers of these genes are differentially expressed at the various stages of the inflammatory and repair phases. Importantly, ablation of BACH1 impacts the expression of these eRNAs (**Figure 16B**). To validate these observations, BACH1 ChIP experiments were performed in BMDMs before and after heme treatment (**Figure 16C**). These experiments demonstrated that BACH1 is bound at multiple enhancers, at various genomic locations and distances from the TSS of these genes. These observations propose that BACH1 directly regulates important inflammatory and repair related genes in the context of muscle regeneration (such as Igf1, Slc40a1, Il6, Il10, Gdf3, Pparg, Dusp1, Cebpb), which further explains the severity of the Bach1 KO delayed muscle regeneration phenotype. Overall, we show that Bach1 is an acute damage signal dependent TF having a much larger gene regulation repertoire that expands beyond iron and heme related pathways.

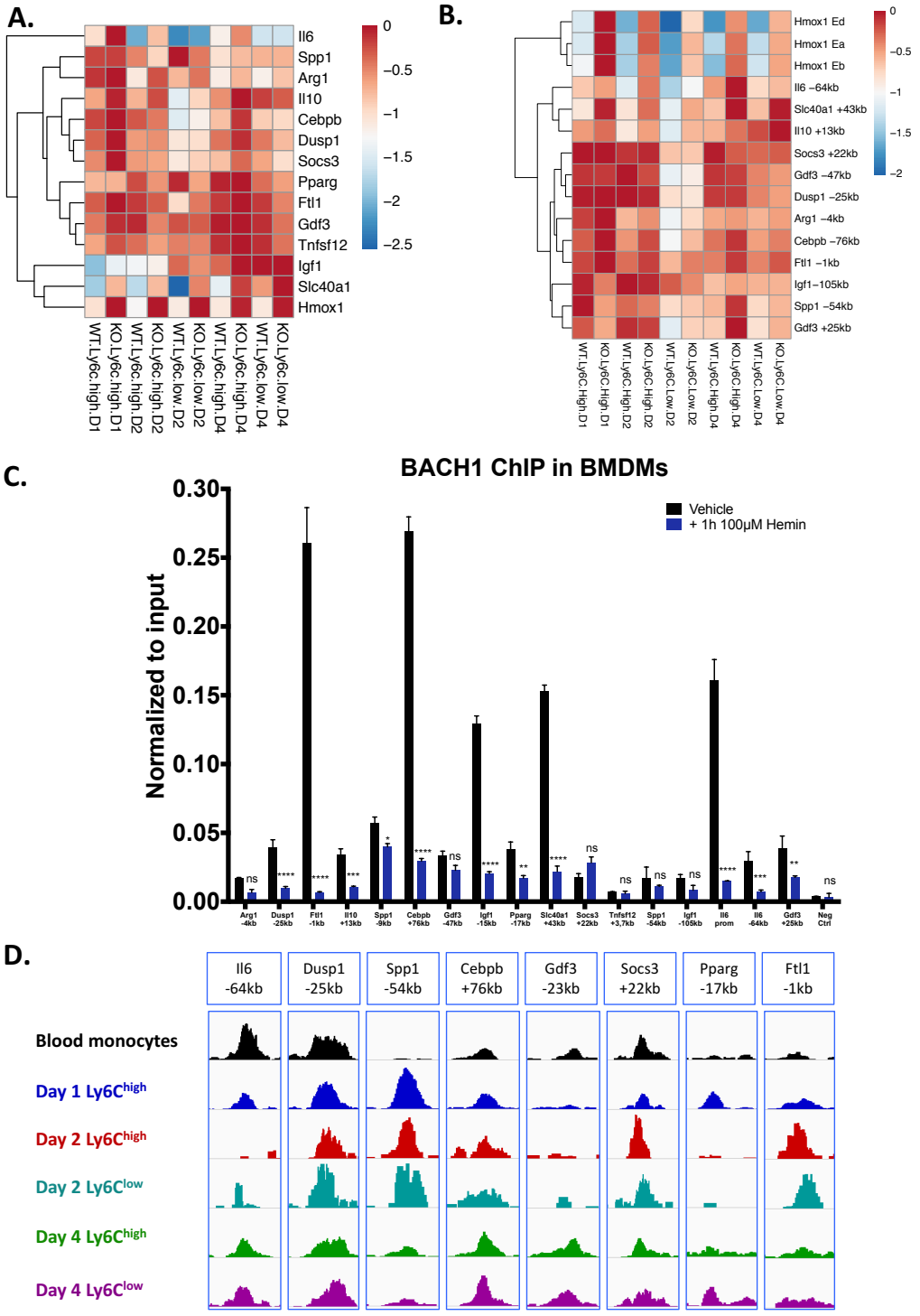

Figure 16. Defective regeneration related gene expression in Bach1 KO muscle derived macrophages.

A. Real-time PCR expression analysis of pro-inflammatory and repair markers in Bach1 KO muscle-derived macrophages upon CTX injury. Heatmap represents $-\log_{10}$(normalized mRNA expression) for each gene over Ppia.

B. Enhancer RNA expression of pro-inflammatory and repair markers in Bach1 KO muscle-derived macrophages upon CTX injury. Heatmap represents $-\log_{10}$(normalized expression) over Ppia.

C. BACH1-ChIP on the putative enhancer regions in BMDMs reveal Bach1 binding in all marked enhancers around the pro-inflammatory and repair markers mentioned in A and B. Heme treatment for 1 h was used to decipher the direct heme regulated Bach1 targets.

D. IGV genome browser view of ATAC-seq signals from muscle-derived macrophages at the indicated genomic regions showing differential intensities.

In all bar graphs, bars represent mean ± SEM.

Part 3. Reciprocal satellite-myeloid cell communication during regeneration

Aside from the transcriptional regulation of muscle infiltrating macrophages that we studied so far, we wanted to identify what are the cell interactions within the injured tissue cell milieu that contribute or potentially control the macrophage phenotypic switch. Here, by using the cardiotoxin (CTX) induced skeletal muscle injury combined with (1) irradiation as a means to alter cellular composition prior to injury, (2) bone marrow transplantation to replenish myeloid cells, (3) *in vivo* imaging to monitor the myeloid cell phenotypic switch *in situ*, and (4) focusing on *in vivo* ablation of a specific muscle cell population (paired box 7 (PAX7) positive cells) as a proof of concept, we tried to show that muscle tissue integrity and cell composition prior to the injury is required for *in situ* macrophage phenotypic shift and subsequently for proper and complete tissue regeneration.

The satellite cell pool is radiation sensitive and is required for proper muscle regeneration

We first sought to validate whether muscle regeneration is indeed impaired in irradiated muscles (Wakeford, Watt et al. 1991), and second whether this effect is due to diminished satellite cell populations (Barton, Shoturma et al. 1999), (Caiozzo, Giedzinski et al. 2010). The radiation dose we chose was 11 Gy because it has been reported that C57BL/6J mice can tolerate radiation doses of 10 to 11 Gy (Duran-Struuck, Hartigan et al. 2008). We used a method, which we termed lower body irradiation where mouse hindlimbs were irradiated and left to recover for 8 weeks after the radiation exposure (for details check the Methods section). For this method, non-irradiated and radioprotected (irradiated but simultaneously lead shielded) muscles served as control. Please note that the irradiated and radioprotected control belong to the same animal. TA muscles were then injured with CTX, and analyzed 8 days later using histology and morphometry. Importantly, muscle regeneration in the irradiated muscles is severely impaired, even after 2 months post irradiation, in comparison to control non-irradiated or radioprotected muscles as shown by histological analysis (**Figure 17A**). This impairment can also be illustrated by a significant shift to the left of the distribution of the myofiber Cross Sectional Area (**Figure 17B**), a decrease in the mean CSA of regenerating myofibers (-46%, $p < 0.0001$), (**Figure 17B right panel**) and a dramatic increase in necrotic fibers (**Figure 17C**). Macroscopically one can observe more than 35% reduction in the mass of the irradiated muscles compare to the contralateral radioprotected muscles of the same animals and also compared to age and weight matched non-irradiated control animals of the same genetic background (**Figure 18A**). The fact that we observe differences even after 2 months post irradiation is an important feature of the experimental setup because in this way one can avoid any short-term effects of irradiation induced toxicity.

To assess the effect of irradiation on the local muscle cell pool and more specifically on satellite cell pool, we measured the mRNA expression of a commonly used satellite cell marker; Pax7 (von Maltzahn, Jones et al. 2013), via qPCR and validated PAX7 through immunohistochemistry. Our data show that indeed Pax7 (**Figure 17D**) mRNA expression is decreased in the irradiated muscles compared to controls and radioprotected muscles at 8 weeks following irradiation. Interestingly, this effect is evident in both injured (Day 8 post CTX) and uninjured irradiated muscles (Day 0). Furthermore, PAX7 staining revealed fewer $PAX7^{+}$ cells in the irradiated muscles (**Figure 17E**) both at day 0 (**Figures 17E and 17F**) and day 8 post CTX injury

(**Figures 17E and 17G**). Radioprotected muscles served as control and showed similar numbers of $PAX7^+$ cells to non-irradiated control muscles. These results suggest that $PAX7^+$ satellite cells are indeed radiosensitive and are likely to be the major cause of the muscle regeneration deficiency observed in irradiated muscles.

Delayed phenotypic transition of myeloid cells in irradiated muscles following CTX injury

Next, we asked whether the impaired muscle integrity, and the altered cellular composition induced by irradiation prior to an acute injury, would have any effect on the cellular dynamics of the myeloid cell infiltrate during muscle regeneration (even after 2 months post irradiation). Hence, we injected both TA muscles of irradiated mice with CTX and the myeloid cells were isolated at Day 4 and 6 after the injury using $CD45^+$ magnetic bead selection. Interestingly, we found a statistically significant increase in the numbers of invading myeloid cells ($CD45^+$) in the irradiated versus radioprotected muscles at both timepoints (**Figure 18B**), thus excluding the possibility of a massively diminished myeloid cell invasion contributing to the muscle regeneration impairment we observed in **Figure 17A**.

However, this finding did not exclude the possibility of a change in the cellular composition and differentiation of the infiltrating myeloid cells. Therefore, we examined the dynamics of the infiltrating myeloid cell populations during the course of the regeneration period in irradiated and radioprotected muscles (**Figure 18C**). At day 4 post CTX, the ratio of $Ly6C^{high}$ $F4/80^{low}$ and $Ly6C^{low}$ $F4/80^{high}$ macrophages in injured muscle between irradiated versus non-radiated or radioprotected controls show remarkable differences (**Figures 18C-D**). Normally, in an uncompromised tissue, by day 4 after CTX injury, $Ly6C^{high}$ inflammatory macrophages are progressively differentiating into $Ly6C^{low}$ repair macrophages (**Figure 4B**). This is the case for non-irradiated and radioprotected controls (**Figure 18C-D**). Surprisingly, in the case of irradiated muscles, this shift starts later and is completed only by day 6 (**Figures 18C-E**). In summary, we observe a remarkably long 2-day delay (in the context of an 8-day regeneration process) in the phenotypic transition of infiltrating myeloid cells in the irradiated muscles. In addition, it also showed that radioprotection (in the form of lead shielding) during irradiation exposure prevented the delay of muscle regeneration following CTX injury, by preserving the local muscle cell composition and by maintaining the infiltrating myeloid cell kinetics. However, we reached the limit of this method because we are unable to differentiate between the BM-derived and the tissue resident macrophages as the source of the infiltration.

Bone marrow transplantation allows establishing the source of myeloid cell invasion and phenotypic shift

In order to control the source of the infiltrating cells (BM-derived), and to exclude the possibility that the restoration of the infiltration dynamics in the radioprotected muscles is due to the protection of the resident tissue macrophages, we performed bone marrow transplantation (BMT). This method allowed us to investigate whether the infiltrating myeloid cells in both the radioprotected and irradiated muscles share the same features, and originate from the donor C57BL/6J bone marrow (CD45.2 positive). We used C57BL/6 congenic mice (BoyJ)

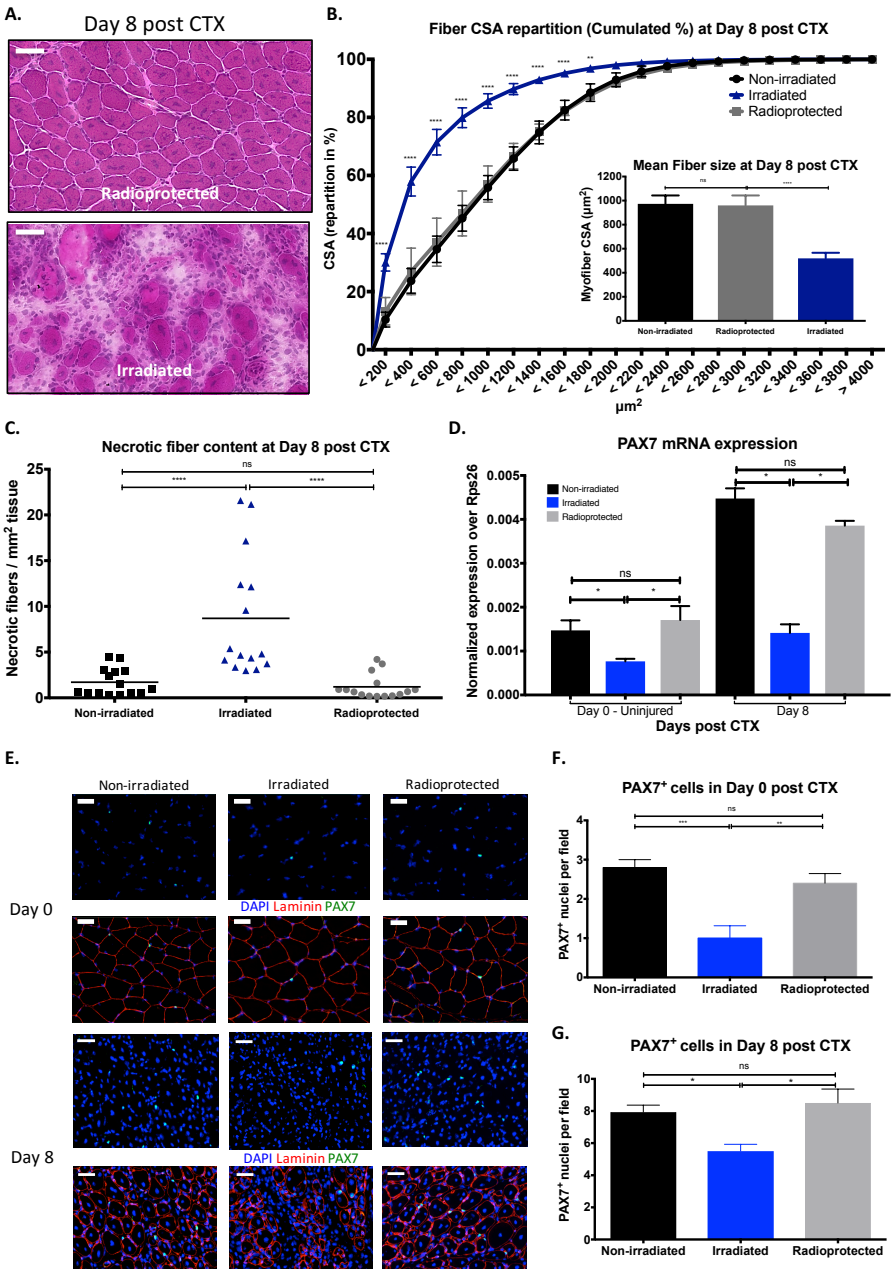

Figure 17. Diminished satellite cell numbers in radiation-exposed muscles impairs skeletal muscle regeneration.

A. Representative images of H&E stained TA muscles from 11 Gy irradiated and radioprotected muscles at day 8 post CTX induced injury. Scale bars represent 100 µm.
B. Myofiber cross sectional area repartition (cumulated) and mean CSA (right panel) in control non-irradiated, irradiated and radioprotected animals at day 8 post CTX injury (n=8 per group).
C. The ratio of phagocytic and/or necrotic fiber area relative to the regeneration area (in mm^2) at day 8 post CTX injury in control non-irradiated, irradiated and radioprotected muscle sections are shown (n=8 per group).
D. mRNA expression (±SD) of satellite cell lineage marker, Pax7 in control non-radiated, irradiated and radioprotected muscles at Day 0 (uninjured) and Day 8 post CTX injury (n=5 for each group).
E. Representative images from IHC detection of lamimin (red), PAX7 (green) and nuclei (blue) from control non-radiated, irradiated and radioprotected muscles at day 0 (upper panel) and day 8 (lower panel) post CTX injury. Scale bars represent 50 µm.
F. $PAX7^+$ cell quantification (PAX7 positive cells per field of view) in control non-radiated, irradiated and radioprotected muscles at day 0 post CTX injury.
G. $PAX7^+$ cell quantification (PAX7 positive cells per field of view) in control non-radiated, irradiated and radioprotected muscles at day 8 post CTX injury.

In all graphs, mean values ± SEM are shown.

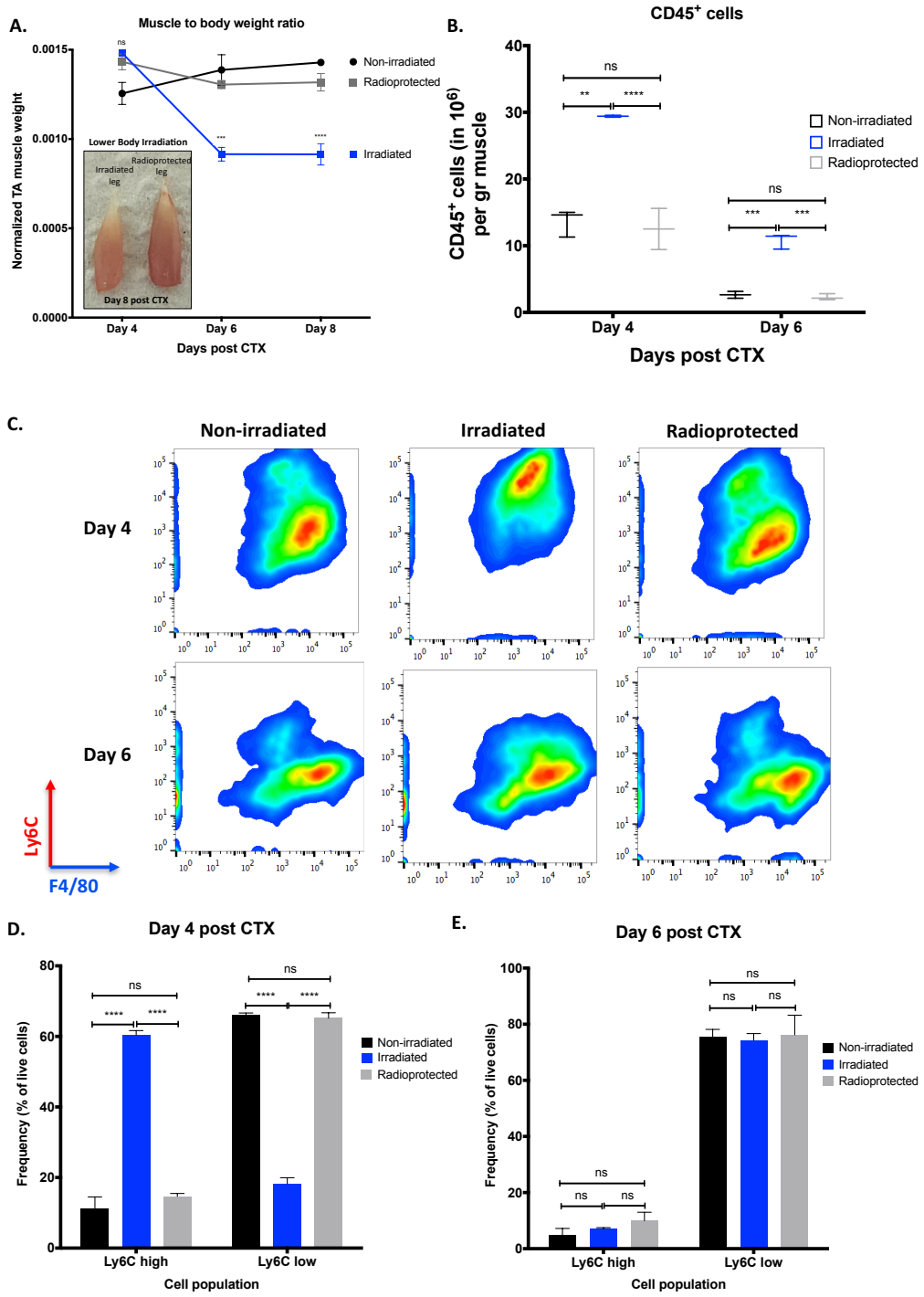

Figure 18. Delayed phenotypic transition of infiltrating myeloid cells in irradiated animals following CTX injury.

A. Normalized TA muscle weight to body weight ratio from control non-irradiated and WBS animals at indicated timepoints following CTX injury (n=4 per group). Left panel shows representative macroscopical images of recovered WBS animals and muscles at day 8 post CTX injury.

B. Number of infiltrating myeloid ($CD45^{+}$) cells in regenerating muscle from control non-irradiated, irradiated and radioprotected muscles at day 4 and 6 post CTX injury (n = 8 muscles per group).

C. Representative FACS images of inflammatory and repair macrophages from control non-irradiated, irradiated and radioprotected muscles at day 4 and 6 post CTX injury.

D. Percentage of inflammatory ($Ly6C^{high}$ $F4/80^{low}$) and repair ($Ly6C^{low}$ $F4/80^{high}$) MFs from control non-irradiated, irradiated and radioprotected muscles at day 4 following CTX injury, respectively (n = 8 mice per group).

E. Percentage of inflammatory ($Ly6C^{high}$ $F4/80^{low}$) and repair ($Ly6C^{low}$ $F4/80^{high}$) MFs from control non-irradiated, irradiated and radioprotected muscles at day 6 following CTX injury, respectively (n = 8 mice per group).

In all graphs, mean values ± SEM are shown.

which carry a differential CD45 pan leukocyte marker (CD45.1), compared to WT C57BL/6J inbred mice that express the CD45.2 allele allowing discrimination between donor and recipient BM-derived cells. After a radiation dose of 11 Gy, animals were transplanted with C57BL/6J bone marrows (BM) and left to recover for 8 weeks after the BMT. It is important to note that total body irradiation precedes BMT thus giving us the unique opportunity to combine irradiation induced cell ablation and myeloid cell tracing. TA muscles were then injured with CTX, and analyzed 8 days later using histology and morphometry. Macroscopically there is almost a 48% reduction in the mass of the muscles compare to age and weight matched non-BMT control animals of the same genetic background (**Figures 19A-B**). Thus, in agreement with our previous lower body irradiation experiments (**Figure 17A**), muscle regeneration in these BMT animals is severely impaired, even after 2 months post irradiation and BMT, in comparison to control non-BMT animals (**Figure 19C**). This impairment can also be illustrated by a significant shift to the left of the distribution of the myofiber Cross Sectional Area (**Figure 19D**), a decrease in the mean CSA of regenerating myofibers (-42%, $p < 0.0001$), (**Figure 19D right panel**) and an increase in necrotic fiber content (**Figure 19E**). In addition, when we further followed up the regeneration period in the BMT animals we observed that recovery to a morphologically and histochemically mature muscle takes at least 2 more weeks (Day 20 post CTX) compared to the non-BMT animals (**Figure 19F**), as shown by the mean CSA of regenerating myofibers (**Figure 19G**). Reducing the radiation dose to 9.5 Gy (sub-lethal dose) and increasing the number of BM cells to be injected from $5x10^6$ to $20x10^6$ had only a small effect in improving the outcome of regeneration (**Figures 19C-E**) although bone marrow chimerism did improve (**Figures 19B-C**). Chimerism measurements were performed as shown before (Mócsai, Zhou et al. 2002) by using CD45.1 and CD45.2 markers to distinguish between the leukocytes, of the donor and that of the recipient. The gating strategy we followed to determine the chimerism in the BMT animals is illustrated in **Figure 20A**.

There were no statistically significant differences found between the numbers of invading myeloid cells ($CD45^+$) in BMT versus non-BMT controls except from Day 4 in which an increase of cell number in the BMT animals was observed (**Figure 20D**), validating our previous results (**Figure 18B**). Next, we examined the dynamics of the infiltrating myeloid cell populations during the course of the regeneration in non-BMT controls and BMT animals. At day 1 post CTX injury, the predominant cell populations within the muscle are neutrophils and $Ly6C^{high}$ macrophages (**Figure 4B**). The ratio of the $Ly6G^{high}$ $Ly6C^{med}$ $F4/80^-$ neutrophils and the $Ly6C^{high}$ $F4/80^{low}$ macrophages among the $CD45^+$ cells isolated from injured muscle at day 1 was not significantly altered (**Figures 20E-F**). At day 2 the ratio of $Ly6C^{high}$ $F4/80^{low}$ (**Figure 20F**) and $Ly6C^{low}$ $F4/80^{high}$ (**Figure 20G**) macrophages in injured muscle between BMT and non-BMT controls, was altered (**Figures 20E-G**). More importantly, the difference in the ratio of $Ly6C^{high}$ $F4/80^{low}$ and $Ly6C^{low}$ $F4/80^{high}$ we observe at day 2 can be detected all the way through day 6 after the CTX injury (**Figures 20E-G**). In summary, we consistently observe a 2-day delay in the phenotypic transition of the infiltrating myeloid cells from inflammatory to the repair phenotype. These experiments reported to us, as expected, that irradiation is impacting regeneration in the bone marrow transplantation model as well, while we can readily assess the origin of the myeloid infiltration.

In order to maintain the contralateral leg as a control following irradiation and BMT, we decided to optimize our radioprotection strategy. Thus, we devised a method to both preserve the satellite cell number and replace the bone marrow derived macrophages to be able to assess infiltrating macrophage phenotypic dynamics. Methods of radioprotection from radiation-

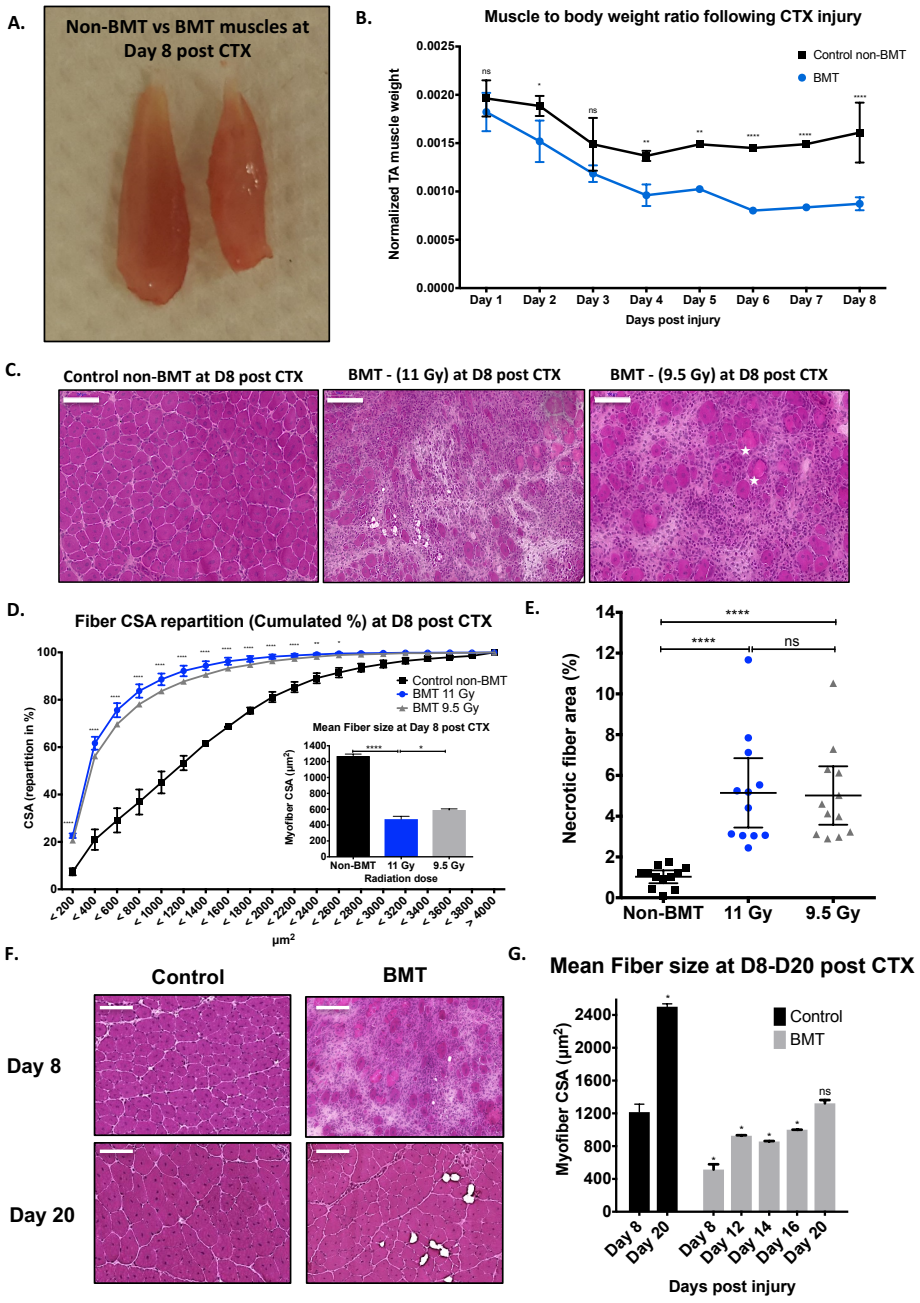

Figure 19. Impaired regeneration of skeletal muscle in bone marrow transplanted animals.

A. Normalized TA muscle to body weight from aged and weight matched control non-BMT and bone marrow transplanted (BMT) animals at indicated timepoints following CTX injury. By day 8 post CTX TA muscle weight drops from 0.056 gr to 0.046 gr in the control non-BMT animals and from 0.053 gr to 0.025 gr in the BMT animals.

B. Representative macroscopical image of TA muscle from control (left) and BMT (right) animals at day 8 post CTX injury.

C. Representative images of H&E stained muscle from control (non-BMT) and BMT animals radiated with 11 or 9.5 Gy at day 8 post CTX induced injury. Asterisks label phagocytic and/or necrotic fibers. Scale bars represent 100 µm.

D. Myofiber cross sectional area repartition (cumulated) and mean CSA (right panel) in control and BMT animals (radiated with 11 or 9.5 Gy) at day 8 post CTX injury (number of fibers counted > 20000). Significance is shown for control *vs.* BMT 11 Gy.

E. The ratio of phagocytic and/or necrotic fiber area relative to the regeneration area at day 8 in control and BMT muscle sections are shown.

F. Representative images of H&E stained muscle from control (non-BMT) and BMT animals at the indicated timepoints post CTX injury.

G. Average fiber cross sectional area (CSA) of regenerating muscle at indicated timepoints post CTX injury in control and BMT animals. All data timepoints were compared to day 8 controls. n = (numbers of individual muscles, derived from controls or BMT animals): at least 8 muscles for each sample per timepoint.

In all graphs, mean values ± SEM are shown.

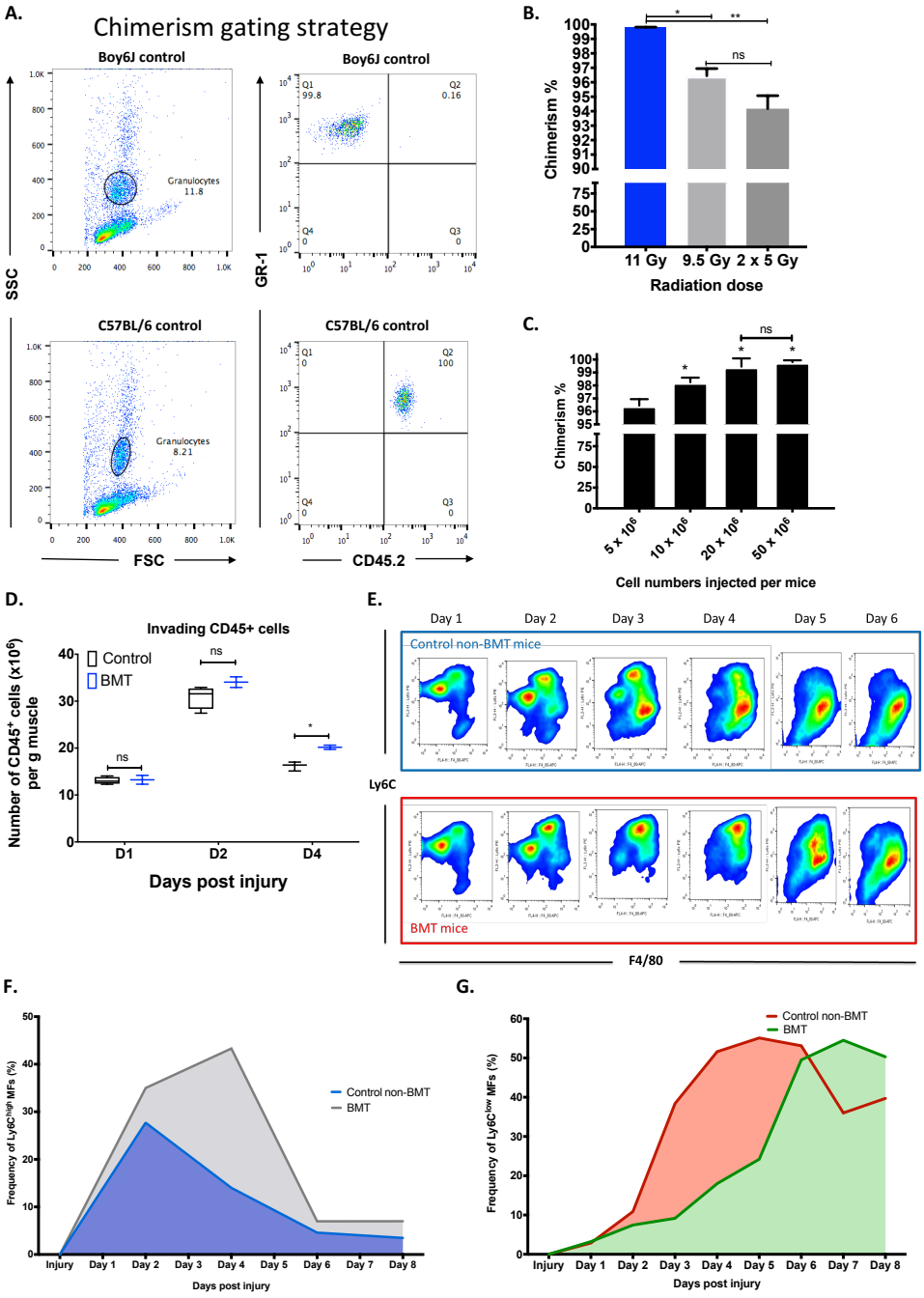

Figure 20. Delayed phenotypic transition of infiltrating myeloid cells in BMT animals following CTX injury.

A. FACS gating strategy to calculate chimerism levels following BMT. The ratio of donor ($CD45.2^+$) to host ($CD45.1^+$) bone marrow repopulation is gated on the granulocyte fraction using CD45.2 and GR1 antibodies.

B. Percentage of chimerism in BMT animals receiving different radiation doses (one single dose of 11 Gy or 9.5Gy and 2 consecutive doses of 5 Gy with a 24h rest period between them).

C. Percentage of chimerism in BMT animals injected with different numbers of donor cells (5, 10, 20 and 50 x 10^6 cells). In both chimerism experiments n>8 per group.

D. Number of infiltrating myeloid ($CD45^+$) cells in regenerating muscle at day 1,2 and 4 post CTX injury (n = 8 muscles per group).

E. FACS gating strategy to enumerate muscle infiltrative $Ly6C^{high}$ $F4/80^{low}$ and $Ly6C^{low}$ $F4/80^{high}$ macrophages at day 1 - 6 post CTX injury. Upper panel (blue) shows representative samples from control animals and lower (red) from BMT animals.

F. Percentage of $Ly6C^{high}$ $F4/80^{low}$ muscle MFs at indicated timepoints following CTX injury (n = 12 mice per group) in control non-BMT and BMT samples. Day 2 – Day 6 comparisons between groups give statistically significant results (** p-value < 0.01).

G. Percentage of $Ly6C^{low}$ $F4/80^{high}$ muscle MFs at indicated timepoints following CTX injury (n = 12 mice per group) in control non-BMT and BMT samples. Day 2 – Day 6 comparisons between groups give statistically significant results (** p-value < 0.01).

In all graphs, mean values ± SEM are shown.

induced toxicity include dose fractionation (**Figure 19C**) and lead shielding (**Figure 21A**). We measured chimerism at 6, 8, and 12-week intervals after transplantation and found that chimerism increased with longer recovery periods (**Figure 21B**), higher radiation doses (**Figure 21B**) and one versus both hindlimbs radioprotected (through lead shielding) (**Figure 21C**). Radioprotecting one leg protects/shields the bone marrow; resulting in slightly decreased chimerism (**Figure 21C**) but still high enough (>90%) to allow us to assess the contribution of myeloid cell infiltration. This observation suggests that the optimization of the leg hindlimb radioprotection setup worked without sacrificing chimerism efficiency. Now this optimized method allows us (1) to ablate satellite cells, (2) assess muscle regeneration outcome, (3) control the origin, and (4) assess the dynamics of myeloid cell infiltration, all these in the same animal. In order to simplify the nomenclature, and keeping in mind that we are assessing muscles of the same animal, we call BMT-shielded the muscle of an animal that underwent irradiation with hindlimb radioprotection (by the usage of lead shields) followed by BMT and BMT-unshielded refers to the contralateral muscle of the same animal that underwent irradiation (without radioprotection) followed by BMT. In a typical experiment, we have 3 kinds of muscle, (1) control; meaning muscles from non-irradiated, non-shielded, non-BMT animals which reports to us the normal regeneration kinetics, (2) BMT-shielded; meaning muscles from irradiated, radioprotected and BMT animals, (3) BMT unshielded; meaning muscles from irradiated, non-radioprotected and BMT animals. Importantly muscles from group 2 and 3 come from the same animal. In agreement with our hypothesis, muscle regeneration and TA muscle mass at day 8 post CTX injury in unshielded BMT animals was significantly impaired compared to contralateral BMT shielded muscles, as illustrated by the muscle mass (**Figures 21D-E**), H&E histology staining (**Figure 22B**), the distribution (**Figure 22D**) and mean (**Figure 22D right panel**) myofiber CSA, and necrotic fiber content (**Figure 22E**). The efficiency of the radioprotection can also be seen by the preservation of coat colors only in the radiation-protected regions (**Figure 21E left panel**). Interestingly, no apparent difference in muscle mass (**Figure 21D**) or CSA (**Figures 22A and 22C**) of uninjured BMT-shielded *versus* uninjured BMT-unshielded muscles was observed. In addition, no central myonuclei in the BMT-unshielded muscles was observed, suggesting that the radiation does not have a direct long-term effect on muscle morphology. Albeit reduced numbers of PAX7 positive cells were observed at 8 weeks following irradiation (**Figure 17F**) it appears that an acute insult to the muscle like CTX, is needed to reveal the muscle regeneration deficiency.

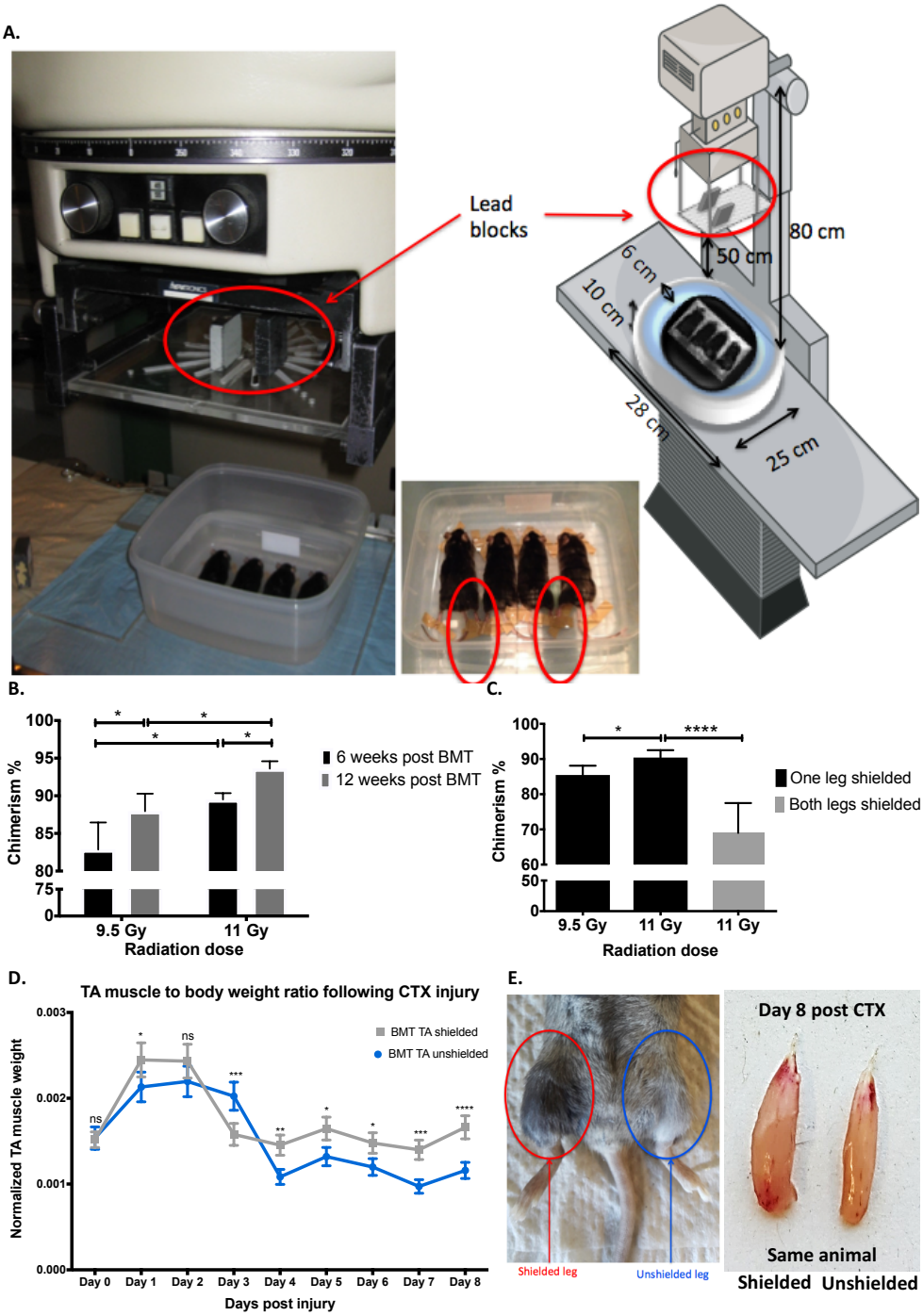

Figure 21. BMT with radioprotection optimized setup.

A. Representative images of the shielding adaptation during irradiation. The mice were put into a plastic box, with double wall and water was used for scattering medium. Two 5 cm high led blocks on the PMMA shadow tray were used for protection one of the legs (red circles) of the mouse at 20 cm distance to the surface of the plastic box. The source surface distance (SSD) and source axis distance (SAD) was 80 cm. The beam size is 21x21 cm. Illustration model uses a modified version of art from Servier Medical Art under a Creative Commons (CC) license.

B. Percentage of chimerism in animals left to recover for 6 *vs.* 12 weeks post irradiation and BMT (n=8 per group).

C. Percentage of chimerism in BMT animals with one *vs.* both legs shielded (n=8 per group).

D. Normalized TA muscle to body weight ratio from BMT shielded *vs.* unshielded animals at indicated timepoints following CTX injury (n=16 per group).

E. Representative macroscopical images of recovered BMT shielded animals (left) and muscles at day 8 post CTX (right). The fur color was preserved in the shielded leg (red circle) but not in the unshielded leg (blue cirlce) of the same animal.

In all graphs, mean values ± SEM are shown.

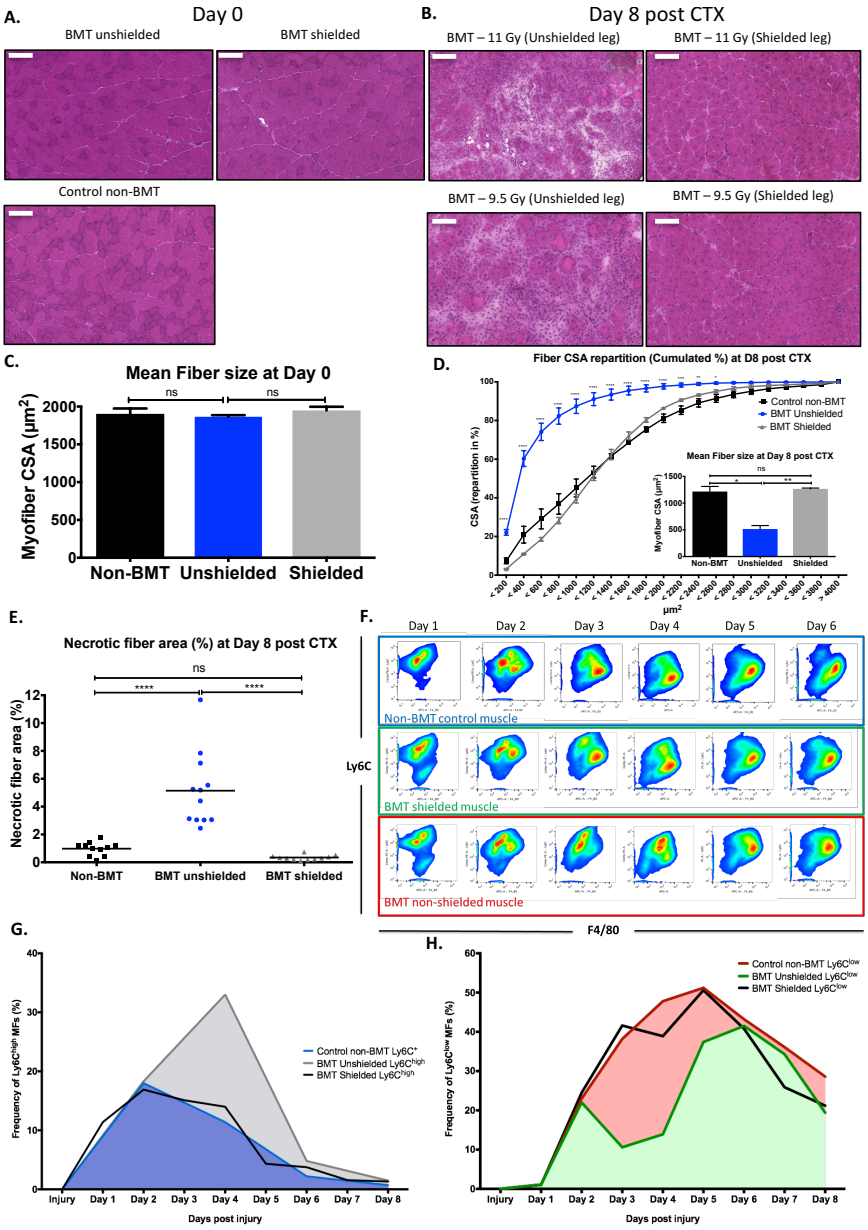

Figure 22. Radioprotected muscles during BMT have normal recovery time following CTX injury.

A. Representative images of H&E stained uninjured TA muscles from control non-BMT, BMT-shielded and BMT-unshielded muscles. Scale bars represent 100 µm.

B. Representative images of H&E stained TA muscle from control non-BMT, BMT-shielded and BMT-unshielded muscles radiated with 11 or 9.5 Gy at day 8 post CTX induced injury. Scale bars represent 100 µm.

C. Average fiber cross sectional area (CSA) of uninjured (Day 0) TA muscle from control non-BMT, BMT-shielded and BMT-unshielded muscles (n = 12 muscles per group).

D. Myofiber cross sectional area repartition (cumulated) and mean CSA (right panel) in control non-BMT, BMT-shielded and BMT-unshielded muscles (n = 12 muscles per group) at day 8 post CTX (number of fibers counted > 20 000).

E. The ratio of phagocytic and/or necrotic fiber area relative to the regeneration area at day 8 in control non-BMT, BMT-shielded and BMT-unshielded muscle sections are shown.

F. FACS gating strategy to enumerate muscle infiltrative Ly6C^{high} F4/80^{low} and Ly6C^{low} F4/80^{high} macrophages at day 1 - 6 post CTX injury. Upper panel (blue) shows representative samples from control non-BMT animals; middle panel (green) shows samples from BMT-shielded muscles and lower panel (red) from BMT-unshielded muscles.

G. Percentage of Ly6C^{high} F4/80^{low} muscle MFs from control non-BMT, BMT- shielded and BMT-unshielded animals at indicated timepoints following CTX injury (n = 12 mice per group).

H. Percentage of Ly6C^{low} F4/80^{high} muscle MFs from control non-BMT, BMT-shielded and BMT-unshielded animals at indicated timepoints following CTX injury (n = 12 mice per group).

In all graphs, mean values ± SEM are shown.

Local radioprotection during BMT allows the assessment of donor bone marrow derived invading macrophages in an intact muscle tissue environment

The next obvious question was to determine whether radioprotection (lead shielding) in the BMT-shielded animals sustains the cellular dynamics of the myeloid cell invasion following CTX injury at control levels. Hence, we injected BMT-shielded and BMT-unshielded muscles (from the same animal) with CTX and myeloid cells were isolated from them at Day 1 to Day 6 after the injury using $CD45^+$ magnetic bead selection and Ly6G, Ly6C and F4/80 antibody labeling. Within the same animal the contralateral BMT-unshielded muscle showed the two-day delay in the phenotypic switch from $Ly6C^{high}$ to $Ly6C^{low}$ (**Figures 22F-H**), in accordance with the histopathological assessment (**Figure 22B**). To prove that the infiltrating cells in both the BMT-shielded and BMT-unshielded muscles originate from the donor C57BL/6J bone marrow (CD45.2 positive) and share the same features, we quantified $CD45^+$ positive cells according to the myeloid lineage markers CD45.1 (recipient BoyJ bone marrow stains positive for CD45.1 but not CD45.2) and CD45.2 by FACS (**Figure 23A**). Over 90% of the infiltrating cells in both the BMT-shielded and BMT-unshielded muscles were CD45.2 positive which is in line with the level of chimerism detected in the blood from the same animals (**Figure 23B**), thus excluding the contributions of tissue resident macrophages in the observed phenotype. By demonstrating that the donor-derived cells infiltrate (CD45.1 vs. CD45.2 %) is present, even when the host limb is radioprotected during BMT; suggest that this BMT modification could be a viable model for muscle regeneration studies despite the tibia and femur not being irradiated.

Taken together, these results suggest that radioprotection by lead shielding effectively attenuated radiation effects and protected muscle tissue integrity. This also suggested that the cause of the delay in regeneration is the effect of irradiation of the leg itself and not elsewhere in the body for example in the bone marrow, blood or spleen that are sites where myeloid cells could be derived from.

^{18}F-FDG PET-MRI allows *in vivo* monitoring of the infiltrating immune response and reveals that the invading myeloid cells are metabolically distinct

The analysis of myeloid cells following the injury based on surface markers requires long (over 6 hours) and tedious tissue processing. In order to obtain additional and truly *in vivo* non-invasive reading of myeloid cell invasion we turned to *in vivo* imaging. Positron Emission Tomography (PET) imaging technique is a widely used noninvasive method in clinical and preclinical studies for the detection of tumors, staging and monitoring the effect of cancer therapy (Wester 2007). Glucose analogue, 2-[^{18}F] fluoro-2-deoxy-d-glucose (^{18}F-FDG) is the most commonly used and validated tracer, which is up taken by activated cells where it is metabolically trapped and accumulates in proportion to intracellular demands. Increased FDG uptake was observed in several energy-intensive processes, such as infections and inflammation (Glaudemans, de Vries et al. 2013), (Vaidyanathan, Patel et al. 2015) and has been associated with activated neutrophils and macrophages, so we hypothesized that using FDG as a tracer and combining it with MRI (Signore and Glaudemans 2011), (Gondin, Théret et al. 2015), could be a novel and effective method to monitor the events following the acute muscle injury and specifically the metabolism of the immune cells during the inflammatory response.

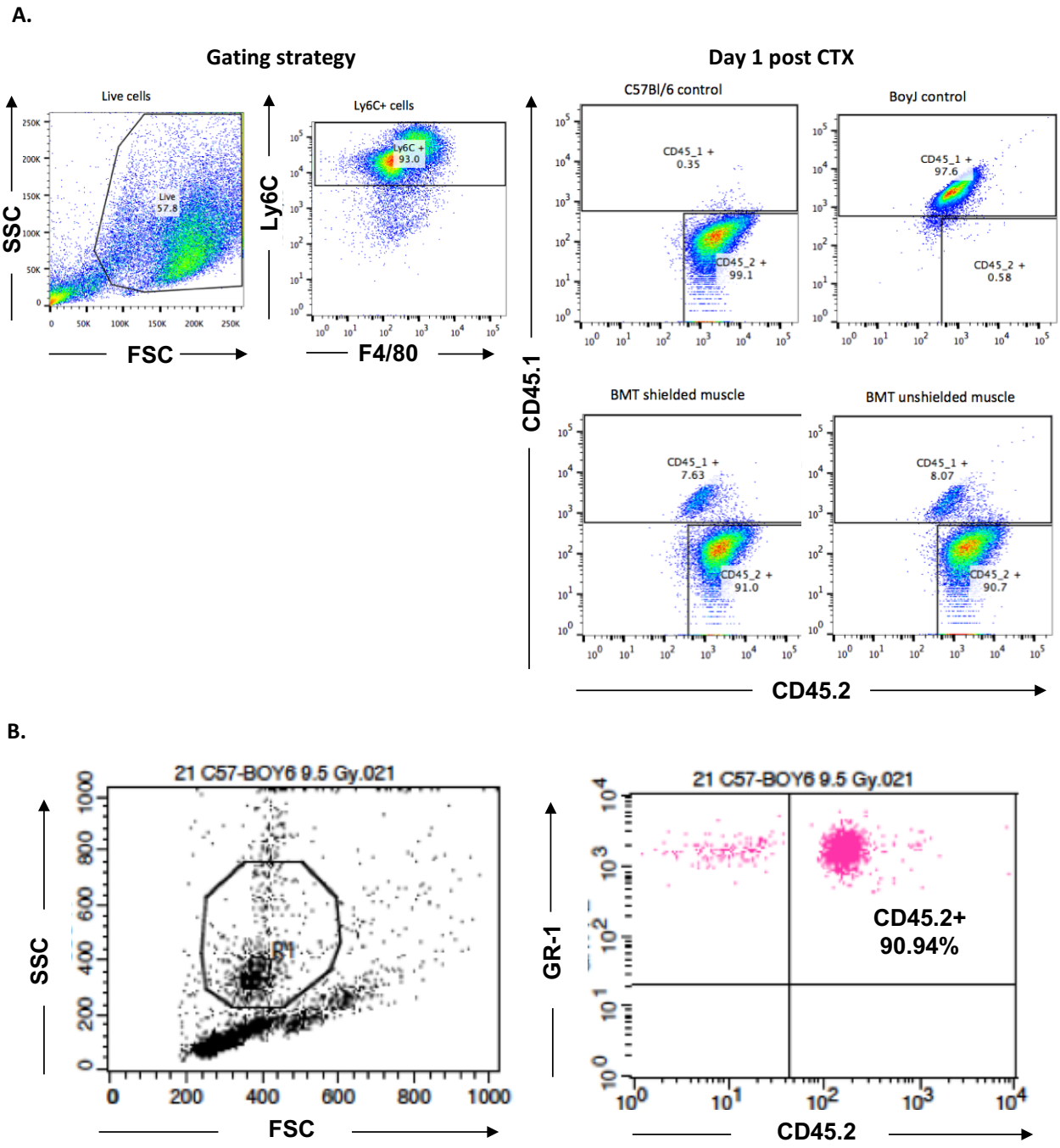

Figure 23. Infiltrating cells in both the BMT-shielded and BMT-unshielded muscles share the same features and originate from the donor C57BL/6J bone marrow.

A. Muscle macrophages origin tracing based on the myeloid lineage markers CD45.1 (host BoyJ bone marrow stains positive for CD45.1 but not CD45.2) and CD45.2 (donor bone marrow stains positive for CD45.2 but not CD45.1) at day 1 post CTX injury. Both the BMT-shielded and BMT-unshielded muscles were over 90% CD45.2 positive (n=4 per group).

B. Blood chimerism levels from the same BMT animals prior to the above terminal experiment (n=4 per group).

In order to make sure that muscle metabolism is not interfering with our labeling, PET-MRI experiments were always performed during the light cycle in which the activity of the mice is minimal and thus muscles considered being at rest. In addition, in various exercise physiology studies (Tashiro, Fujimoto et al. 1999), (Kemppainen, Fujimoto et al. 2002), (Slimani, Oikonen et al. 2006), (Haddock, Holm et al. 2016) FDG uptake in resting muscles is minimal and thus in our experiments Day 0 served as the baseline, allowing us to follow the metabolic changes in the muscle, as the result of CTX injury, and exclude the contribution of skeletal muscle activity. By the quantitative analysis of the decay-corrected ^{18}F-FDG PET images we found significant differences in the mean standardized uptake values (SUV) of the indicated TA muscle tissues 50 min after tracer injection and at various time points (Day 0-8) post CTX injury (**Figure 24A**).

The ^{18}F-FDG accumulation in the leg was overall significantly higher in the injured TA muscle area in all the timepoints we checked, compared to control uninjured animals (mean SUV was 0.21 ± 0.01) (**Figures 24A and 24C**). The ^{18}F-FDG accumulation of the gastrocnemius (GAST) muscle area showed very low signal and served as a negative control in all timepoints (mean SUV: 0.17 ± 0.02). The radiotracer uptake from injured muscle region at Day 2 was approximately two-fold higher (0.55 ± 0.01) compared to all other timepoints followed by Day 1 (0.42 ± 0.01) and Day 4 (0.37 ± 0.01) post injury (**Figure 24C**). Next, based on the significantly increased PET signal we observed at Day 2 post CTX, we asked whether the signal comes from the muscle resident cells or the infiltrating immune cells. To tackle this question, we decided to perform an *ex vivo* ^{18}F-FDG uptake on isolated myeloid CD45^{+} versus non-myeloid CD45^{-} cells from D1 and D2 injured muscles (10^{6} live cells sorted based on FSC/SSC gating were used for each group). In accordance with our hypothesis myeloid CD45^{+} cells seem to uptake and utilize more ^{18}F-FDG compared to non-myeloid CD45^{-} cells (**Figure 24D**), which is line with previous observations (Gamelli, Liu et al. 1994), (Hyafil, Cornily et al. 2009), (de Prost, Tucci et al. 2010), where macrophages co-localize with the *in vivo* PET signal in inflamed tissues. Furthermore, the increased ^{18}F-FDG uptake of the myeloid cells (**Figure 24D**), overlaps with the kinetics of the myeloid cell numbers infiltrating the injured muscle (**Figure 20D**). However, one should note that CD45^{-} cell fraction might contain a low percentage of dead cells.

In summary, we demonstrated that ^{18}F-FDG PET-MRI is a valuable tool to monitor immune cell invasion *in vivo*. Thus, we used it in order to delineate and further explain the difference in the regeneration process between BMT-shielded and BMT-unshielded muscles. By the quantitative analysis of the decay-corrected ^{18}F-FDG PET images we found significant differences in the mean SUV of the BMT-shielded *versus* BMT-unshielded muscles at various time points (Day 2-6) post CTX injury (**Figures 24B and 24E**) which overlaps with the delayed dynamics of the inflammatory response (**Figures 22F-H**) we observed previously with FACS. More specifically we detected a significantly lower accumulation of ^{18}F-FDG in the BMT-unshielded muscles compared to the BMT-shielded muscles of the same animal at Day 2, Day 4, Day 5 and Day 6 post CTX.

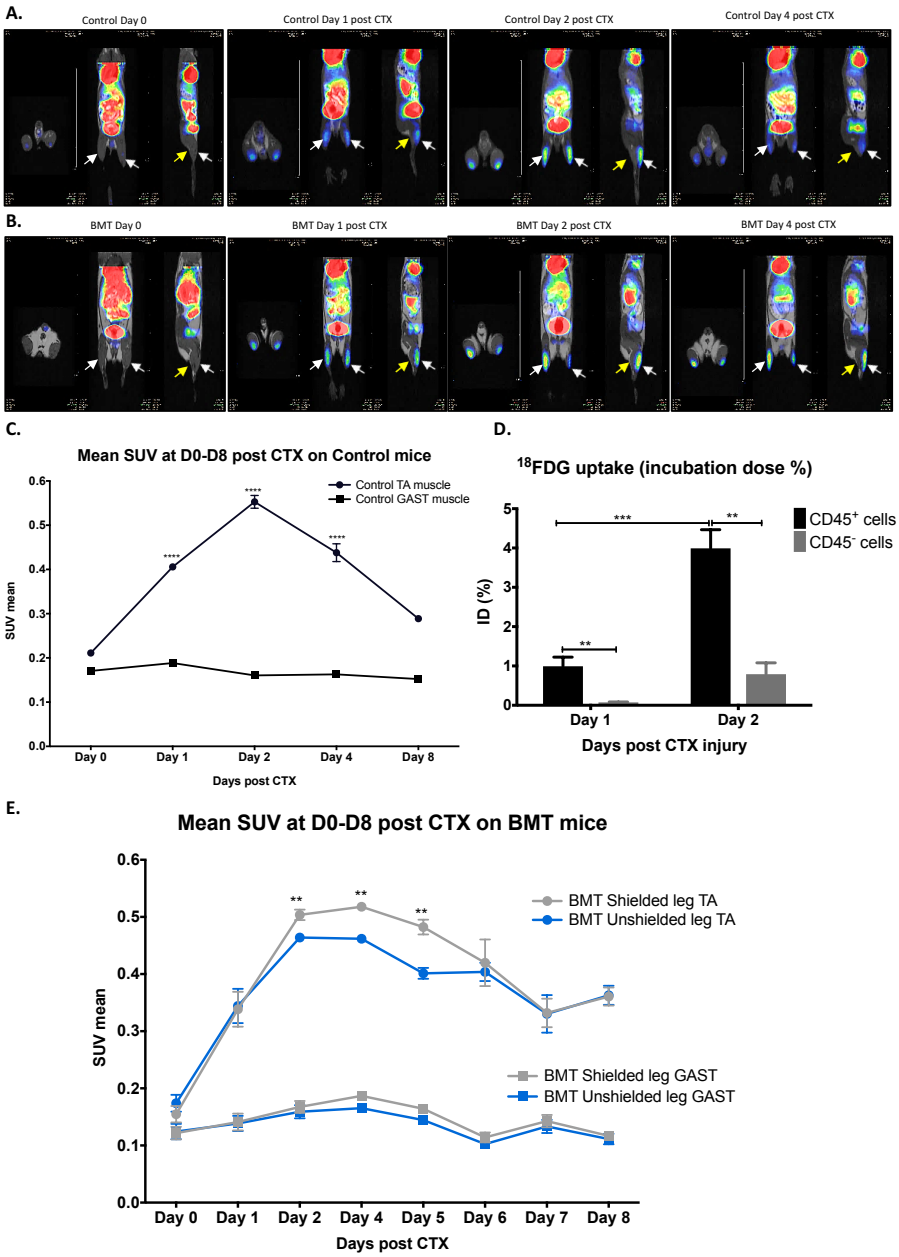

Figure 24. *In vivo* monitoring of the infiltrating immune response with ^{18}F-FDG PET-MRI.

A. Representative whole body PET-MRI images (axial, coronal and sagittal planes are shown) of control non-BMT at indicated timepoints post CTX injury. Images were obtained 50 mins after i.v. injection with 8.0±0.2 MBq ^{18}F-FDG. Arrows show muscles under consideration (white arrows indicate Tibialis anterior and yellow arrows indicate Gastrocnemius). Corresponding video images are included in Supplementary material.

B. Representative whole body PET-MRI images (axial, coronal and sagittal planes are shown) of BMT mice with right leg radioprotection (lower panel) at indicated timepoints post CTX injury. Images were obtained 50 mins after i.v. injection with 8.0±0.2 MBq ^{18}F-FDG. Arrows show muscles under consideration (white arrows indicate TA and yellow arrows indicate GAST). Corresponding video images are included in Supplementary material.

C. Quantitative analysis of the ^{18}F-FDG uptake of the injured TA muscles in control non-BMT at indicated timepoints post CTX injury. ^{18}F-FDG-Standardized Uptake Value (SUV) mean of TA and GAST (used as baseline muscle SUV mean) muscles are shown (n=8).

D. *Ex vivo* ^{18}F-FDG uptake (shown as incubation dose % per 10^6 live cells) of the myeloid CD45$^+$ versus non-myeloid CD45$^-$ cell fractions (10^6 live cells were sorted in each group/experiment) of the injured TA muscles in control non-BMT at indicated timepoints post CTX injury (n=4).

E. ^{18}F-FDG-Standardized Uptake Value (SUV) mean of injured TA and uninjured GAST muscles from BMT-shielded versus BMT-unshielded muscles of the same animal at indicated timepoints are shown (n=8).

In all graphs, mean values ± SEM are shown.

In vivo ablation of Pax7^{+} cells produces similar phenotypic transition delay on infiltrating macrophages

The radioprotection and *in vivo* imaging experiments presented in this dissertation showed that lead shielding during radiation exposure prevented the delay of muscle regeneration following CTX injury, preserved the local muscle cell composition and sustained infiltrating myeloid cell kinetics and metabolic properties at control levels, suggesting that the infiltrating immune response of skeletal muscle regeneration is regulated by a local radiosensitive tissue compartment, including PAX7^{+} satellite cells. In order to determine if the decrease in satellite cell numbers observed following radiation is contributing to delayed macrophage phenotypic shift, we decided to deplete satellite cells *in vivo* before the injury. By using a transgenic mouse model for selective diphtheria toxin-induced depletion of PAX7^{+} satellite cells (Nishijo, Hosoyama et al. 2009), we observed that satellite cell ablation (Pax7 Cre^{ER}-DTA), leads to a significantly decreased muscle mass following the injury (**Figures 25A-B**). This result is in agreement with the current literature in which PAX7 positive satellite cells are indispensable for skeletal muscle regeneration both for development (Fry, Lee et al. 2014) and following an acute injury (Lepper, Partridge et al. 2011), (Sambasivan, Yao et al. 2011). Interestingly satellite cell ablation led to alterations not only in muscle macrophage infiltration numbers both at Day 4 and Day 6 post CTX (**Figure 25C**) but also in dynamic MFs phenotype shift (**Figures 25D-G**), similar to irradiated and BMT-unshielded muscles. Therefore, these data suggest that it is indeed Pax7-lineage cell pool, which is regulating, at least in part, the repair macrophage phenotype transition.

Taken together, our data reveal the existence of a reciprocal cross talk between the skeletal muscle tissue and myeloid cells recruited following the injury and establish an experimental paradigm suitable to dissect the components of immune cell invasion assisted tissue repair.

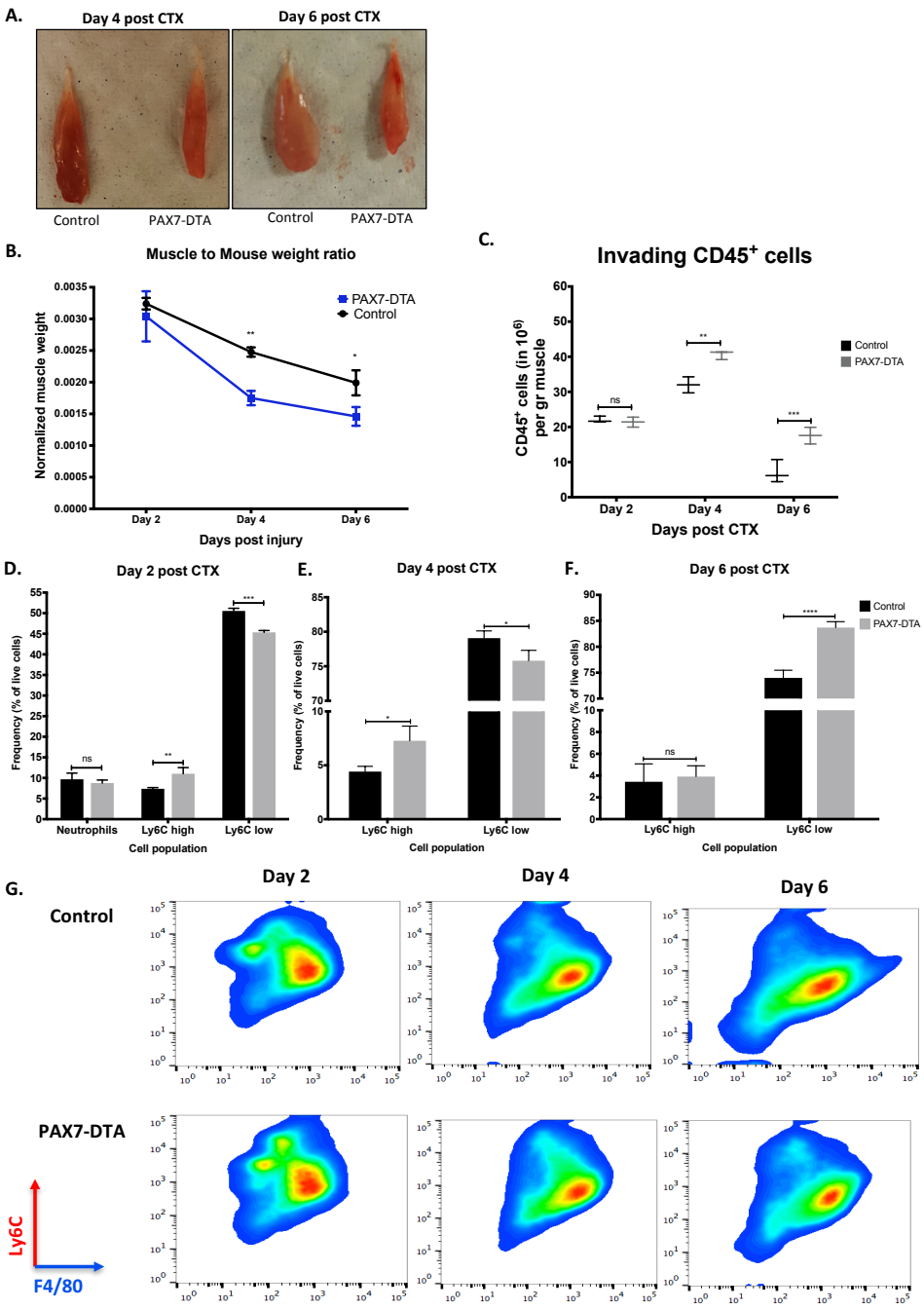

Figure 25. Delayed phenotypic transition of infiltrating myeloid cells in satellite cell depleted animals following CTX injury.

A. Representative macroscopical image of TA muscles from control (left) and satellite cell ablated PAX7^{ER} – DTA (right) animals at day 4 and 6 post CTX injury.

B. TA muscle weight from control versus PAX7^{ER} – DTA animals at indicated timepoints following CTX injury (n=4 per group).

C. Number of infiltrating myeloid (CD45^{+}) cells in regenerating muscle of satellite cell depleted animals (PAX7^{ER} – DTA), at day 2, 4 and 6 post CTX injury (n = 16 muscles per group).

D. Percentage of inflammatory (Ly6C^{high} F4/80^{low}) and repair (Ly6C^{low} F4/80^{high}) muscle MFs from control and PAX7^{ER} – DTA animals at day 2 following CTX injury, respectively (n = 12 mice per group).

E. Percentage of inflammatory (Ly6C^{high} F4/80^{low}) and repair (Ly6C^{low} F4/80^{high}) muscle MFs from control and PAX7^{ER} – DTA animals at day 4 following CTX injury, respectively (n = 12 mice per group).

F. Percentage of inflammatory (Ly6C^{high} F4/80^{low}) and repair (Ly6C^{low} F4/80^{high}) muscle MFs from control and PAX7^{ER} – DTA animals at day 6 following CTX injury, respectively (n = 12 mice per group).

G. Representative FACS images of Ly6C^{high} F4/80^{low} and Ly6C^{low} F4/80^{high} macrophages at day 2, 4 and 6 post CTX injury. Upper panel shows representative samples from control animals while lower panel from PAX7^{ER} – DTA animals.

In all graphs, mean values ± SEM are shown.

Limitations

There are some technical limitations of this part of the work. By using this modified BMT method in studies to assess myeloid contribution in muscle regeneration, the sample size might be too small (using only the shielded leg) and thus it could be difficult to find significant relationships among the data, due to the fact that statistical tests for such quantitative (i.e. CSA) studies will require a larger sample size. This will lead to doubling the number of animals in order to ensure a representative distribution of myofiber size and to reliably conclude as to the outcome of regeneration. Furthermore, the increase in cell numbers to be transplanted from $5x10^6$ to $20x10^6$ will also increase the number of donor BM animals. Another limitation of our study is the usage of a human cobalt radiation source (gamma rays being used). Since various radiation sources (some are exclusively build for small animal research use) and types exist, such as gamma rays, and X-rays (lower energy and longer wavelength compared to gamma rays), with the latter being the most frequently used in radiation and BMT research, one cannot exclude the possibility of slightly different satellite cell ablation, chimerism and shielding efficiency depending on the aforementioned parameters. In addition, the radiation dose we chose and optimize was specific for the C57BL/6J strain. One needs to keep in mind that different inbred strains can tolerate different radiation doses (Duran-Struuck R et al. 2008). Thus, minor dose and shielding optimization will be needed to attain comparable results. Finally, a conceptual limitation is that the contribution of other cell types to the observed phenotype cannot be excluded with absolute certainty.

G. Discussion

Inflammation triggers a broad array of physiological and pathological processes and is evolved as a response to restore homeostasis. Although the pathological features of many types of inflammation are well understood, their physiological functions are mostly unknown. Thus, in order to develop specific therapeutic interventions of tissue malfunction or homeostatic imbalance (caused by dysregulated inflammation), the origins and physiological features of an inflammatory response need to be understood in a broader physiological context. The cardiotoxin (CTX) induced skeletal muscle injury model is an ideal experimental system to study physiological inflammation dynamics and tissue environment dependent monocyte-to-effector macrophage transition processes (Tidball 2017). This model induces a synchronous inflammation process allowing the isolation of homogenous cell populations. Upon injury, circulating monocytes enter the damaged tissue area and differentiate to macrophages with an inflammatory phenotype (Ly6C^{high}) and that very fast (within 1-2 days) the same cells shift to a Ly6C^{low} repair macrophage phenotype (Varga, Mounier et al. 2013), (Tidball 2017). The present work reveals unexpected highly dynamic changes of gene expression by macrophage populations during acute inflammation and subsequent tissue repair, confirming the highly versatile nature of these cells, that can hardly be addressed *in vitro*. We show that macrophages from regenerating muscle are distinct from resting macrophages in other tissues, while they still are true macrophages. Unbiased analysis of gene expression by macrophage populations during muscle regeneration revealed that time segregation, much more then Ly6C status segregation showed the highest differential gene expression. Thus, the time course of inflammation is the predominant organizing force in gene expression by macrophages, with an important time point at day 2-4 post injury, which corresponds to the full skewing of macrophages from Ly6C^{high} to Ly6C^{low} status and the starting of resolution of inflammation.

Several groups have independently demonstrated that Ly6C^{high} macrophages express higher levels of pro-inflammatory cytokines (IL-1β, TNFα) and lower levels of anti-inflammatory cytokines (TGFβ, IL-10) than Ly6C^{low} macrophages. Therefore, these macrophage subsets were identified as M1 and M2 macrophages, respectively, to parallel the expression of these cytokines by *in vitro* LPS/IFNγ and IL-4 activated macrophages, respectively (Xue, Schmidt et al. 2014). The data presented here show that although Ly6C^{high} macrophages preferentially expressed pro-inflammatory markers and Ly6C^{low} macrophages preferentially expressed anti-inflammatory markers, the differences are not large, despite the limitation of global RNA analysis and the fact that low change in mRNA expression may lead to big changes in function at the protein level. These results indicate that *in vivo*, macrophages cannot be restricted and defined according to the M1/M2 nomenclature and display highly different inflammatory profiles than those previously described *in vitro*.

Comparison of Ly6C^{high} versus Ly6C^{low} macrophages, as well as comparison of the same cell subset with time revealed high dynamic changes of gene expression by macrophage subsets during muscle regeneration. These dynamics allowed to highlight 3 main features of macrophages during muscle regeneration. The first feature is early expression of acute phase proteins and scavenger receptors by Ly6C^{high} and Ly6C^{low} macrophages, respectively. These macrophages were the most numerous at day 2 and they highly expressed a series of genes involved in inflammation. Acute phase proteins, defined as proteins which plasmatic

concentration highly increases (or decreases) upon acute inflammation, exert a plethora or both pro- and anti-inflammatory functions during both the initiation and the resolution of inflammation (Gabay and Kushner 1999). Scavenger receptors on the other hand are thought to participate in the removal of necrotic debris in the living body by extensive ligand specificity and a variety of receptor molecules (Politz, Gratchev et al. 2002). Here we show that Stabilin-1 is upregulated in the Ly6C^{low} fraction. Its molecular mechanism and mode of action needs further investigation.

Second, expression of ECM components during the early phase of the regeneration process. Data presented here show that Ly6C^{high} macrophages expressed ECM proteins at day 1 of regeneration. These ECM proteins are usually involved in cell-cell interactions, intercellular communication processes and regulation of ECM organization (Mouw, Ou et al. 2014). Among them, Versican seems to be involved and differentially regulated in skeletal muscle regeneration. While the majority of such molecules have been shown to exert some effects on macrophages; mainly through chemotactic activity; their expression by macrophages themselves has been less documented (Wight, Kang et al. 2014). By being exclusively expressed on day 1 Ly6C^{high} MFs it implies that it might be involved in the phenotypic transition of macrophages. In addition, our results suggest that macrophages may directly act on the ECM environment by participating to the synthesis of ECM components and molecules that regulate ECM constituents. Further investigation would decipher the significance of such an expression beside that of interstitial cells at the early phases of tissue healing.

The third feature, is the metabolic change of macrophages at the time of resolution of inflammation. Between day 2 and day 4 of regeneration, Ly6C^{high} macrophages undergo a switch of their phenotype, to acquire an anti-inflammatory phenotype and become Ly6C^{low} cells. Apart from the genes directly linked to the inflammatory process (chemokines, cytokines, etc.), genes involved in the regulation of cell metabolism have been shown to vary according to the inflammatory status of macrophages. However, while metabolism is foreseen as an important regulator of macrophage function, notably in diseases (Biswas and Mantovani 2012), few studies addressed specific metabolic pathways linked to a specific macrophage inflammatory status (Haschemi, Kosma et al. 2012). For example, GDF15 has been shown to prevent obesity by increasing thermogenesis, lipolysis and oxidative metabolism (Chrysovergis, Wang et al. 2014). Here we identified GDF15 been differentially upregulated during the repair process in the Ly6C^{low} MFs and its absence negatively impacts muscle regeneration. A potential mechanism by which GDF15 exerts its action is by directly acting on satellite cells controlling their proliferation and expansion following the injury. In addition, we observed a strong upregulation of PPARg, which is characteristic of M2 (IL-4) macrophages *in vitro* (Jha, Huang et al. 2015), at the late steps of muscle regeneration (day 4) in Ly6C^{low} macrophages.

In this dissertation, we have identified the ligand activated transcription factor, PPARg as a regulator of macrophage functions during muscle regeneration (findings summarized in **Figure 26**). By using two distinct genetic models (conditional macrophage specific KO and BMT), it allowed us to focus on the role of PPARg in MFs. The delay in regeneration in PPARg deficient animals was profound and detectable as long as three weeks after the initial injury, thus appearing to be among the most dramatic reported deficiencies in regeneration caused by impairments in MF functions (Mounier, Théret et al. 2013). It is interesting to note that several distinct features of the regeneration delay, such as impairment in CSA, and persistent presence

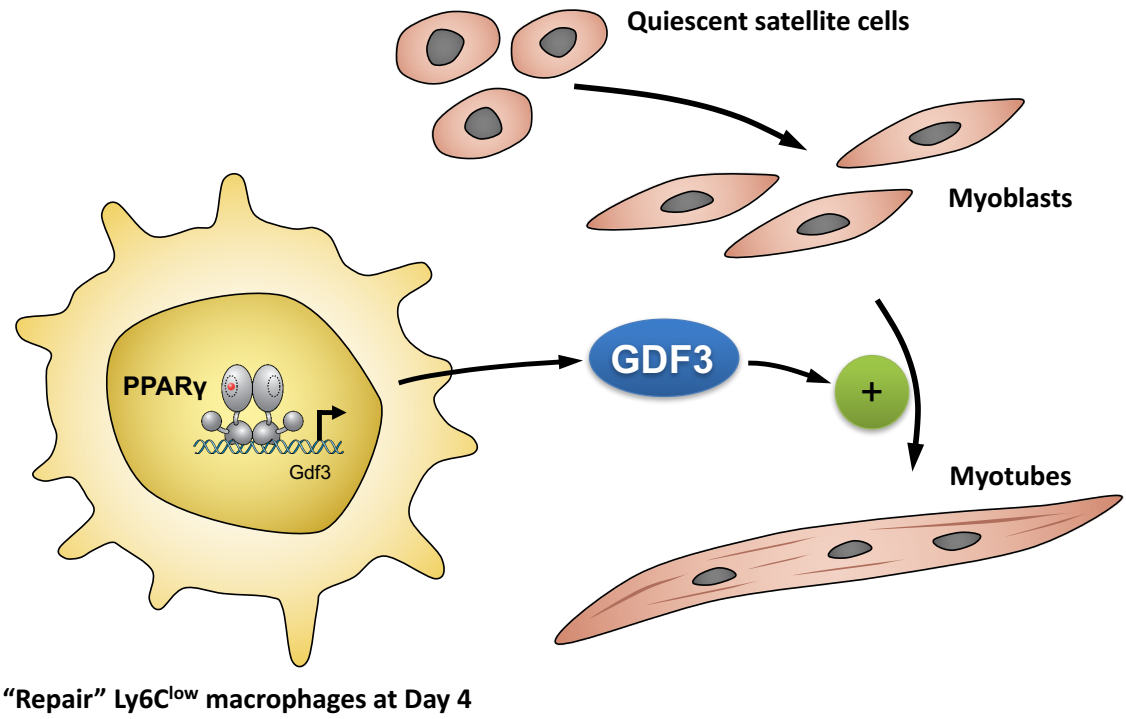

Figure 26. Macrophage PPARg, a lipid activated transcription factor controls Growth Differentiation Factor-3 and skeletal muscle regeneration.

of necrotic fibers were present after CTX injury in PPARg MacKO animals. Systematic transcriptomic analyses, provided clues about both the sensory and the regulatory roles of PPARg in muscle infiltrating MFs. We here described several potential new PPARg target genes. It is important to stress that earlier descriptions of direct PPARg target genes often reported lipid metabolic genes as the main targets PPARg of in MFs, which could poorly explain the anti-inflammatory role of the receptor (Szanto, Balint et al. 2010). We report here that the transcriptional activity of PPARg is unique in muscle macrophages, because the most robustly changing genes (such as Saa3, Hebp1) are linked to inflammation, rather than to lipid metabolism. The most intriguing interpretation of the available data would be the involvement of a yet unidentified endogenous ligand for PPARg whose activity is restricted to the Ly6C^{low} compartment. Importantly, PPARg activity in the Ly6C^{low} MF subtype, which dominates the regenerative phase of muscle injury suggests that PPARg is a licensing factor for repair MFs. From the perspective of muscle regeneration, the most important finding was the identification of GDF3, which showed consistent regulation by PPARg in all relevant MF subtypes. Importantly, GDF3 is a strong candidate as a MF derived paracrine factor with muscle regenerative functions, whose diminished macrophage-linked expression is consistent with the impaired regeneration seen in PPARg deficient animals. To link macrophage biology to tissue regeneration, we analyzed the role of MF derived GDF3 in muscle regeneration in a combination of *in vivo* and *in vitro* approaches. Foremost, two genetic models of GDF3 deficiency (full body KO and BMT) reported a delay in regeneration. While the decrease in average CSA in Gdf3 KO animals was comparable to that seen in PPARg MacKO animals, Gdf3 KO animals did not display persistent inflammation and delayed clearance of necrotic fibers. This suggested that PPARg regulates several other

pathways during regeneration. Importantly, a gain of function experiment revealed that exogenous GDF3 administered locally *in vivo* could counteract the deleterious effect of PPARg deficiency in MFs. In addition, GDF3 appeared to be an especially robust enhancer of myoblast fusion. Taken together, GDF3, which is expressed in and secreted by muscle infiltrating MFs within injured and regenerating muscles, has the capacity to elicit biologically relevant responses in primary myoblasts and differentiating myotubes and is a regulator of both *in vitro* muscle differentiation and muscle regeneration *in vivo*. As other cell types are also involved in the regeneration process (Heredia, Mukundan et al. 2013), (Joe, Yi et al. 2010), (Uezumi, Fukada et al. 2010), it cannot be excluded that other TGFβ family members such as GDF15 are active during regeneration and that it has effects on other cell types such as fibro/adipogenic progenitors as well (Hidestrand, Richards-Malcolm et al. 2008), (Joe, Yi et al. 2010), (Lemos, Babaeijandaghi et al. 2015).

Our findings also carry potential implications for pathological circumstances in which muscle damage and asynchrony in repair due to aging leads to severe impairment in muscle function. Here, we show that GDF3 seems to be a regulator of muscle regeneration in geriatric models as well, which are most of the time associated with the permanent presence of inflammatory cells (findings summarized in **Figure 27**). These findings suggest that MF derived factors such as GDF3 and GDF15 could also be used as part of other therapeutics to regulate not only regeneration, but also muscle and bone growth (Chen, Walton et al. 2015). To conclude the present work, so far, highlights an unexpected dynamic of the molecular signature of macrophage subsets during skeletal muscle regeneration and the identified PPARg is a required metabolic sensor and transcriptional regulator of repair macrophages, that controls the expression of GDF3, which in turn regulates the restoration of skeletal muscle integrity by promoting muscle progenitor cell fusion (Varga, Mounier et al. 2016). However, our understanding is fairly limited regarding the role of other transcription factors sensing the macrophage's tissue environment especially in the context of epigenetic and transcriptional regulation as well as contributing to macrophage effector functions. A logical extension to these studies was to employ unbiased epigenomic profiling, to identify molecules regulating phenotypic transition and effector functions of inflammatory and repair macrophages.

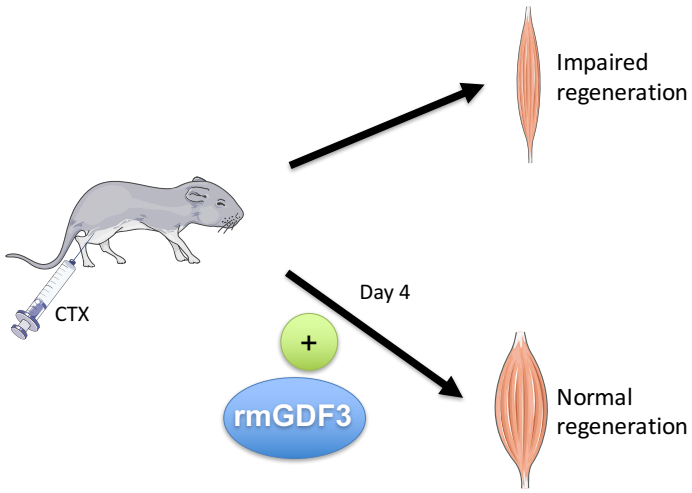

Figure 27. Growth Differentiation Factor-3 restores muscle regeneration kinetics in geriatric mice following acute sterile muscle injury.

The phenotypic transition from the monocyte progenitors to inflammatory Ly6C^{high} and then to repair Ly6C^{low} cells is highly correlated with the tissue regeneration kinetics and is accompanied by a dynamic crosstalk between macrophages and other muscle tissue components that lead to a hierarchical chromatin and transcriptional reprogramming process. In order to delineate the order of transcriptional events during monocyte infiltration and *in situ* macrophage differentiation and to identify novel candidate genes and signaling pathways regulating *in situ* macrophage function and tissue regeneration, we sought first to map these changes by generating chromatin accessibility maps (genomic regions that are highly bound by transcription complexes) using the ATAC-seq method (Buenrostro, Giresi et al. 2013). By using ATAC-seq on circulating monocytes and muscle infiltrating macrophages from day 1, 2 and 4, detection of differentially opening sites in time allowed us to expand our analysis and look for the actual transcriptional regulators that might be responsible for these changes. Coupling standard bioinformatic analysis with innovative clustering algorithms, we found that a large class of more than 9000 genomic regulatory elements is becoming *de novo* accessible during monocyte infiltration in the muscle. Importantly, motif analysis showed that these sites were very highly enriched (58% of sites) to AP-1 motif (including the Maf recognition element - MARE) compared to other common macrophage specific motifs (PU.1, C/EBP). This intriguing finding prompted us to ask the following questions: 1) what are the AP-1 motif binding transcription factors that potentially regulate these *de novo* accessible sites, and 2) how these AP-1 factors contribute overall to macrophage polarization during muscle regeneration. Potential candidates would include known AP-1 factors such as Jun, Fos, NF-E2 and others that have been shown to form homo- or hetero- dimers to activate their gene targets. However, such factors are usually inducible and bind to DNA by continuously competing with other AP-1 family members. This mode of action is interesting as it suggests that repressor factors bind to low accessible sites and precede activators and that such early chromatin priming by bookmarking transcription factors might be important to activator recruitment and thus to the effective control of transient activation programs. We hypothesized that such transcription factors are in place in our experimental system and we set the following criteria to narrow down candidate regulator transcription factors: 1) ability to bind AP-1 motifs with repressor activity, 2) high expression in monocytes and macrophage populations and 3) direct sensor of cellular environment changes (such as metabolite concentration changes). It has been shown that during muscle damage, profound changes in heme and iron involved genes can be observed (Corna, Caserta et al. 2016). Muscle-infiltrating macrophages carry out this function thus preventing the deleterious effects caused by its oxidizing action (Hentze, Muckenthaler et al. 2010). In addition, the ability of infiltrating macrophages to export iron is crucial to avoid fat accumulation during the regeneration process (Corna, Caserta et al. 2016). Myoglobin, which is released because of the muscle necrosis possibly influences the expression of iron homeostatic genes which in turn might reflect on macrophage phenotype switch. Thus, based both on literature search and available transcriptomic data, we narrowed down to the heme sensing transcription factor BACH1 (findings summarized in **Figure 28**).

The transcription factor BACH1 forms heterodimers with small Maf proteins that binds to the Maf recognition element (MARE), a subcategory of AP-1 motif, to act as transcription repressor (Zhou et al., 2016). BACH1 is expressed in most cell types, but it is more highly upregulated in hematopoietic cells (macrophages, dendritic cells and thymic T cells). Notably,

BACH1 possesses a heme-binding region and thus can be directly bound by free heme that is released by many hemoproteins such as hemoglobin and myoglobin usually following acute tissue damage. Heme binding destabilizes BACH1, thus inhibiting its DNA binding capacity, and subsequently BACH1 is exported from nucleus and degraded in the proteasome. Subsequently, the transcription factor NF-E2, competing for the same MARE sites, heterodimerizes with small Mafs and activates BACH1 target genes, such as the heme oxygenase 1 enzyme (Hmox1) to further degrade heme to less harmful metabolites (**Figure 12B**), to biliverdin, ferrous iron, and carbon monoxide (Alam, Devalaraja et al. 2017). Absence of BACH1 leads to constitutive expression of Hmox1 (Sun, Hoshino et al. 2002). Thus, according to existing literature, BACH1 functions as a metabolite driven regulator of heme and iron metabolism, metal detoxification and cellular signaling programs. BACH1 has largely an invariable gene expression profile among different populations of macrophages and, interestingly, it has been predicted by transcriptomic analysis of the Immunological Genome Project (Immgen) to be among the core regulator of macrophage identity, along with TCEF3, C/EBP-α, and CREG-1. However, contrary to expectations based on its importance and ubiquitous presence, the existing mouse model has minimal macrophage developmental defect and no overall physiological defects in mouse development and lifespan (So, Garcia-Flores et al. 2012), (Ota, Brydun et al. 2014). In addition, in experimental injury and inflammatory models, these animals show protective phenotypes and dampened overall inflammatory responses (Harusato, Naito et al. 2009), (So, Garcia-Flores et al. 2012). To test our hypothesis that the heme-BACH1-Hmox1 axis contributes to macrophage function during muscle injury and regeneration, we performed CTX experiments in heme treated, Bach1 KO and Hmox1 conditional KO mice. Histology and morphometric analysis showed that these mice have delayed muscle repair and regeneration kinetics (extensive and persistent necrotic content in the muscle tissue and smaller mean muscle fiber size compared to controls).

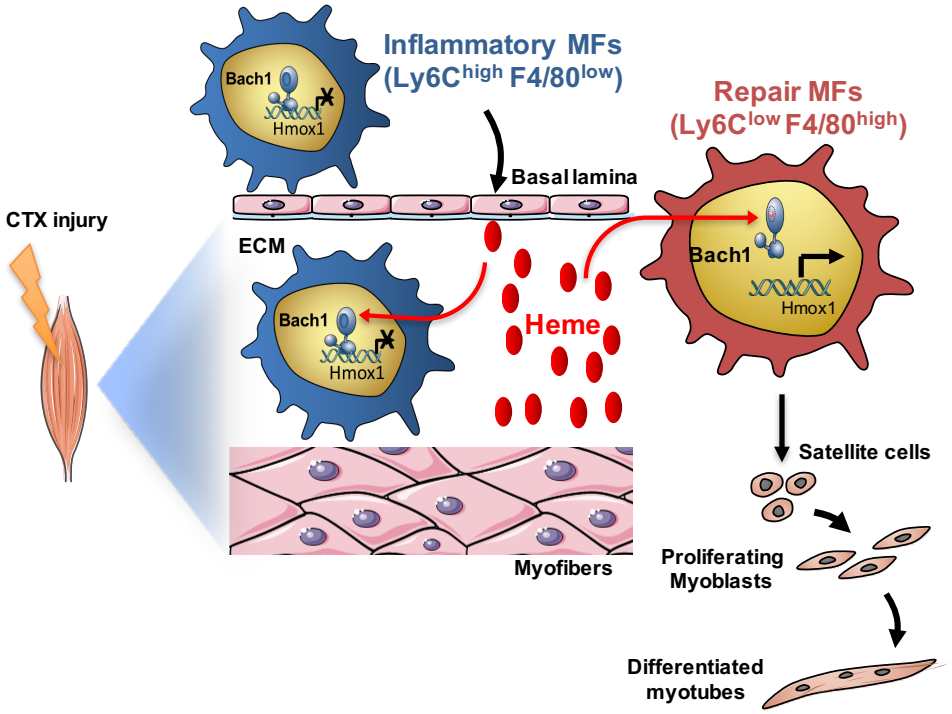

Figure 28. A regulatory axis, involving heme, BTB Domain And CNC Homolog-1, and Heme Oxygenase-1, controls the phenotype and function of the infiltrating myeloid cells upon tissue damage, shaping the overall tissue repair kinetics.

Bone marrow transplantation experiments showed that this defect is intrinsic to myeloid cells and not attributed to BACH1 function in muscle cells. FACS analysis showed comparable cell numbers of infiltrating myeloid cells but a reproducible higher (in the case of Bach1 KO and heme treated mice) or lower (in the case of the macrophage conditional Hmox1 KO) ratio of repair ($Ly6C^{low}$) to inflammatory ($Ly6C^{high}$) macrophages at day 4 post CTX. To our knowledge only three other experimental systems (DUSP1, AMPKa1 or IGF1 deficiency in muscle infiltrative MFs) were reported to lead to altered MF differentiation (Perdiguero, Sousa-Victor et al. 2011), (Mounier, Théret et al. 2013), (Tonkin, Temmerman et al. 2015). Notably, neutrophil invasion is a generic and indispensable response to acute muscle injury. This early invasion of neutrophils in injured muscle allows them to condition the inflammatory environment and to influence the activation state of subsequent immune cell populations. For example, circulating monocytes and macrophages extravasate and enter a muscle environment that is enriched with pro-inflammatory cytokines produced by neutrophil. Thus, it is not impossible that Bach1 in neutrophils contributes to the overall macrophage phenotypic impairment observed in the KO. Further investigation would decipher the significance of such interactions at the early phases of the inflammatory responses.

Complementary to this *in vivo* analysis and to gain insights to the molecular function of BACH1, we used eRNA measurements, and the BMDM differentiation system to map BACH1 novel binding sites and potential target genes using ChIP. We found that BACH1 binds to a large number of activated enhancers and accessible sites in the genome based on the ATAC-seq mapping. Importantly, BACH1 extensively binds to a number of gene loci (Il6, Il10, Cebpb, Dusp1, PPARg, Igf1, Slc40a1, GDF3) previously shown to participate and heavily impact the regeneration process. These observations expand the current view of BACH1 as mere rheostat of heme-oxygenase 1 expression and potentially suggest BACH1 involvement in a bookmarking mechanism of genomic sites yet to be activated in macrophages when appropriate signals become present or of an active repressing mode action to genomic regions, active in other cellular states, environments or lineages. Taken together, these results suggest that proper muscle regeneration depends on tightly and timely regulated inflammatory responses following acute injury and that BACH1 likely acts to fine-tune activation, phenotypic transition and resolution of inflammatory programs. Lastly, BACH1's protein structure and capacity to bind metabolites and sense the tissue micro-environment makes it an attractive model to test how such signal integrators sense different tissue stimuli and shape different transcriptional programs and diverse macrophage subtypes.

Tissue regeneration is a complex but precisely coordinated array of processes involving cellular recruitment, differentiation, phenotype switches, and intercellular communications. It is remarkable, though, that the key elements of the myogenic cross talk between macrophages and myoblasts suggest that these two cell types and their interactions are critical to support regeneration. In the final part of this work, we document that (1) altered cellular composition affects the *in situ* phenotypic transition of invading myeloid cells to repair macrophages, thus (2) revealing the existence of reciprocal intercellular communication between satellite cells and recruited macrophages during skeletal muscle regeneration, and (3) establish a combination of methods to use bone marrow transplantation, with local muscle radiation shielding, to identify myeloid cell contribution to tissue repair and monitor the myeloid cells metabolic activity *in vivo* (findings summarized in **Figure 29**).

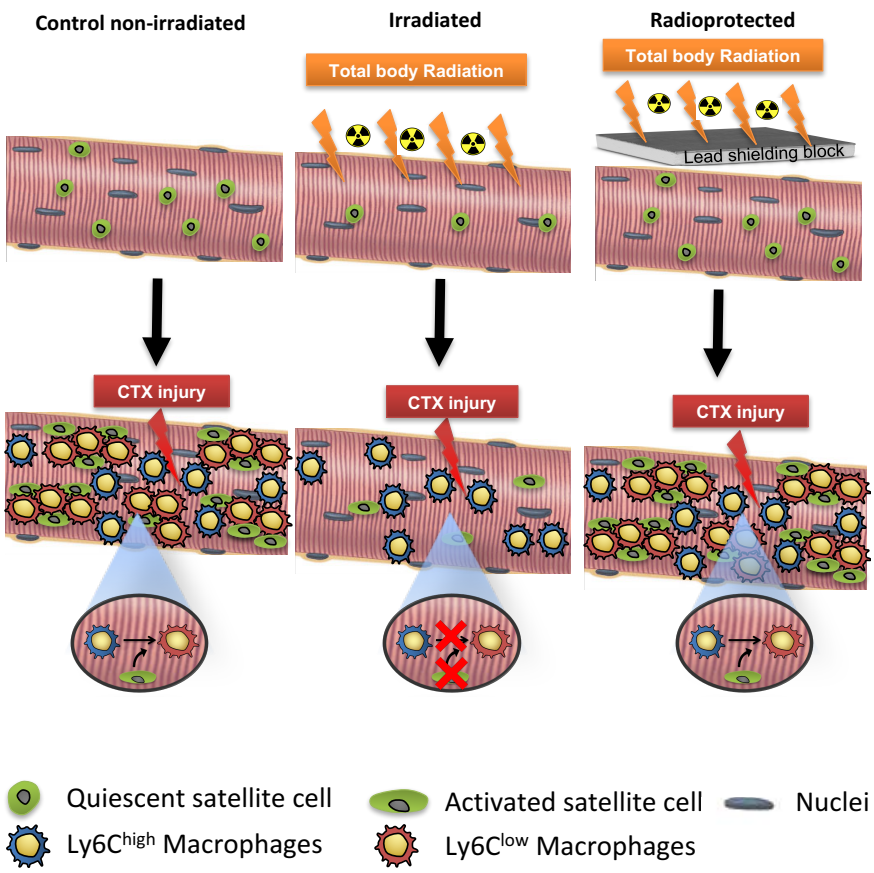

Figure 29. Satellite cells and other local populations affects macrophage transition from inflammatory (Ly6C^{high}F4/80^{low}) to repair(Ly6C^{low}F4/80^{high}) phenotype, which is critical for normal muscle tissue repair dynamics.

As mentioned several times in this dissertation the skeletal muscle microenvironment is very heterogeneous, with distinct cell types such as satellite cells, fibroblasts, fibro/adipogenic progenitors (FAPs) adipocytes, epithelial cells, Schwann cells, and blood cells, all of which may influence and, in turn, be influenced by local structural and biochemical cues (Bentzinger, Wang et al. 2013). The general consensus holds that satellite cells are required for muscle regeneration. Here we show that both, radiation-induced or *in vivo* ablation (PAX7-DTA) of these cells, leads to delayed repair macrophage phenotypic transition and muscle regeneration. While there have been several papers demonstrating that infiltrating macrophages influence satellite cell behavior (Cantini, Massimino et al. 1994), (Cantini and Carraro 1995), (Saclier, Yacoub-Youssef et al. 2013), our data indicate that the reverse is also true, and that Pax7-lineage cells are regulating a degree of the *in situ* macrophage phenotypic shift. However, there are also additional cell types that are abundant in healthy muscle, and it's been recently shown that FAPs (Joe, Yi et al. 2010), (Uezumi, Fukada et al. 2010), fibroblasts (Murphy, Lawson et al. 2011), endothelial cells (Christov, Chretien et al. 2007), and other interstitial cells like pericytes (Dellavalle, Maroli et al. 2011), (Birbrair, Zhang et al. 2014), (Kostallari, Baba-Amer et al. 2015), expand following acute muscle damage, to transiently establish an environment that enhances myogenic differentiation. This raises the question whether perturbations of their cellular interplay with satellite cells or macrophages could further explain the delay in the macrophage phenotype switch. For example, it is known that angiogenesis is crucial for muscle repair and satellite cell survival. In this context, endothelial

cells strongly stimulate myogenic cell growth while myogenic cells promote angiogenesis (reviewed in (Latroche, Gitiaux et al. 2015)). On the other hand, during return to homeostasis, periendothelial cells facilitate the return to quiescence of a subset of muscle precursor cells that ensures self-renewal of the satellite cell pool (Abou-Khalil, Mounier et al. 2010). Irradiation activates endothelial cells which then participate in the recruitment of circulating cells, especially by overexpressing cell adhesion molecules (Jaillet, Morelle et al. 2017). Thus, it is possible that they directly influence the macrophage phenotypic shift in our system as well. Interestingly, depletion of $PAX7^+$ cells *in vivo* has no impact on vasculature ($CD31^+$ endothelial cells), innervation or neuromuscular junctions (Sambasivan, Yao et al. 2011). The same group also documented that FAPs and fibroblasts are unchanged in the $PAX7^+$ ablated muscles (Sambasivan, Yao et al. 2011), which suggests that the interaction of satellite cells with macrophages is unique and likely to be specific.

Substantially less is known about the role of the adaptive immune system in the regeneration process. Lymphocytes consistently infiltrate the muscle in conditions of chronic injury, including muscular dystrophies (Burzyn, Kuswanto et al. 2013), (Villalta, Rosenthal et al. 2014) and during aging (Kuswanto, Burzyn et al. 2016). Recent studies have shown that in acute injury models, like the CTX model, lymphocytes are recruited and required for the healing of the muscle (reviewed in (Schiaffino, Pereira et al. 2016). More specifically, T regulatory cells (Tregs) seem to be involved in muscle repair by directly interacting with satellite cells, inducing their expansion (Castiglioni, Corna et al. 2015). It was also shown that Tregs efficiently induced the phenotypic and functional switch to M2 macrophage differentiation *in vivo* (Liu, Duan et al. 2011), (Liu, Ma et al. 2011). Thus, it will be interesting for future studies to explore possible interactions of Tregs with satellite cells and macrophages in our system, which could potentially influence the phenotypic shift of the muscle infiltrating macrophages.

Our findings that PAX7 positive satellite cells affect macrophage phenotypic transition poses several more questions, regarding a potential niche for macrophages formed by satellite cells, what signaling molecules/cytokines influence the communication between these cell types and whether satellite cells produce signals that instruct macrophage functions such debris clearance, phagocytosis and myogenesis. It will require selective depletion or replenishment of satellite cells and other cell types to establish the cause and effect relationships between them and macrophage invasion, phenotypic switching and contribution to repair. Future studies should test whether radiation causes a depletion of these and other local interstitial cells with myogenic potential that could affect also the cross talk with the immune cells following acute damage, which in turn can affect macrophage infiltration and phenotypic dynamics, and subsequently muscle regeneration outcome.

In order to understand these complex interactions one needs more complex methodologies. We believe that our work here goes to some distance to address these needs. Cardiotoxin injection in TA muscles is very well suited to study immune cell infiltration because it induces extensive, homogenous and synchronous damage. Myeloid cells are invading the injured muscle, and during the course of regeneration, dynamically alter their phenotype by day 4 in a highly ordered and reproducible manner, leading to complete regeneration (*ad integrum*) of the muscle fibers by day 8. A recent study (Wang, Melton et al. 2014) provides mechanistic insights into the contribution of monocyte-derived subsets by eliminating $CD11b^+$ monocyte and macrophage subsets using a diphtheria toxin inducible system and the CTX injury model. They

were able to show by transient and differential ablation that not only monocyte-derived macrophages, but also the phenotypic transition is necessary for proper regeneration. In this context, our data suggest that the delayed transition is likely to be causative of impaired regeneration.

Several important signaling pathways and transcriptional regulators such as IGF-1, CEBPb, AMPKa1 and P-38/MKP (Tonkin, Temmerman et al. 2015), (Ruffell, Mourkioti et al. 2009), (Mounier, Théret et al. 2013), (Perdiguero, Sousa-Victor et al. 2011), have been implicated in the phenotypic transition of these muscle macrophages (from the pro-inflammatory/phagocytic phenotype ($Ly6C^{high}$) to the anti-inflammatory/reparatory phenotype ($Ly6C^{low}$)) using the CTX model. However, many more pathways could be implicated (reviewed in (Lawrence and Natoli 2011)) and further work towards their identification is needed. To this end, loss of function experiments, have been employed to identify key genes, by crossing gene specific floxed allele containing mice with the myeloid-specific LysM-CRE strain (Clausen, Burkhardt et al. 1999), in order to generate myeloid-specific knock out strains. However, the availability of conditional myeloid specific knockout mice for most genes is a limiting factor in delineating their role in the macrophage phenotype switch during muscle injury and regeneration. A commonly used method to assess the contribution of myeloid cell populations in *in vivo* murine disease models is bone marrow transplantation (BMT). During this CD45 congenic method, the bone marrow of animals is eliminated by total body irradiation and then reconstituted by injecting a fresh bone marrow isolated from specific donor animals that are usually genetically manipulated. The fact that the congenic donor cells can be easily tracked is also highly beneficial. However, the requirement for total body irradiation leads to unwanted inflammation, tissue injuries and fibrosis (Johnston, Williams et al. 2002), (Ghosh, Wu et al. 2009) if not properly optimized. Despite the fact that it has been previously reported that muscle regeneration is impaired in irradiated muscles (Gulati 1987), (Wakeford, Watt et al. 1991), BMT experiments to generate chimeric mice have been used extensively as an alternative tool in muscle regeneration studies (Mounier, Théret et al. 2013), (Perdiguero, Sousa-Victor et al. 2011). Therefore, we reasoned that the combination of an optimized BMT method with dose fractionation and *in vivo* imaging would allow us to trace and characterize myeloid cell invasion and cellular interactions and overcome the radiation effect. Low radiation doses lead to incomplete engraftment due to survival of the host bone marrow (Soderling, Song et al. 1985), (Baśkiewicz-Masiuk, Grymuła et al. 2009) but at the same time can also lead to macrophage activation (Finkelstein, Johnston et al. 1994), (Lorimore, Coates et al. 2001), (Coates, Rundle et al. 2008). Thus, an optimum radiation dose is needed to achieve complete BM ablation without causing any local organ damage. According to the current literature irradiation doses of 7 to 13 Gy are myeloablative but one needs to be aware that the higher the dose, the higher the risk for the animals to die from irradiation-induced toxicity (Hardee, Puppa et al. 2014). As mentioned above methods for reducing radiation toxicity include dose fractionation (in which smaller doses of radiation are administered sequentially) and lead shielding. The latter method was successfully used by Labar et al and Murphy et al. to protect the lungs and study alveolar macrophage turnover following BMT, but were limited by high levels of mixed chimerism in the circulation due to head and forelimbs being lead shielded as well (Labar, Bogdanic et al. 1992), (Murphy, Summer et al. 2008). In our study and in order to bypass these limitations, (1) we used radioprotection sparingly, focused on protecting only one hindlimb (to minimize radioprotection of the recipient animal's BM), (2) increase the number of transplanted

cells to $20x10^6$ cells/BMT animal in order to increase the degree of chimerism in favor of donor BM repopulation (hindlimb radioprotection increases survival of host BM that in turn increases the competition with the donor BM), and (3) increase recovery time to 12 weeks post BMT, thus allowing us, both to reach high levels of blood chimerism (>90%) and protect the local radiosensitive muscle compartments (e.g. satellite cell pool).

Our combined method with *in vivo* tracing of myeloid cells by PET-MRI is an important advance allowing real time assessment of cell invasion as opposed to cell sorting that requires several hours of processing. These findings have general ramifications because it may be possible to extend the utility of this system to other organs, for studies that require preservation of resident cell populations in bone marrow transplanted animals, and especially in cases of immune cell invasion. In addition, this method allowed us to examine, monitor and characterize the immune cell invasion following acute injury by CTX. The PET-MRI *in vivo* imaging studies showed that these invading cells seem to have special metabolic properties biased towards glycolysis. In support of this observation, Mounier and his colleagues showed that M2a macrophages had an increased basal and maximal oxygen consumption rate (OCR) in comparison to M1 and M2c macrophages which could further explain the increased SUV signal at Day 2 following the injury (Mounier, Theret et al. 2013). Our findings suggest that ^{18}F-FDG PET-MRI is a useful tool to monitor immune cell invasion and to help to delineate and further explain the difference in the regeneration process in the irradiated muscles and especially the difference between BMT-shielded and BMT-unshielded muscles. Further acute sterile injury models in other tissues, such as liver or skin injury, could validate our PET-MRI results.

In conclusion, our work has translational implications on the muscle regenerative potential of the elderly following radiation therapy. Our findings suggest that irradiation of skeletal muscle might impair the ability of satellite cells to orchestrate macrophage phenotypic transition further impacting regeneration potential. This is in addition to other known side effects of irradiation such as direct effects on myoblasts (Jurdana, Cemazar et al. 2013). Our findings also convey potential ramifications for pathological circumstances in which recurrent muscle damage and satellite cell mediated regeneration asynchrony leads to devastating muscle diseases, such as Duchenne Muscular Dystrophy, which are usually associated with the permanent presence (and potential interaction) of inflammatory cells, especially macrophages.

H. Summary

Skeletal muscle regeneration is a complex interplay between various cell types including invading macrophages. Their recruitment to damaged tissues upon acute sterile injuries is necessary for necrotic debris clearance and for coordination of tissue regeneration. This highly dynamic process is characterized by an *in situ* transition of infiltrating monocytes from an inflammatory ($Ly6C^{high}$) to a repair ($Ly6C^{low}$) macrophage phenotype. System-level gene expression analysis revealed that the time course of muscle regeneration, much more than Ly6C status, was correlated with the largest differential gene expression. This indicated that the time course of inflammation was the predominant driving force of macrophage gene expression. These findings validate the dynamic nature of the macrophage response and associate a specific gene signature to predictive specialized functions of macrophages at each step of muscle regeneration. However, the gene regulatory events supporting the sensory and effector functions of macrophages involved in tissue repair are not well understood. Here, we show that the lipid activated transcription factor (TF), PPARg is required for proper skeletal muscle regeneration acting in repair MFs. PPARg controls the expression of the TGFb family member, GDF3, which in turn regulates the restoration of skeletal muscle integrity by stimulating myoblast cell fusion. In addition, to delineate the order of transcriptional events during monocyte infiltration and *in situ* macrophage differentiation we generated chromatin accessibility maps using ATAC-seq. We found that a large class of genomic regulatory elements is becoming *de novo* accessible during monocyte infiltration in the muscle, and motif analysis showed that these sites are highly enriched to the MARE motif, compared to other common macrophage specific motifs. We also identified BACH1, a heme-regulated MARE-binding TF, as a novel regulatory molecule. The contribution of this molecule and downstream targets such as Hmox1, have been evaluated using full body and macrophage-specific knock-outs. Surprisingly, the inactivation of either Bach1 or Hmox1 in macrophages impairs muscle regeneration by altering the dynamics of the macrophage phenotypic transition. In addition, Bach1 deletion leads to transcriptional deregulation of critical inflammatory genes in macrophages upon injury. By using bone marrow-derived macrophages, we found BACH1 to bind extensively to enhancers of these genes, suggesting that fine-tuning of transient inflammatory transcriptional programs in macrophages during tissue injury, largely depend on MARE-binding TFs. Overall, this work establishes PPARg and BACH1 as required environment sensors and transcriptional regulators of muscle infiltrating MFs. Moreover, this work also establishes GDF3 as a secreted extrinsic effector protein acting on myoblasts and serving as a regeneration factor in tissue repair.

The importance of the macrophage phenotypic shift and the cell cross-talk of the local muscle tissue with the infiltrating macrophages during tissue regeneration upon injury are also not fully understood and their study lacks adequate methodology. Here, by using an acute sterile skeletal muscle injury model combined with irradiation, bone marrow transplantation and *in vivo* imaging we show that preserved muscle integrity and cell composition prior to the injury is necessary for repair macrophage phenotypic transition and subsequently for proper and complete tissue regeneration. Importantly, by using a model of *in vivo* ablation of PAX7 positive cells, we show that this radiosensitive skeletal muscle progenitor pool contributes to macrophage phenotypic transition following acute sterile muscle injury. Taken together, our data suggest the existence of a more extensive and reciprocal cross-talk between muscle tissue compartments,

including satellite cells, and infiltrating myeloid cells upon tissue damage. These interactions are shaping the macrophages in-situ phenotypic shift, which is indispensable for normal muscle tissue repair dynamics.

I. New Findings

- Infiltrating macrophages display a dynamic gene expression signature during muscle regeneration.
- GDF15 is produced by macrophages and enhances primary myoblast proliferation.
- Macrophage PPARg is required for skeletal muscle regeneration.
- PPARg regulates GDF3 in muscle infiltrating Ly6C^{low} repair macrophages.
- GDF3 regulates muscle regeneration and enhances primary myoblast fusion.
- GDF3 restores muscle regeneration in geriatric models.
- The chromatin structure is dynamically changing during Ly6C^{high} inflammatory to Ly6C^{low} repair macrophage transition.
- AP-1 factors shape the active enhancer landscape of macrophages upon an acute tissue injury and BACH-1 genomic binding sites are overrepresented in the opening chromatin cluster.
- Myeloid BACH-1 and HMOX1 are required for proper Ly6C^{high} – Ly6C^{low} transition and skeletal muscle regeneration.
- BACH1 fine-tunes inflammatory transcriptional programs in macrophages following acute skeletal muscle injury.
- The *in situ* phenotypic switch of macrophages is delayed in acute injury following irradiation.
- The combination of bone marrow transplantation and local muscle radiation protection allows for the identification of a myeloid cell contribution to tissue repair.
- PET-MRI allows monitoring of myeloid cell invasion and metabolism.
- Altered cellular composition prior to acute sterile injury affects the *in situ* phenotypic transition of invading myeloid cells to repair macrophages.
- There is reciprocal intercellular communication between local muscle cell compartments, such as PAX7 positive cells, and recruited macrophages during skeletal muscle regeneration.

J. List of Keywords

monocytes, macrophages, muscle regeneration, tissue repair, inflammation, BACH1, HMOX1, PPARg, GDF3, GDF15, bone marrow transplantation, satellite cells, cardiotoxin, irradiation, acute injury, chromatin dynamics.

K. Acknowledgements

Foremost, I would like to express my sincere gratitude to my supervisor Professor Laszlo Nagy for the continuous support during my PhD studies and research, for his patience, motivation, enthusiasm, and immense knowledge. His guidance helped me through all aspects of research and writing of this thesis. I could not have imagined having a better advisor and mentor for my PhD studies. Dr. Nagy it has been an honor to work with you.

I am grateful to Prof. Jozsef Tozser, the head of the Department of Biochemistry and Molecular Biology, and my advisory committee: Dr Laszlo Fesus, Dr. Gabor Koncz and Dr. Attila Toth for their encouragement and insightful comments.

I owe my deepest gratitude to Dr. Tamas Varga who was my first tutor and introduced me to the fields of muscle biology and inflammation.

I am also thankful to the many collaborators who not only provided data but I could really learn from them: Dr. Dezso Balazs, Dr. Eva Pintye, Dr. Gyorgy Trencsenyi, Dr. Gerardo Alvarado Contreras, Dr. Gergely Nagy, Dr. Szilard Poliska, Dr. Peter Gogolak, Konstantina Lyroni, Dr. Ioannis Talianidis, Dr. Babis Spilianakis, Dr. Zoltan Papp, Dr Vassiliki Koliaraki, and Dr. Hideto Watanabe.

Special thanks to Attila Pap, and Petros Tzerpos. There are not enough words to describe your excellent work and support for these projects. My sincere thanks also go to secretaries Judit Halmos, and Bernadett Fodorné Kurgyis. I was so privileged to have someone like you helping me in all aspects of my daily PhD life.

My gratitude also goes to all the past and current members of the Nuclear Receptor Research Group for their help and scientific discussions. I thank my fellow lab mates: Nikolas Giannakis, Dr. Bence Daniel, Attila Horvath, Dr. Zoltan Simandi, Dr. Ixchelt Cuaranta-Monroy, and Zsolt Csimmerer for the stimulating discussions, and for all the fun we have had all this time. I should also acknowledge the endless help I received from technicians: Marta Beladi, Timea Cseh, Monika Porcelan, Matt Peloquin and Tristan Hays.

Last but not the least, I would like to express my deepest gratitude to my beloved family, who has supported me throughout the entire process, both by keeping me harmonious and helping me putting pieces together.

This work was financially supported by the Marie Curie Initial Training Network - “NR-NET” [PITN-GA- 2013-606806 from the EU-FP7 PEOPLE-2013 program].

L. References

Abou-Khalil, R., R. Mounier and B. Chazaud (2010). "Regulation of myogenic stem cell behaviour by vessel cells: The "ménage à trois" of satellite cells, periendothelial cells and endothelial cells." Cell Cycle **9**(5): 892-896.

Alam, M. Z., S. Devalaraja and M. Haldar (2017). "The Heme Connection: Linking Erythrocytes and Macrophage Biology." Front Immunol **8**: 33.

Amthor, H., R. Macharia, R. Navarrete, M. Schuelke, S. C. Brown, A. Otto, T. Voit, F. Muntoni, G. Vrbova, T. Partridge, P. Zammit, L. Bunger and K. Patel (2007). "Lack of myostatin results in excessive muscle growth but impaired force generation." Proc Natl Acad Sci U S A **104**(6): 1835-1840.

Anders, H. J. and M. Lech (2013). "NOD-like and Toll-like receptors or inflammasomes contribute to kidney disease in a canonical and a non-canonical manner." Kidney Int **84**(2): 225-228.

Anderson, P. (2008). "Post-transcriptional control of cytokine production." Nat Immunol **9**(4): 353-359.

Arnold, L., A. Henry, F. Poron, Y. Baba-Amer, N. van Rooijen, A. Plonquet, R. K. Gherardi and B. Chazaud (2007). "Inflammatory monocytes recruited after skeletal muscle injury switch into antiinflammatory macrophages to support myogenesis." The Journal of Experimental Medicine **204**(5): 1057-1069.

Aurora, A. B. and E. N. Olson (2014). "Immune modulation of stem cells and regeneration." Cell Stem Cell **15**(1): 14-25.

Aurora, A. B., E. R. Porrello, W. Tan, A. I. Mahmoud, J. A. Hill, R. Bassel-Duby, H. A. Sadek and E. N. Olson (2014). "Macrophages are required for neonatal heart regeneration." J Clin Invest **124**(3): 1382-1392.

Baeza-Raja, B. and P. Munoz-Canoves (2004). "p38 MAPK-induced nuclear factor-kappaB activity is required for skeletal muscle differentiation: role of interleukin-6." Mol Biol Cell **15**(4): 2013-2026.

Barnard, W., J. Bower, M. A. Brown, M. Murphy and L. Austin (1994). "Leukemia inhibitory factor (LIF) infusion stimulates skeletal muscle regeneration after injury: injured muscle expresses lif mRNA." J Neurol Sci **123**(1-2): 108-113.

Barton, D., Shoturma and Sweeney (1999). "Contribution of satellite cells to IGF-I induced hypertrophy of skeletal muscle." Acta Physiologica Scandinavica **167**(4): 301-305.

Baśkiewicz-Masiuk, M., K. Grymuła, M. Hałasa, E. Pius, M. Boehlke and B. Machaliński (2009). "Induction of Mixed Chimerism in Mice by Employing Different Conditioning Protocols and Bone Marrow Cell Transplantation." Transplantation Proceedings **41**(5): 1894-1899.

Bensinger, S. J. and P. Tontonoz (2008). "Integration of metabolism and inflammation by lipid-activated nuclear receptors." Nature **454**(7203): 470-477.

Bentzinger, C. F., Y. X. Wang, N. A. Dumont and M. A. Rudnicki (2013). "Cellular dynamics in the muscle satellite cell niche." EMBO reports **14**(12): 1062-1072.

Berse, B., L. F. Brown, L. Van de Water, H. F. Dvorak and D. R. Senger (1992). "Vascular permeability factor (vascular endothelial growth factor) gene is expressed differentially in normal tissues, macrophages, and tumors." Mol Biol Cell **3**(2): 211-220.

Birbrair, A., T. Zhang, Z.-M. Wang, M. L. Messi, A. Mintz and O. Delbono (2014). "Pericytes: multitasking cells in the regeneration of injured, diseased, and aged skeletal muscle." Frontiers in Aging Neuroscience **6**.

Biswas, S. K. and A. Mantovani (2012). "Orchestration of metabolism by macrophages." Cell Metab **15**(4): 432-437.

Boulter, L., O. Govaere, T. G. Bird, S. Radulescu, P. Ramachandran, A. Pellicoro, R. A. Ridgway, S. S. Seo, B. Spee, N. Van Rooijen, O. J. Sansom, J. P. Iredale, S. Lowell, T. Roskams and S. J. Forbes (2012). "Macrophage-derived Wnt opposes Notch signaling to specify hepatic progenitor cell fate in chronic liver disease." Nat Med **18**(4): 572-579.

Broholm, C., M. J. Laye, C. Brandt, R. Vadalasetty, H. Pilegaard, B. K. Pedersen and C. Scheele (2011). "LIF is a contraction-induced myokine stimulating human myocyte proliferation." J Appl Physiol (1985) **111**(1): 251-259.

Broholm, C. and B. K. Pedersen (2010). "Leukaemia inhibitory factor--an exercise-induced myokine." Exerc Immunol Rev **16**: 77-85.

Bryant, D. M. and K. E. Mostov (2008). "From cells to organs: building polarized tissue." Nat Rev Mol Cell Biol **9**(11): 887-901.

Bryder, D., D. J. Rossi and I. L. Weissman (2006). "Hematopoietic stem cells: the paradigmatic tissue-specific stem cell." Am J Pathol **169**(2): 338-346.

Buenrostro, J. D., P. G. Giresi, L. C. Zaba, H. Y. Chang and W. J. Greenleaf (2013). "Transposition of native chromatin for fast and sensitive epigenomic profiling of open chromatin, DNA-binding proteins and nucleosome position." Nat Methods **10**(12): 1213-1218.

Bunting, M. D., I. Comerford, N. Seach, M. V. Hammett, D. L. Asquith, H. Korner, R. L. Boyd, R. J. Nibbs and S. R. McColl (2013). "CCX-CKR deficiency alters thymic stroma impairing thymocyte development and promoting autoimmunity." Blood **121**(1): 118-128.

Burzyn, D., W. Kuswanto, D. Kolodin, Jennifer L. Shadrach, M. Cerletti, Y. Jang, E. Sefik, Tze G. Tan, Amy J. Wagers, C. Benoist and D. Mathis (2013). "A Special Population of Regulatory T Cells Potentiates Muscle Repair." Cell **155**(6): 1282-1295.

Caiozzo, V. J., E. Giedzinski, M. Baker, T. Suarez, A. Izadi, M. Lan, J. Cho-Lim, B. P. Tseng and C. L. Limoli (2010). "The Radiosensitivity of Satellite Cells: Cell Cycle Regulation, Apoptosis and Oxidative Stress." Radiation Research **174**(5): 582-589.

Cantini, M. and U. G. O. Carraro (1995). "Macrophage-released Factor Stimulates Selectively Myogenic Cells in Primary Muscle Culture." Journal of Neuropathology and Experimental Neurology **54**(1): 121-128.

Cantini, M., M. L. Massimino, A. Bruson, C. Catani, L. Dallalibera and U. Carraro (1994). "Macrophages Regulate Proliferation and Differentiation of Satellite Cells." Biochemical and Biophysical Research Communications **202**(3): 1688-1696.

Castiglioni, A., G. Corna, E. Rigamonti, V. Basso, M. Vezzoli, A. Monno, A. E. Almada, A. Mondino, A. J. Wagers, A. A. Manfredi and P. Rovere-Querini (2015). "FOXP3+ T Cells Recruited to Sites of Sterile Skeletal Muscle Injury Regulate the Fate of Satellite Cells and Guide Effective Tissue Regeneration." PLOS ONE **10**(6): e0128094.

Charge, S. B., A. S. Brack and S. M. Hughes (2002). "Aging-related satellite cell differentiation defect occurs prematurely after Ski-induced muscle hypertrophy." Am J Physiol Cell Physiol **283**(4): C1228-1241.

Chazaud, B. (2014). "Macrophages: Supportive cells for tissue repair and regeneration." Immunobiology **219**(3): 172-178.

Chazaud, B., M. Brigitte, H. Yacoub-Youssef, L. Arnold, R. Gherardi, C. Sonnet, P. Lafuste and F. Chretien (2009). "Dual and beneficial roles of macrophages during skeletal muscle regeneration." Exerc Sport Sci Rev **37**(1): 18-22.

Chazaud, B., C. Sonnet, P. Lafuste, G. Bassez, A. C. Rimaniol, F. Poron, F. J. Authier, P. A. Dreyfus and R. K. Gherardi (2003). "Satellite cells attract monocytes and use macrophages as a support to escape apoptosis and enhance muscle growth." J Cell Biol **163**(5): 1133-1143.

Chen, F., Z. Liu, W. Wu, C. Rozo, S. Bowdridge, A. Millman, N. Van Rooijen, J. F. Urban, Jr., T. A. Wynn and W. C. Gause (2012). "An essential role for TH2-type responses in limiting acute tissue damage during experimental helminth infection." Nat Med **18**(2): 260-266.

Chen, J. L., K. L. Walton, S. L. Al-Musawi, E. K. Kelly, H. Qian, M. La, L. Lu, G. Lovrecz, M. Ziemann, R. Lazarus, A. El-Osta, P. Gregorevic and C. A. Harrison (2015). "Development of novel activin-targeted therapeutics." Mol Ther **23**(3): 434-444.

Cheung, T. H. and T. A. Rando (2013). "Molecular regulation of stem cell quiescence." Nature Reviews Molecular Cell Biology **14**(6): 329-340.

Christov, C., F. Chretien, R. Abou-Khalil, G. Bassez, G. Vallet, F. J. Authier, Y. Bassaglia, V. Shinin, S. Tajbakhsh, B. Chazaud and R. K. Gherardi (2007). "Muscle Satellite Cells and Endothelial Cells: Close Neighbors and Privileged Partners." Molecular Biology of the Cell **18**(4): 1397-1409.

Chrysovergis, K., X. Wang, J. Kosak, S. H. Lee, J. S. Kim, J. F. Foley, G. Travlos, S. Singh, S. J. Baek and T. E. Eling (2014). "NAG-1/GDF-15 prevents obesity by increasing thermogenesis, lipolysis and oxidative metabolism." Int J Obes (Lond) **38**(12): 1555-1564.

Chujo, S., F. Shirasaki, M. Kondo-Miyazaki, Y. Ikawa and K. Takehara (2009). "Role of connective tissue growth factor and its interaction with basic fibroblast growth factor and macrophage chemoattractant protein-1 in skin fibrosis." J Cell Physiol **220**(1): 189-195.

Clausen, B. E., C. Burkhardt, W. Reith, R. Renkawitz and I. Förster (1999). Transgenic Research **8**(4): 265-277.

Coates, P. J., J. K. Rundle, S. A. Lorimore and E. G. Wright (2008). "Indirect Macrophage Responses to Ionizing Radiation: Implications for Genotype-Dependent Bystander Signaling." Cancer Research **68**(2): 450-456.

Cochain, C., C. Auvynet, L. Poupel, J. Vilar, E. Dumeau, A. Richart, A. Recalde, Y. Zouggari, K. Y. Yin, P. Bruneval, G. Renault, C. Marchiol, P. Bonnin, B. Levy, R. Bonecchi, M. Locati, C. Combadiere and J. S. Silvestre (2012). "The chemokine decoy receptor D6 prevents excessive inflammation and adverse ventricular remodeling after myocardial infarction." Arterioscler Thromb Vasc Biol **32**(9): 2206-2213.

Cohen, D. E. and D. Melton (2011). "Turning straw into gold: directing cell fate for regenerative medicine." Nat Rev Genet **12**(4): 243-252.

Collins, C. A., P. S. Zammit, A. P. Ruiz, J. E. Morgan and T. A. Partridge (2007). "A population of myogenic stem cells that survives skeletal muscle aging." Stem Cells **25**(4): 885-894.

Corna, G., I. Caserta, A. Monno, P. Apostoli, A. A. Manfredi, C. Camaschella and P. Rovere-Querini (2016). "The Repair of Skeletal Muscle Requires Iron Recycling through Macrophage Ferroportin." J Immunol **197**(5): 1914-1925.

Costamagna, D., P. Costelli, M. Sampaolesi and F. Penna (2015). "Role of Inflammation in Muscle Homeostasis and Myogenesis." Mediators Inflamm **2015**: 805172.

Csete, M., J. Walikonis, N. Slawny, Y. Wei, S. Korsnes, J. C. Doyle and B. Wold (2001). "Oxygen-mediated regulation of skeletal muscle satellite cell proliferation and adipogenesis in culture." J Cell Physiol **189**(2): 189-196.

Dadgar, S., Z. Wang, H. Johnston, A. Kesari, K. Nagaraju, Y. W. Chen, D. A. Hill, T. A. Partridge, M. Giri, R. J. Freishtat, J. Nazarian, J. Xuan, Y. Wang and E. P. Hoffman (2014). "Asynchronous remodeling is a driver of failed regeneration in Duchenne muscular dystrophy." J Cell Biol **207**(1): 139-158.

Dal-Secco, D., J. Wang, Z. Zeng, E. Kolaczkowska, C. H. Wong, B. Petri, R. M. Ransohoff, I. F. Charo, C. N. Jenne and P. Kubes (2015). "A dynamic spectrum of monocytes arising from the in situ reprogramming of CCR2+ monocytes at a site of sterile injury." J Exp Med **212**(4): 447-456.

Daniel, B., B. L. Balint, Z. S. Nagy and L. Nagy (2014). "Mapping the genomic binding sites of the activated retinoid X receptor in murine bone marrow-derived macrophages using chromatin immunoprecipitation sequencing." Methods Mol Biol **1204**: 15-24.

Daniel, B., G. Nagy, N. Hah, A. Horvath, Z. Czimmerer, S. Poliska, T. Gyuris, J. Keirsse, C. Gysemans, J. A. Van Ginderachter, B. L. Balint, R. M. Evans, E. Barta and L. Nagy (2014). "The active enhancer network operated by liganded RXR supports angiogenic activity in macrophages." Genes Dev **28**(14): 1562-1577.

Das, A., M. Sinha, S. Datta, M. Abas, S. Chaffee, C. K. Sen and S. Roy (2015). "Monocyte and macrophage plasticity in tissue repair and regeneration." Am J Pathol **185**(10): 2596-2606.

Davies, L. C., S. J. Jenkins, J. E. Allen and P. R. Taylor (2013). "Tissue-resident macrophages." Nat Immunol **14**(10): 986-995.

de Prost, N., M. R. Tucci and M. F. V. Melo (2010). "Assessment of Lung Inflammation With 18F-FDG PET During Acute Lung Injury." American Journal of Roentgenology **195**(2): 292-300.

Dellavalle, A., G. Maroli, D. Covarello, E. Azzoni, A. Innocenzi, L. Perani, S. Antonini, R. Sambasivan, S. Brunelli, S. Tajbakhsh and G. Cossu (2011). "Pericytes resident in postnatal skeletal muscle differentiate into muscle fibres and generate satellite cells." Nature Communications **2**: 499.

Deng, B., M. Wehling-Henricks, S. A. Villalta, Y. Wang and J. G. Tidball (2012). "IL-10 triggers changes in macrophage phenotype that promote muscle growth and regeneration." J Immunol **189**(7): 3669-3680.

Duffield, J. S., S. J. Forbes, C. M. Constandinou, S. Clay, M. Partolina, S. Vuthoori, S. Wu, R. Lang and J. P. Iredale (2005). "Selective depletion of macrophages reveals distinct, opposing roles during liver injury and repair." J Clin Invest **115**(1): 56-65.

Duran-Struuck, R., A. Hartigan, S. G. Clouthier, M. C. Dyson, K. Lowler, E. Gatza, I. Tawara, T. Toubai, E. Weisiger, K. Hugunin, P. Reddy and J. E. Wilkinson (2008). "Differential susceptibility of C57BL/6NCr and B6.Cg-Ptprca mice to commensal bacteria after whole body irradiation in translational bone marrow transplant studies." Journal of Translational Medicine **6**(1): 10.

Ehrhardt, J. and J. Morgan (2005). "Regenerative capacity of skeletal muscle." Curr Opin Neurol **18**(5): 548-553.

Epelman, S., K. J. Lavine, A. E. Beaudin, D. K. Sojka, J. A. Carrero, B. Calderon, T. Brija, E. L. Gautier, S. Ivanov, A. T. Satpathy, J. D. Schilling, R. Schwendener, I. Sergin, B. Razani, E. C. Forsberg, W. M. Yokoyama, E. R. Unanue, M. Colonna, G. J. Randolph and D. L. Mann (2014). "Embryonic and adult-derived resident cardiac macrophages are maintained through distinct mechanisms at steady state and during inflammation." Immunity **40**(1): 91-104.

Epelman, S., K. J. Lavine and G. J. Randolph (2014). "Origin and functions of tissue macrophages." Immunity **41**(1): 21-35.

Evans, T. A., D. S. Barkauskas, J. T. Myers, E. G. Hare, J. Q. You, R. M. Ransohoff, A. Y. Huang and J. Silver (2014). "High-resolution intravital imaging reveals that blood-derived macrophages but not resident microglia facilitate secondary axonal dieback in traumatic spinal cord injury." Exp Neurol **254**: 109-120.

Fadok, V. A., D. L. Bratton, A. Konowal, P. W. Freed, J. Y. Westcott and P. M. Henson (1998). "Macrophages that have ingested apoptotic cells in vitro inhibit proinflammatory cytokine production through autocrine/paracrine mechanisms involving TGF-beta, PGE2, and PAF." J Clin Invest **101**(4): 890-898.

Favas, C. and D. A. Isenberg (2009). "B-cell-depletion therapy in SLE--what are the current prospects for its acceptance?" Nat Rev Rheumatol **5**(12): 711-716.

Finkelstein, J. N., C. J. Johnston, R. Baggs and P. Rubin (1994). "Early alterations in extracellular matrix and transforming growth factor β gene expression in mouse lung indicative of late radiation fibrosis." International Journal of Radiation Oncology*Biology*Physics **28**(3): 621-631.

Fry, C. S., J. D. Lee, J. Mula, T. J. Kirby, J. R. Jackson, F. Liu, L. Yang, C. L. Mendias, E. E. Dupont-Versteegden, J. J. McCarthy and C. A. Peterson (2014). "Inducible depletion of satellite cells in adult, sedentary mice impairs muscle regenerative capacity without affecting sarcopenia." Nature Medicine **21**(1): 76-80.

Fullerton, J. N. and D. W. Gilroy (2016). "Resolution of inflammation: a new therapeutic frontier." Nat Rev Drug Discov **15**(8): 551-567.

Gabay, C. and I. Kushner (1999). "Acute-phase proteins and other systemic responses to inflammation." N Engl J Med **340**(6): 448-454.

Gage, F. H. and S. Temple (2013). "Neural stem cells: generating and regenerating the brain." Neuron **80**(3): 588-601.

Galli, S. J., N. Borregaard and T. A. Wynn (2011). "Phenotypic and functional plasticity of cells of innate immunity: macrophages, mast cells and neutrophils." Nat Immunol **12**(11): 1035-1044.

Gallucci, S., C. Provenzano, P. Mazzarelli, F. Scuderi and E. Bartoccioni (1998). "Myoblasts produce IL-6 in response to inflammatory stimuli." Int Immunol **10**(3): 267-273.

Gamelli, R. L., H. Liu, L.-K. He and C. A. Hofmann (1994). "ALTERATIONS OF GLUCOSE TRANSPORTER MRNA AND PROTEIN LEVELS IN BRAIN FOLLOWING THERMAL INJURY AND SEPSIS IN MICE." Shock **1**(6): 395-400.

Ghosh, S. N., Q. Wu, M. Mäder, B. L. Fish, J. E. Moulder, E. R. Jacobs, M. Medhora and R. C. Molthen (2009). "Vascular Injury After Whole Thoracic X-Ray Irradiation in the Rat." International Journal of Radiation Oncology*Biology*Physics **74**(1): 192-199.

Glaudemans, A. W. J. M., E. F. J. de Vries, F. Galli, R. A. J. O. Dierckx, R. H. J. A. Slart and A. Signore (2013). "The Use of18F-FDG-PET/CT for Diagnosis and Treatment Monitoring of Inflammatory and Infectious Diseases." Clinical and Developmental Immunology **2013**: 1-14.

Godwin, J. W., A. R. Pinto and N. A. Rosenthal (2013). "Macrophages are required for adult salamander limb regeneration." Proc Natl Acad Sci U S A **110**(23): 9415-9420.

Goh, Y. P., N. C. Henderson, J. E. Heredia, A. Red Eagle, J. I. Odegaard, N. Lehwald, K. D. Nguyen, D. Sheppard, L. Mukundan, R. M. Locksley and A. Chawla (2013). "Eosinophils secrete IL-4 to facilitate liver regeneration." Proc Natl Acad Sci U S A **110**(24): 9914-9919.

Gomez Perdiguero, E., K. Klapproth, C. Schulz, K. Busch, E. Azzoni, L. Crozet, H. Garner, C. Trouillet, M. F. de Bruijn, F. Geissmann and H. R. Rodewald (2015). "Tissue-resident macrophages originate from yolk-sac-derived erythro-myeloid progenitors." Nature **518**(7540): 547-551.

Gondin, J., M. Théret, G. Duhamel, K. Pegan, J. R. R. Mathieu, C. Peyssonnaux, S. Cuvellier, C. Latroche, B. Chazaud, D. Bendahan and R. Mounier (2015). "Myeloid HIFs Are Dispensable for Resolution of Inflammation during Skeletal Muscle Regeneration." The Journal of Immunology **194**(7): 3389-3399.

Gulati, A. K. (1987). "The effect of X-irradiation on skeletal muscle regeneration in the adult rat." Journal of the Neurological Sciences **78**(1): 111-120.

Gundra, U. M., N. M. Girgis, D. Ruckerl, S. Jenkins, L. N. Ward, Z. D. Kurtz, K. E. Wiens, M. S. Tang, U. Basu-Roy, A. Mansukhani, J. E. Allen and P. Loke (2014). "Alternatively activated macrophages derived from monocytes and tissue macrophages are phenotypically and functionally distinct." Blood **123**(20): e110-122.

Haddock, B., S. Holm, J. M. Poulsen, L. H. Enevoldsen, H. B. W. Larsson, A. Kjær and C. Suetta (2016). "Assessment of muscle function using hybrid PET/MRI: comparison of 18F-FDG PET and T2-weighted MRI for quantifying muscle activation in human subjects." European Journal of Nuclear Medicine and Molecular Imaging **44**(4): 704-711.

Han, M. S., D. Y. Jung, C. Morel, S. A. Lakhani, J. K. Kim, R. A. Flavell and R. J. Davis (2013). "JNK expression by macrophages promotes obesity-induced insulin resistance and inflammation." Science **339**(6116): 218-222.

Hansen, W. R., J. A. Keelan, S. J. Skinner and M. D. Mitchell (1999). "Key enzymes of prostaglandin biosynthesis and metabolism. Coordinate regulation of expression by cytokines in gestational tissues: a review." Prostaglandins Other Lipid Mediat **57**(4): 243-257.

Hardee, J. P., M. J. Puppa, D. K. Fix, S. Gao, K. L. Hetzler, T. A. Bateman and J. A. Carson (2014). "The effect of radiation dose on mouse skeletal muscle remodeling." Radiology and Oncology **48**(3).

Hardy, D., A. Besnard, M. Latil, G. Jouvion, D. Briand, C. Thépenier, Q. Pascal, A. Guguin, B. Gayraud-Morel, J.-M. Cavaillon, S. Tajbakhsh, P. Rocheteau and F. Chrétien (2016). "Comparative Study of Injury Models for Studying Muscle Regeneration in Mice." PLOS ONE **11**(1): e0147198.

Harusato, A., Y. Naito, T. Takagi, S. Yamada, K. Mizushima, Y. Hirai, R. Horie, K. Inoue, K. Fukumoto, I. Hirata, T. Omatsu, E. Kishimoto, K. Uchiyama, O. Handa, T. Ishikawa, S. Kokura, H. Ichikawa, A. Muto, K. Igarashi and T. Yoshikawa (2009). "Inhibition of Bach1 ameliorates indomethacin-induced intestinal injury in mice." J Physiol Pharmacol **60 Suppl 7**: 149-154.

Haschemi, A., P. Kosma, L. Gille, C. R. Evans, C. F. Burant, P. Starkl, B. Knapp, R. Haas, J. A. Schmid, C. Jandl, S. Amir, G. Lubec, J. Park, H. Esterbauer, M. Bilban, L. Brizuela, J. A. Pospisilik, L. E. Otterbein and O. Wagner (2012). "The sedoheptulose kinase CARKL directs macrophage polarization through control of glucose metabolism." Cell Metab **15**(6): 813-826.

Haugen, F., F. Norheim, H. Lian, A. J. Wensaas, S. Dueland, O. Berg, A. Funderud, B. S. Skalhegg, T. Raastad and C. A. Drevon (2010). "IL-7 is expressed and secreted by human skeletal muscle cells." Am J Physiol Cell Physiol **298**(4): C807-816.

Hawke, T. J. and D. J. Garry (2001). "Myogenic satellite cells: physiology to molecular biology." J Appl Physiol (1985) **91**(2): 534-551.

Hearps, A. C., G. E. Martin, T. A. Angelovich, W. J. Cheng, A. Maisa, A. L. Landay, A. Jaworowski and S. M. Crowe (2012). "Aging is associated with chronic innate immune activation and dysregulation of monocyte phenotype and function." Aging Cell **11**(5): 867-875.

Heinz, S., C. Benner, N. Spann, E. Bertolino, Y. C. Lin, P. Laslo, J. X. Cheng, C. Murre, H. Singh and C. K. Glass (2010). "Simple combinations of lineage-determining transcription factors prime cis-regulatory elements required for macrophage and B cell identities." Mol Cell **38**(4): 576-589.

Henson, P. M. and D. A. Hume (2006). "Apoptotic cell removal in development and tissue homeostasis." Trends Immunol. **27**: 244-250.

Hentze, M. W., M. U. Muckenthaler, B. Galy and C. Camaschella (2010). "Two to tango: regulation of Mammalian iron metabolism." Cell **142**(1): 24-38.

Heredia, J. E., L. Mukundan, F. M. Chen, A. A. Mueller, R. C. Deo, R. M. Locksley, T. A. Rando and A. Chawla (2013). "Type 2 innate signals stimulate fibro/adipogenic progenitors to facilitate muscle regeneration." Cell **153**(2): 376-388.

Hidestrand, M., S. Richards-Malcolm, C. M. Gurley, G. Nolen, B. Grimes, A. Waterstrat, G. V. Zant and C. A. Peterson (2008). "Sca-1-expressing nonmyogenic cells contribute to fibrosis in aged skeletal muscle." J Gerontol A Biol Sci Med Sci **63**(6): 566-579.

Hoene, M., H. Runge, H. U. Haring, E. D. Schleicher and C. Weigert (2013). "Interleukin-6 promotes myogenic differentiation of mouse skeletal muscle cells: role of the STAT3 pathway." Am J Physiol Cell Physiol **304**(2): C128-136.

Horsley, V., K. M. Jansen, S. T. Mills and G. K. Pavlath (2003). "IL-4 acts as a myoblast recruitment factor during mammalian muscle growth." Cell **113**(4): 483-494.

Hotamisligil, G. S. (2006). "Inflammation and metabolic disorders." Nature **444**: 860-867.

Hume, D. A., K. M. Summers and M. Rehli (2016). "Transcriptional Regulation and Macrophage Differentiation." Microbiol Spectr **4**(3).

Hyafil, F., J. C. Cornily, J. H. F. Rudd, J. Machac, L. J. Feldman and Z. A. Fayad (2009). "Quantification of Inflammation Within Rabbit Atherosclerotic Plaques Using the Macrophage-Specific CT Contrast Agent N1177: A Comparison with 18F-FDG PET/CT and Histology." Journal of Nuclear Medicine **50**(6): 959-965.

Jaillet, C., W. Morelle, M. C. Slomianny, V. Paget, G. Tarlet, V. Buard, S. Selbonne, F. Caffin, E. Rannou, P. Martinez, A. Francois, F. Foulquier, F. Allain, F. Milliat and O. Guipaud (2017). "Radiation-induced changes in the glycome of endothelial cells with functional consequences." Sci Rep **7**(1): 5290.

Jenkins, S. J., D. Ruckerl, P. C. Cook, L. H. Jones, F. D. Finkelman, N. van Rooijen, A. S. MacDonald and J. E. Allen (2011). "Local macrophage proliferation, rather than recruitment from the blood, is a signature of TH2 inflammation." Science **332**(6035): 1284-1288.

Jenkins, S. J., D. Ruckerl, G. D. Thomas, J. P. Hewitson, S. Duncan, F. Brombacher, R. M. Maizels, D. A. Hume and J. E. Allen (2013). "IL-4 directly signals tissue-resident macrophages to proliferate beyond homeostatic levels controlled by CSF-1." J Exp Med **210**(11): 2477-2491.

Jha, A. K., S. C. Huang, A. Sergushichev, V. Lampropoulou, Y. Ivanova, E. Loginicheva, K. Chmielewski, K. M. Stewart, J. Ashall, B. Everts, E. J. Pearce, E. M. Driggers and M. N. Artyomov (2015). "Network integration of parallel metabolic and transcriptional data reveals metabolic modules that regulate macrophage polarization." Immunity **42**(3): 419-430.

Joe, A. W. B., L. Yi, A. Natarajan, F. Le Grand, L. So, J. Wang, M. A. Rudnicki and F. M. V. Rossi (2010). "Muscle injury activates resident fibro/adipogenic progenitors that facilitate myogenesis." Nature Cell Biology **12**(2): 153-163.

Johnston, C. J., J. P. Williams, P. Okunieff and J. N. Finkelstein (2002). "Radiation-Induced Pulmonary Fibrosis: Examination of Chemokine and Chemokine Receptor Families." Radiation Research **157**(3): 256-265.

Jurdana, M., M. Cemazar, K. Pegan and T. Mars (2013). "Effect of ionizing radiation on human skeletal muscle precursor cells." Radiol Oncol **47**(4): 376-381.

Kawai, T. and S. Akira (2010). "The role of pattern-recognition receptors in innate immunity: update on Toll-like receptors." Nat Immunol **11**(5): 373-384.

Kemppainen, J., T. Fujimoto, K. K. Kalliokoski, T. Viljanen, P. Nuutila and J. Knuuti (2002). "Myocardial and skeletal muscle glucose uptake during exercise in humans." The Journal of Physiology **542**(2): 403-412.

Khalil, N., O. Bereznay, M. Sporn and A. H. Greenberg (1989). "Macrophage production of transforming growth factor beta and fibroblast collagen synthesis in chronic pulmonary inflammation." J Exp Med **170**(3): 727-737.

Korf-Klingebiel, M., M. R. Reboll, S. Klede, T. Brod, A. Pich, F. Polten, L. C. Napp, J. Bauersachs, A. Ganser, E. Brinkmann, I. Reimann, T. Kempf, H. W. Niessen, J. Mizrahi, H. J. Schonfeld, A. Iglesias, M. Bobadilla, Y. Wang and K. C. Wollert (2015). "Myeloid-derived growth factor (C19orf10) mediates cardiac repair following myocardial infarction." Nat Med **21**(2): 140-149.

Kostallari, E., Y. Baba-Amer, S. Alonso-Martin, P. Ngoh-Melame, F. Relaix, P. Lafuste and R. Gherardi (2015). "Pericytes in the myovascular niche promote postnatal myofiber growth and satellite cell quiescence." Morphologie **99**(327): 155.

Kurek, J. B., S. Nouri, G. Kannourakis, M. Murphy and L. Austin (1996). "Leukemia inhibitory factor and interleukin-6 are produced by diseased and regenerating skeletal muscle." Muscle Nerve **19**(10): 1291-1301.

Kuswanto, W., D. Burzyn, M. Panduro, K. K. Wang, Y. C. Jang, A. J. Wagers, C. Benoist and D. Mathis (2016). "Poor Repair of Skeletal Muscle in Aging Mice Reflects a Defect in Local, Interleukin-33-Dependent Accumulation of Regulatory T Cells." Immunity **44**(2): 355-367.

Labar, B., V. Bogdanic, D. Nemet, M. Mrsic, M. Vrtar, L. Grgic-Markulin, S. Kalenic, S. Vujasinovic, V. Presecki, J. Jakic-Razumovic and et al. (1992). "Total body irradiation with or without lung shielding for allogeneic bone marrow transplantation." Bone Marrow Transplant **9**(5): 343-347.

Latroche, C., C. Gitiaux, F. Chrétien, I. Desguerre, R. Mounier and B. Chazaud (2015). "Skeletal Muscle Microvasculature: A Highly Dynamic Lifeline." Physiology **30**(6): 417-427.

Lavin, Y., D. Winter, R. Blecher-Gonen, E. David, H. Keren-Shaul, M. Merad, S. Jung and I. Amit (2014). "Tissue-Resident Macrophage Enhancer Landscapes Are Shaped by the Local Microenvironment." Cell **159**(6): 1312-1326.

Lawrence, T. and G. Natoli (2011). "Transcriptional regulation of macrophage polarization: enabling diversity with identity." Nature Reviews Immunology **11**(11): 750-761.

Lawrence, T. and G. Natoli (2011). "Transcriptional regulation of macrophage polarization: enabling diversity with identity." Nat Rev Immunol **11**(11): 750-761.

Lemos, D. R., F. Babaeijandaghi, M. Low, C. K. Chang, S. T. Lee, D. Fiore, R. H. Zhang, A. Natarajan, S. A. Nedospasov and F. M. Rossi (2015). "Nilotinib reduces muscle fibrosis in chronic muscle injury by promoting TNF-mediated apoptosis of fibro/adipogenic progenitors." Nat Med **21**(7): 786-794.

Lepper, C., T. A. Partridge and C. M. Fan (2011). "An absolute requirement for Pax7-positive satellite cells in acute injury-induced skeletal muscle regeneration." Development **138**(17): 3639-3646.

Levine, A. J. and A. H. Brivanlou (2006). "GDF3, a BMP inhibitor, regulates cell fate in stem cells and early embryos." Development **133**(2): 209-216.

Levine, A. J., Z. J. Levine and A. H. Brivanlou (2009). "GDF3 is a BMP inhibitor that can activate Nodal signaling only at very high doses." Dev Biol **325**(1): 43-48.

Li, H. and R. Durbin (2009). "Fast and accurate short read alignment with Burrows-Wheeler transform." Bioinformatics **25**(14): 1754-1760.

Li, H., B. Handsaker, A. Wysoker, T. Fennell, J. Ruan, N. Homer, G. Marth, G. Abecasis, R. Durbin and S. Genome Project Data Processing (2009). "The Sequence Alignment/Map format and SAMtools." Bioinformatics **25**(16): 2078-2079.

Lira, S. A., P. Zalamea, J. N. Heinrich, M. E. Fuentes, D. Carrasco, A. C. Lewin, D. S. Barton, S. Durham and R. Bravo (1994). "Expression of the chemokine N51/KC in the thymus and epidermis of transgenic mice results in marked infiltration of a single class of inflammatory cells." J Exp Med **180**(6): 2039-2048.

Liu, G., K. Duan, H. Ma, Z. Niu, J. Peng and Y. Zhao (2011). "An instructive role of donor macrophages in mixed chimeras in the induction of recipient CD4(+)Foxp3(+) Treg cells." Immunol Cell Biol **89**(8): 827-835.

Liu, G., H. Ma, L. Qiu, L. Li, Y. Cao, J. Ma and Y. Zhao (2011). "Phenotypic and functional switch of macrophages induced by regulatory CD4+CD25+ T cells in mice." Immunol Cell Biol **89**(1): 130-142.

Liu, J., Z. Zhang, L. Chai, Y. Che, S. Min and R. Yang (2013). "Identification and characterization of a unique leucine-rich repeat protein (LRRC33) that inhibits Toll-like receptor-mediated NF-kappaB activation." Biochem Biophys Res Commun **434**(1): 28-34.

Lorchner, H., J. Poling, P. Gajawada, Y. Hou, V. Polyakova, S. Kostin, J. M. Adrian-Segarra, T. Boettger, A. Wietelmann, H. Warnecke, M. Richter, T. Kubin and T. Braun (2015). "Myocardial healing requires Reg3beta-dependent accumulation of macrophages in the ischemic heart." Nat Med **21**(4): 353-362.

Lorimore, S. A., P. J. Coates, G. E. Scobie, G. Milne and E. G. Wright (2001). "Inflammatory-type responses after exposure to ionizing radiation in vivo: a mechanism for radiation-induced bystander effects?" Oncogene **20**(48): 7085-7095.

Lu, H., D. Huang, N. Saederup, I. F. Charo, R. M. Ransohoff and L. Zhou (2011). "Macrophages recruited via CCR2 produce insulin-like growth factor-1 to repair acute skeletal muscle injury." FASEB J **25**(1): 358-369.

Lyroni, K., A. Patsalos, M. G. Daskalaki, C. Doxaki, B. Soennichsen, M. Helms, I. Liapis, V. Zacharioudaki, S. C. Kampranis and C. Tsatsanis (2017). "Epigenetic and Transcriptional Regulation of IRAK-M Expression in Macrophages." J Immunol **198**(3): 1297-1307.

Mahla, R. S., M. C. Reddy, D. V. Prasad and H. Kumar (2013). "Sweeten PAMPs: Role of Sugar Complexed PAMPs in Innate Immunity and Vaccine Biology." Front Immunol **4**: 248.

Mantovani, A., A. Sica, S. Sozzani, P. Allavena, A. Vecchi and M. Locati (2004). "The chemokine system in diverse forms of macrophage activation and polarization." Trends Immunol **25**(12): 677-686.

Massague, J., S. Cheifetz, T. Endo and B. Nadal-Ginard (1986). "Type beta transforming growth factor is an inhibitor of myogenic differentiation." Proc Natl Acad Sci U S A **83**(21): 8206-8210.

McPherron, A. C., A. M. Lawler and S. J. Lee (1997). "Regulation of skeletal muscle mass in mice by a new TGF-beta superfamily member." Nature **387**(6628): 83-90.

McQuibban, G. A., J. H. Gong, E. M. Tam, C. A. McCulloch, I. Clark-Lewis and C. M. Overall (2000). "Inflammation dampened by gelatinase A cleavage of monocyte chemoattractant protein-3." Science **289**(5482): 1202-1206.

McQuibban, G. A., J. H. Gong, J. P. Wong, J. L. Wallace, I. Clark-Lewis and C. M. Overall (2002). "Matrix metalloproteinase processing of monocyte chemoattractant proteins generates CC chemokine receptor antagonists with anti-inflammatory properties in vivo." Blood **100**(4): 1160-1167.

Medzhitov, R. (2008). "Origin and physiological roles of inflammation." Nature **454**(7203): 428-435.

Mills, C. D. and K. Ley (2014). "M1 and M2 macrophages: the chicken and the egg of immunity." J Innate Immun **6**(6): 716-726.

Miron, V. E., A. Boyd, J. W. Zhao, T. J. Yuen, J. M. Ruckh, J. L. Shadrach, P. van Wijngaarden, A. J. Wagers, A. Williams, R. J. M. Franklin and C. Ffrench-Constant (2013). "M2 microglia and macrophages drive oligodendrocyte differentiation during CNS remyelination." Nat Neurosci **16**(9): 1211-1218.

Mirza, R., L. A. DiPietro and T. J. Koh (2009). "Selective and Specific Macrophage Ablation Is Detrimental to Wound Healing in Mice." The American Journal of Pathology **175**(6): 2454-2462.

Mócsai, A., M. Zhou, F. Meng, V. L. Tybulewicz and C. A. Lowell (2002). "Syk Is Required for Integrin Signaling in Neutrophils." Immunity **16**(4): 547-558.

Mosser, D. M. and J. P. Edwards (2008). "Exploring the full spectrum of macrophage activation." Nat Rev Immunol **8**(12): 958-969.

Mounier, R., F. Chretien and B. Chazaud (2011). "Blood vessels and the satellite cell niche." Curr Top Dev Biol **96**: 121-138.

Mounier, R., M. Theret, L. Arnold, S. Cuvellier, L. Bultot, O. Goransson, N. Sanz, A. Ferry, K. Sakamoto, M. Foretz, B. Viollet and B. Chazaud (2013). "AMPKalpha1 regulates macrophage skewing at the time of resolution of inflammation during skeletal muscle regeneration." Cell Metab **18**(2): 251-264.

Mounier, R., M. Théret, L. Arnold, S. Cuvellier, L. Bultot, O. Göransson, N. Sanz, A. Ferry, K. Sakamoto, M. Foretz, B. Viollet and B. Chazaud (2013). "AMPKα1 Regulates Macrophage Skewing at the Time of Resolution of Inflammation during Skeletal Muscle Regeneration." Cell Metabolism **18**(2): 251-264.

Mouw, J. K., G. Ou and V. M. Weaver (2014). "Extracellular matrix assembly: a multiscale deconstruction." Nat Rev Mol Cell Biol **15**(12): 771-785.

Munoz-Canoves, P. and A. L. Serrano (2015). "Macrophages decide between regeneration and fibrosis in muscle." Trends Endocrinol Metab **26**(9): 449-450.

Murphy, J., R. Summer, A. A. Wilson, D. N. Kotton and A. Fine (2008). "The Prolonged Life-Span of Alveolar Macrophages." American Journal of Respiratory Cell and Molecular Biology **38**(4): 380-385.

Murphy, M. M., J. A. Lawson, S. J. Mathew, D. A. Hutcheson and G. Kardon (2011). "Satellite cells, connective tissue fibroblasts and their interactions are crucial for muscle regeneration." Development **138**(17): 3625-3637.

Murray, P. J. and T. A. Wynn (2011). "Protective and pathogenic functions of macrophage subsets." Nat Rev Immunol **11**(11): 723-737.

Nagy, G., B. Daniel, D. Jonas, L. Nagy and E. Barta (2013). "A novel method to predict regulatory regions based on histone mark landscapes in macrophages." Immunobiology **218**(11): 1416-1427.

Nathan, C. (2006). "Neutrophils and immunity: challenges and opportunities." Nat Rev Immunol **6**(3): 173-182.

Newson, J., M. Stables, E. Karra, F. Arce-Vargas, S. Quezada, M. Motwani, M. Mack, S. Yona, T. Audzevich and D. W. Gilroy (2014). "Resolution of acute inflammation bridges the gap between innate and adaptive immunity." Blood **124**(11): 1748-1764.

Nishijo, K., T. Hosoyama, C. R. R. Bjornson, B. S. Schaffer, S. I. Prajapati, A. N. Bahadur, M. S. Hansen, M. C. Blandford, A. T. McCleish, B. P. Rubin, J. A. Epstein, T. A. Rando, M. R. Capecchi and C. Keller (2009). "Biomarker system for studying muscle, stem cells, and cancer in vivo." The FASEB Journal **23**(8): 2681-2690.

Novak, M. L., E. M. Weinheimer-Haus and T. J. Koh (2014). "Macrophage activation and skeletal muscle healing following traumatic injury." J Pathol **232**(3): 344-355.

Nyugen, J., S. Agrawal, S. Gollapudi and S. Gupta (2010). "Impaired functions of peripheral blood monocyte subpopulations in aged humans." J Clin Immunol **30**(6): 806-813.

O'Brien, A. J., J. N. Fullerton, K. A. Massey, G. Auld, G. Sewell, S. James, J. Newson, E. Karra, A. Winstanley, W. Alazawi, R. Garcia-Martinez, J. Cordoba, A. Nicolaou and D. W. Gilroy (2014). "Immunosuppression in acutely decompensated cirrhosis is mediated by prostaglandin E2." Nat Med **20**(5): 518-523.

Odegaard, J. I. and A. Chawla (2011). "Alternative Macrophage Activation and Metabolism." Annual Review of Pathology: Mechanisms of Disease **6**(1): 275-297.

Ogawa, K., J. Sun, S. Taketani, O. Nakajima, C. Nishitani, S. Sassa, N. Hayashi, M. Yamamoto, S. Shibahara, H. Fujita and K. Igarashi (2001). "Heme mediates derepression of Maf recognition element through direct binding to transcription repressor Bach1." EMBO J **20**(11): 2835-2843.

Okabe, Y. and R. Medzhitov (2014). "Tissue-Specific Signals Control Reversible Program of Localization and Functional Polarization of Macrophages." Cell **157**(4): 832-844.

Ota, K., A. Brydun, A. Itoh-Nakadai, J. Sun and K. Igarashi (2014). "Bach1 deficiency and accompanying overexpression of heme oxygenase-1 do not influence aging or tumorigenesis in mice." Oxid Med Cell Longev **2014**: 757901.

Palsson-McDermott, E. M., A. M. Curtis, G. Goel, M. A. Lauterbach, F. J. Sheedy, L. E. Gleeson, M. W. van den Bosch, S. R. Quinn, R. Domingo-Fernandez, D. G. Johnston, J. K. Jiang, W. J. Israelsen, J. Keane, C. Thomas, C. Clish, M. Vander Heiden, R. J. Xavier and L. A. O'Neill (2015). "Pyruvate kinase M2 regulates Hif-1alpha activity and IL-1beta induction and is a critical determinant of the warburg effect in LPS-activated macrophages." Cell Metab **21**(1): 65-80.

Pedersen, B. K. (2011). "Muscles and their myokines." J Exp Biol **214**(Pt 2): 337-346.

Pedersen, B. K. and M. A. Febbraio (2008). "Muscle as an endocrine organ: focus on muscle-derived interleukin-6." Physiol Rev **88**(4): 1379-1406.

Pedersen, B. K. and M. A. Febbraio (2012). "Muscles, exercise and obesity: skeletal muscle as a secretory organ." Nat Rev Endocrinol **8**(8): 457-465.

Peiser, L., S. Mukhopadhyay and S. Gordon (2002). "Scavenger receptors in innate immunity." Curr Opin Immunol **14**(1): 123-128.

Perdiguero, E., P. Sousa-Victor, V. Ruiz-Bonilla, M. Jardi, C. Caelles, A. L. Serrano and P. Munoz-Canoves (2011). "p38/MKP-1-regulated AKT coordinates macrophage transitions and resolution of inflammation during tissue repair." J Cell Biol **195**(2): 307-322.

Petrof, B. J., J. B. Shrager, H. H. Stedman, A. M. Kelly and H. L. Sweeney (1993). "Dystrophin protects the sarcolemma from stresses developed during muscle contraction." Proc Natl Acad Sci U S A **90**(8): 3710-3714.

Politz, O., A. Gratchev, P. A. McCourt, K. Schledzewski, P. Guillot, S. Johansson, G. Svineng, P. Franke, C. Kannicht, J. Kzhyshkowska, P. Longati, F. W. Velten, S. Johansson and S. Goerdt (2002).

"Stabilin-1 and -2 constitute a novel family of fasciclin-like hyaluronan receptor homologues." Biochem J **362**(Pt 1): 155-164.

Pollock, J. D., D. A. Williams, M. A. Gifford, L. L. Li, X. Du, J. Fisherman, S. H. Orkin, C. M. Doerschuk and M. C. Dinauer (1995). "Mouse model of X-linked chronic granulomatous disease, an inherited defect in phagocyte superoxide production." Nat Genet **9**(2): 202-209.

Qian, H., N. Luo and Y. Chi (2012). "Aging-shifted prostaglandin profile in endothelium as a factor in cardiovascular disorders." J Aging Res **2012**: 121390.

Qian, L., Y. Huang, C. I. Spencer, A. Foley, V. Vedantham, L. Liu, S. J. Conway, J. D. Fu and D. Srivastava (2012). "In vivo reprogramming of murine cardiac fibroblasts into induced cardiomyocytes." Nature **485**(7400): 593-598.

Quinlan, A. R. and I. M. Hall (2010). "BEDTools: a flexible suite of utilities for comparing genomic features." Bioinformatics **26**(6): 841-842.

Ramachandran, P., A. Pellicoro, M. A. Vernon, L. Boulter, R. L. Aucott, A. Ali, S. N. Hartland, V. K. Snowdon, A. Cappon, T. T. Gordon-Walker, M. J. Williams, D. R. Dunbar, J. R. Manning, N. van Rooijen, J. A. Fallowfield, S. J. Forbes and J. P. Iredale (2012). "Differential Ly-6C expression identifies the recruited macrophage phenotype, which orchestrates the regression of murine liver fibrosis." Proc Natl Acad Sci U S A **109**(46): E3186-3195.

Rappolee, D. A., Y. Patel and K. Jacobson (1998). "Expression of fibroblast growth factor receptors in peri-implantation mouse embryos." Mol Reprod Dev **51**(3): 254-264.

Robinson, M. D., D. J. McCarthy and G. K. Smyth (2010). "edgeR: a Bioconductor package for differential expression analysis of digital gene expression data." Bioinformatics **26**(1): 139-140.

Rocheteau, P., B. Gayraud-Morel, I. Siegl-Cachedenier, M. A. Blasco and S. Tajbakhsh (2012). "A subpopulation of adult skeletal muscle stem cells retains all template DNA strands after cell division." Cell **148**(1-2): 112-125.

Roy, S., S. Schmeier, E. Arner, T. Alam, S. P. Parihar, M. Ozturk, O. Tamgue, H. Kawaji, M. J. de Hoon, M. Itoh, T. Lassmann, P. Carninci, Y. Hayashizaki, A. R. Forrest, V. B. Bajic, R. Guler, C. Fantom, F. Brombacher and H. Suzuki (2015). "Redefining the transcriptional regulatory dynamics of classically and alternatively activated macrophages by deepCAGE transcriptomics." Nucleic Acids Res **43**(14): 6969-6982.

Ruffell, D., F. Mourkioti, A. Gambardella, P. Kirstetter, R. G. Lopez, N. Rosenthal and C. Nerlov (2009). "A CREB-C/EBPbeta cascade induces M2 macrophage-specific gene expression and promotes muscle injury repair." Proc Natl Acad Sci U S A **106**(41): 17475-17480.

Saclier, M., H. Yacoub-Youssef, A. L. Mackey, L. Arnold, H. Ardjoune, M. Magnan, F. Sailhan, J. Chelly, G. K. Pavlath, R. Mounier, M. Kjaer and B. Chazaud (2013). "Differentially activated macrophages orchestrate myogenic precursor cell fate during human skeletal muscle regeneration." Stem Cells **31**(2): 384-396.

Saclier, M., H. Yacoub-Youssef, A. L. Mackey, L. Arnold, H. Ardjoune, M. Magnan, F. Sailhan, J. Chelly, G. K. Pavlath, R. Mounier, M. Kjaer and B. Chazaud (2013). "Differentially Activated Macrophages Orchestrate Myogenic Precursor Cell Fate During Human Skeletal Muscle Regeneration." STEM CELLS **31**(2): 384-396.

Sag, D., D. Carling, R. D. Stout and J. Suttles (2008). "Adenosine 5'-monophosphate-activated protein kinase promotes macrophage polarization to an anti-inflammatory functional phenotype." J Immunol **181**(12): 8633-8641.

Said, E. A., F. P. Dupuy, L. Trautmann, Y. Zhang, Y. Shi, M. El-Far, B. J. Hill, A. Noto, P. Ancuta, Y. Peretz, S. G. Fonseca, J. Van Grevenynghe, M. R. Boulassel, J. Bruneau, N. H. Shoukry, J. P. Routy, D. C. Douek, E. K. Haddad and R. P. Sekaly (2010). "Programmed death-1-induced interleukin-10 production by monocytes impairs CD4+ T cell activation during HIV infection." Nat Med **16**(4): 452-459.

Saldanha, A. J. (2004). "Java Treeview--extensible visualization of microarray data." Bioinformatics **20**(17): 3246-3248.

Sambasivan, R., R. Yao, A. Kissenpfennig, L. Van Wittenberghe, A. Paldi, B. Gayraud-Morel, H. Guenou, B. Malissen, S. Tajbakhsh and A. Galy (2011). "Pax7-expressing satellite cells are indispensable for adult skeletal muscle regeneration." Development **138**(17): 3647-3656.

Sanchez Alvarado, A. and S. Yamanaka (2014). "Rethinking differentiation: stem cells, regeneration, and plasticity." Cell **157**(1): 110-119.

Satoh, T., O. Takeuchi, A. Vandenbon, K. Yasuda, Y. Tanaka, Y. Kumagai, T. Miyake, K. Matsushita, T. Okazaki, T. Saitoh, K. Honma, T. Matsuyama, K. Yui, T. Tsujimura, D. M. Standley, K. Nakanishi, K. Nakai and S. Akira (2010). "The Jmjd3-Irf4 axis regulates M2 macrophage polarization and host responses against helminth infection." Nat Immunol **11**(10): 936-944.

Schiaffino, S., M. G. Pereira, S. Ciciliot and P. Rovere-Querini (2016). "Regulatory T cells and skeletal muscle regeneration." The FEBS Journal **284**(4): 517-524.

Serrano, A. L., B. Baeza-Raja, E. Perdiguero, M. Jardi and P. Munoz-Canoves (2008). "Interleukin-6 is an essential regulator of satellite cell-mediated skeletal muscle hypertrophy." Cell Metab **7**(1): 33-44.

Serrano, A. L., B. Baeza-Raja, E. Perdiguero, M. Jardí and P. Muñoz-Cánoves (2008). "Interleukin-6 Is an Essential Regulator of Satellite Cell-Mediated Skeletal Muscle Hypertrophy." Cell Metabolism **7**(1): 33-44.

Shaw, A. C., D. R. Goldstein and R. R. Montgomery (2013). "Age-dependent dysregulation of innate immunity." Nat Rev Immunol **13**(12): 875-887.

Shechter, R., A. London and M. Schwartz (2013). "Orchestrated leukocyte recruitment to immune-privileged sites: absolute barriers versus educational gates." Nat Rev Immunol **13**(3): 206-218.

Shechter, R., O. Miller, G. Yovel, N. Rosenzweig, A. London, J. Ruckh, K. W. Kim, E. Klein, V. Kalchenko, P. Bendel, S. A. Lira, S. Jung and M. Schwartz (2013). "Recruitment of beneficial M2 macrophages to injured spinal cord is orchestrated by remote brain choroid plexus." Immunity **38**(3): 555-569.

Sheedy, F. J., E. Palsson-McDermott, E. J. Hennessy, C. Martin, J. J. O'Leary, Q. Ruan, D. S. Johnson, Y. Chen and L. A. O'Neill (2010). "Negative regulation of TLR4 via targeting of the proinflammatory tumor suppressor PDCD4 by the microRNA miR-21." Nat Immunol **11**(2): 141-147.

Shefer, G., D. P. Van de Mark, J. B. Richardson and Z. Yablonka-Reuveni (2006). "Satellite-cell pool size does matter: Defining the myogenic potency of aging skeletal muscle." Developmental Biology **294**(1): 50-66.

Shen, J. J., L. Huang, L. Li, C. Jorgez, M. M. Matzuk and C. W. Brown (2009). "Deficiency of growth differentiation factor 3 protects against diet-induced obesity by selectively acting on white adipose." Mol Endocrinol **23**(1): 113-123.

Shimokado, K., E. W. Raines, D. K. Madtes, T. B. Barrett, E. P. Benditt and R. Ross (1985). "A significant part of macrophage-derived growth factor consists of at least two forms of PDGF." Cell **43**(1): 277-286.

Shouval, D. S., A. Biswas, J. A. Goettel, K. McCann, E. Conaway, N. S. Redhu, I. D. Mascanfroni, Z. Al Adham, S. Lavoie, M. Ibourk, D. D. Nguyen, J. N. Samsom, J. C. Escher, R. Somech, B. Weiss, R. Beier, L. S. Conklin, C. L. Ebens, F. G. Santos, A. R. Ferreira, M. Sherlock, A. K. Bhan, W. Muller, J. R. Mora, F. J. Quintana, C. Klein, A. M. Muise, B. H. Horwitz and S. B. Snapper (2014). "Interleukin-10 receptor signaling in innate immune cells regulates mucosal immune tolerance and anti-inflammatory macrophage function." Immunity **40**(5): 706-719.

Sica, A. and A. Mantovani (2012). "Macrophage plasticity and polarization: in vivo veritas." Journal of Clinical Investigation **122**(3): 787-795.

Signore, A. and A. W. J. M. Glaudemans (2011). "The molecular imaging approach to image infections and inflammation by nuclear medicine techniques." Annals of Nuclear Medicine **25**(10): 681-700.

Slimani, L., V. Oikonen, K. Hällsten, N. Savisto, J. Knuuti, P. Nuutila and P. Iozzo (2006). "Exercise Restores Skeletal Muscle Glucose Delivery But Not Insulin-Mediated Glucose Transport and Phosphorylation in Obese Subjects." The Journal of Clinical Endocrinology & Metabolism **91**(9): 3394-3403.

So, A. Y., Y. Garcia-Flores, A. Minisandram, A. Martin, K. Taganov, M. Boldin and D. Baltimore (2012). "Regulation of APC development, immune response, and autoimmunity by Bach1/HO-1 pathway in mice." Blood **120**(12): 2428-2437.

Soderling, C. C., C. W. Song, B. R. Blazar and D. A. Vallera (1985). "A correlation between conditioning and engraftment in recipients of MHC-mismatched T cell-depleted murine bone marrow transplants." J Immunol **135**(2): 941-946.

Stein, M., S. Keshav, N. Harris and S. Gordon (1992). "Interleukin 4 potently enhances murine macrophage mannose receptor activity: a marker of alternative immunologic macrophage activation." J Exp Med **176**(1): 287-292.

Stoecklin, G. and P. Anderson (2006). "Posttranscriptional mechanisms regulating the inflammatory response." Adv Immunol **89**: 1-37.

Sun, J., H. Hoshino, K. Takaku, O. Nakajima, A. Muto, H. Suzuki, S. Tashiro, S. Takahashi, S. Shibahara, J. Alam, M. M. Taketo, M. Yamamoto and K. Igarashi (2002). "Hemoprotein Bach1 regulates enhancer availability of heme oxygenase-1 gene." EMBO J **21**(19): 5216-5224.

Szanto, A., B. L. Balint, Z. S. Nagy, E. Barta, B. Dezso, A. Pap, L. Szeles, S. Poliska, M. Oros, R. M. Evans, Y. Barak, J. Schwabe and L. Nagy (2010). "STAT6 transcription factor is a facilitator of the nuclear receptor PPARgamma-regulated gene expression in macrophages and dendritic cells." Immunity **33**(5): 699-712.

Taganov, K. D., M. P. Boldin, K. J. Chang and D. Baltimore (2006). "NF-kappaB-dependent induction of microRNA miR-146, an inhibitor targeted to signaling proteins of innate immune responses." Proc Natl Acad Sci U S A **103**(33): 12481-12486.

Tashiro, M., T. Fujimoto, M. Itoh, K. Kubota, T. Fujiwara, M. Miyake, S. Watanuki, E. Horikawa, H. Sasaki and T. Ido (1999). "18F-FDG PET imaging of muscle activity in runners." J Nucl Med **40**(1): 70-76.

Thorvaldsdottir, H., J. T. Robinson and J. P. Mesirov (2013). "Integrative Genomics Viewer (IGV): high-performance genomics data visualization and exploration." Brief Bioinform **14**(2): 178-192.

Tidball, J. G. (2004). "Inflammatory processes in muscle injury and repair." AJP: Regulatory, Integrative and Comparative Physiology **288**(2): R345-R353.

Tidball, J. G. (2017). "Regulation of muscle growth and regeneration by the immune system." Nat Rev Immunol **17**(3): 165-178.

Tidball, J. G. and S. A. Villalta (2010). "Regulatory interactions between muscle and the immune system during muscle regeneration." AJP: Regulatory, Integrative and Comparative Physiology **298**(5): R1173-R1187.

Tidball, J. G. and M. Wehling-Henricks (2007). "Macrophages promote muscle membrane repair and muscle fibre growth and regeneration during modified muscle loading in mice in vivo." J Physiol **578**(Pt 1): 327-336.

Tonkin, J., L. Temmerman, R. D. Sampson, E. Gallego-Colon, L. Barberi, D. Bilbao, M. D. Schneider, A. Musarò and N. Rosenthal (2015). "Monocyte/Macrophage-derived IGF-1 Orchestrates Murine Skeletal Muscle Regeneration and Modulates Autocrine Polarization." Molecular Therapy **23**(7): 1189-1200.

Turer, E. E., R. M. Tavares, E. Mortier, O. Hitotsumatsu, R. Advincula, B. Lee, N. Shifrin, B. A. Malynn and A. Ma (2008). "Homeostatic MyD88-dependent signals cause lethal inflamMation in the absence of A20." J Exp Med **205**(2): 451-464.

Tussiwand, R. and E. L. Gautier (2015). "Transcriptional Regulation of Mononuclear Phagocyte Development." Front Immunol **6**: 533.

Uezumi, A., S.-i. Fukada, N. Yamamoto, S. i. Takeda and K. Tsuchida (2010). "Mesenchymal progenitors distinct from satellite cells contribute to ectopic fat cell formation in skeletal muscle." Nature Cell Biology **12**(2): 143-152.

Vaidyanathan, S., C. N. Patel, A. F. Scarsbrook and F. U. Chowdhury (2015). "FDG PET/CT in infection and inflammation—current and emerging clinical applications." Clinical Radiology **70**(7): 787-800.

van Duin, D., S. Mohanty, V. Thomas, S. Ginter, R. R. Montgomery, E. Fikrig, H. G. Allore, R. Medzhitov and A. C. Shaw (2007). "Age-associated defect in human TLR-1/2 function." J Immunol **178**(2): 970-975.

Vannella, K. M., L. Barron, L. A. Borthwick, K. N. Kindrachuk, P. B. Narasimhan, K. M. Hart, R. W. Thompson, S. White, A. W. Cheever, T. R. Ramalingam and T. A. Wynn (2014). "Incomplete deletion of IL-4Ralpha by LysM(Cre) reveals distinct subsets of M2 macrophages controlling inflammation and fibrosis in chronic schistosomiasis." PLoS Pathog **10**(9): e1004372.

Varga, T., R. Mounier, P. Gogolak, S. Poliska, B. Chazaud and L. Nagy (2013). "Tissue LyC6- Macrophages Are Generated in the Absence of Circulating LyC6- Monocytes and Nur77 in a Model of Muscle Regeneration." The Journal of Immunology **191**(11): 5695-5701.

Varga, T., R. Mounier, A. Horvath, S. Cuvellier, F. Dumont, S. Poliska, H. Ardjoune, G. Juban, L. Nagy and B. Chazaud (2016). "Highly Dynamic Transcriptional Signature of Distinct Macrophage Subsets during Sterile Inflammation, Resolution, and Tissue Repair." The Journal of Immunology **196**(11): 4771-4782.

Varga, T., R. Mounier, A. Patsalos, P. Gogolák, M. Peloquin, A. Horvath, A. Pap, B. Daniel, G. Nagy, E. Pintye, S. Poliska, S. Cuvellier, S. Ben Larbi, Brian E. Sansbury, M. Spite, Chester W. Brown, B. Chazaud and L. Nagy (2016). "Macrophage PPARγ, a Lipid Activated Transcription Factor Controls the Growth Factor GDF3 and Skeletal Muscle Regeneration." Immunity **45**(5): 1038-1051.

Vats, D., L. Mukundan, J. I. Odegaard, L. Zhang, K. L. Smith, C. R. Morel, D. R. Greaves, P. J. Murray and A. Chawla (2006). "Oxidative metabolism and PGC-1β attenuate macrophage-mediated inflammation." Cell Metabolism **4**(1): 13-24.

Vergadi, E., E. Ieronymaki, K. Lyroni, K. Vaporidi and C. Tsatsanis (2017). "Akt Signaling Pathway in Macrophage Activation and M1/M2 Polarization." J Immunol **198**(3): 1006-1014.

Vidal, B., A. L. Serrano, M. Tjwa, M. Suelves, E. Ardite, R. De Mori, B. Baeza-Raja, M. Martinez de Lagran, P. Lafuste, V. Ruiz-Bonilla, M. Jardi, R. Gherardi, C. Christov, M. Dierssen, P. Carmeliet, J. L. Degen, M. Dewerchin and P. Munoz-Canoves (2008). "Fibrinogen drives dystrophic muscle fibrosis via a TGFbeta/alternative macrophage activation pathway." Genes Dev **22**(13): 1747-1752.

Villalta, S. A., B. Deng, C. Rinaldi, M. Wehling-Henricks and J. G. Tidball (2011). "IFN-gamma promotes muscle damage in the mdx mouse model of Duchenne muscular dystrophy by suppressing M2 macrophage activation and inhibiting muscle cell proliferation." J Immunol **187**(10): 5419-5428.

Villalta, S. A., W. Rosenthal, L. Martinez, A. Kaur, T. Sparwasser, J. G. Tidball, M. Margeta, M. J. Spencer and J. A. Bluestone (2014). "Regulatory T cells suppress muscle inflammation and injury in muscular dystrophy." Science Translational Medicine **6**(258): 258ra142-258ra142.

von Maltzahn, J., A. E. Jones, R. J. Parks and M. A. Rudnicki (2013). "Pax7 is critical for the normal function of satellite cells in adult skeletal muscle." Proceedings of the National Academy of Sciences **110**(41): 16474-16479.

Wakeford, S., D. J. Watt and T. A. Partridge (1991). "X-Irradiation improves mdx mouse muscle as a model of myofiber loss in DMD." Muscle & Nerve **14**(1): 42-50.

Wang, H., D. W. Melton, L. Porter, Z. U. Sarwar, L. M. McManus and P. K. Shireman (2014). "Altered Macrophage Phenotype Transition Impairs Skeletal Muscle Regeneration." The American Journal of Pathology **184**(4): 1167-1184.

Wang, N., H. Liang and K. Zen (2014). "Molecular mechanisms that influence the macrophage m1-m2 polarization balance." Front Immunol **5**: 614.

Wehling, M., M. J. Spencer and J. G. Tidball (2001). "A nitric oxide synthase transgene ameliorates muscular dystrophy in mdx mice." J Cell Biol **155**(1): 123-131.

Wehling-Henricks, M., M. C. Jordan, T. Gotoh, W. W. Grody, K. P. Roos and J. G. Tidball (2010). "Arginine metabolism by macrophages promotes cardiac and muscle fibrosis in mdx muscular dystrophy." PLoS One **5**(5): e10763.

Welch, J. S., M. Ricote, T. E. Akiyama, F. J. Gonzalez and C. K. Glass (2003). "PPARgamma and PPARdelta negatively regulate specific subsets of lipopolysaccharide and IFN-gamma target genes in macrophages." Proc Natl Acad Sci U S A **100**(11): 6712-6717.

Welle, S. (2002). "Cellular and Molecular Basis of Age-Related Sarcopenia." Canadian Journal of Applied Physiology **27**(1): 19-41.

Werner, S. and R. Grose (2003). "Regulation of wound healing by growth factors and cytokines." Physiol. Rev. **83**: 835-870.

Wester, H. J. (2007). "Nuclear Imaging Probes: from Bench to Bedside." Clinical Cancer Research **13**(12): 3470-3481.

Wight, T. N., I. Kang and M. J. Merrilees (2014). "Versican and the control of inflammation." Matrix Biol **35**: 152-161.

Willenborg, S., T. Lucas, G. van Loo, J. A. Knipper, T. Krieg, I. Haase, B. Brachvogel, M. Hammerschmidt, A. Nagy, N. Ferrara, M. Pasparakis and S. A. Eming (2012). "CCR2 recruits an inflammatory macrophage subpopulation critical for angiogenesis in tissue repair." Blood **120**(3): 613-625.

Wu, S. (2006). "Motoneurons and oligodendrocytes are sequentially generated from neural stem cells but do not appear to share common lineage-restricted progenitors in vivo." Development **133**(4): 581-590.

Wynn, T. A. (2008). "Cellular and molecular mechanisms of fibrosis." J Pathol **214**(2): 199-210.

Wynn, T. A. and L. Barron (2010). "Macrophages: master regulators of inflammation and fibrosis." Semin Liver Dis **30**(3): 245-257.

Wynn, T. A., A. Chawla and J. W. Pollard (2013). "Macrophage biology in development, homeostasis and disease." Nature **496**(7446): 445-455.

Xu, G., G. Liu, S. Xiong, H. Liu, X. Chen and B. Zheng (2015). "The histone methyltransferase Smyd2 is a negative regulator of macrophage activation by suppressing interleukin 6 (IL-6) and tumor necrosis factor alpha (TNF-alpha) production." J Biol Chem **290**(9): 5414-5423.

Xu, H., J. Zhu, S. Smith, J. Foldi, B. Zhao, A. Y. Chung, H. Outtz, J. Kitajewski, C. Shi, S. Weber, P. Saftig, Y. Li, K. Ozato, C. P. Blobel, L. B. Ivashkiv and X. Hu (2012). "Notch-RBP-J signaling regulates the transcription factor IRF8 to promote inflammatory macrophage polarization." Nat Immunol **13**(7): 642-650.

Xue, J., S. V. Schmidt, J. Sander, A. Draffehn, W. Krebs, I. Quester, D. De Nardo, T. D. Gohel, M. Emde, L. Schmidleithner, H. Ganesan, A. Nino-Castro, M. R. Mallmann, L. Labzin, H. Theis, M. Kraut, M. Beyer, E. Latz, T. C. Freeman, T. Ulas and J. L. Schultze (2014). "Transcriptome-based network analysis reveals a spectrum model of human macrophage activation." Immunity **40**(2): 274-288.

Yang, T. T., I. M. Liu, H. T. Wu and J. T. Cheng (2009). "Mediation of protein kinase C zeta in mu-opioid receptor activation for increase of glucose uptake into cultured myoblast C2C12 cells." Neurosci Lett **465**(2): 177-180.

Yona, S., K. W. Kim, Y. Wolf, A. Mildner, D. Varol, M. Breker, D. Strauss-Ayali, S. Viukov, M. Guilliams, A. Misharin, D. A. Hume, H. Perlman, B. Malissen, E. Zelzer and S. Jung (2013). "Fate mapping reveals origins and dynamics of monocytes and tissue macrophages under homeostasis." Immunity **38**(1): 79-91.

Yun, M. H., H. Davaapil and J. P. Brockes (2015). "Recurrent turnover of senescent cells during regeneration of a complex structure." Elife **4**.

Zhang, C., Y. Li, Y. Wu, L. Wang, X. Wang and J. Du (2013). "Interleukin-6/signal transducer and activator of transcription 3 (STAT3) pathway is essential for macrophage infiltration and myoblast proliferation during muscle regeneration." J Biol Chem **288**(3): 1489-1499.

Zhang, L., A. Rowe, F. Braet and I. Ramzan (2012). "Macrophage depletion ameliorates kavalactone damage in the isolated perfused rat liver." J Toxicol Sci **37**(2): 447-453.

Zhang, Y., T. Liu, C. A. Meyer, J. Eeckhoute, D. S. Johnson, B. E. Bernstein, C. Nusbaum, R. M. Myers, M. Brown, W. Li and X. S. Liu (2008). "Model-based analysis of ChIP-Seq (MACS)." Genome Biol **9**(9): R137.

Zigmond, E., B. Bernshtein, G. Friedlander, C. R. Walker, S. Yona, K. W. Kim, O. Brenner, R. Krauthgamer, C. Varol, W. Muller and S. Jung (2014). "Macrophage-restricted interleukin-10 receptor deficiency, but not IL-10 deficiency, causes severe spontaneous colitis." Immunity **40**(5): 720-733.

M. Publications Related to Dissertation

UNIVERSITY OF DEBRECEN
UNIVERSITY AND NATIONAL LIBRARY

Registry number: DEENK/293/2017.PL
Subject: PhD Publikációs Lista

Candidate: Andreas Patsalos
Neptun ID: HGIRAK
Doctoral School: Doctoral School of Molecular Cellular and Immune Biology

List of publications related to the dissertation

1. **Patsalos, A.**, Pap, A., Varga, T., Trencsényi, G., Contreras, G. A., Garai, I., Papp, Z., Dezső, B., Pintye, É., Nagy, L.: In situ macrophage phenotypic transition is affected by altered cellular composition prior to acute sterile muscle injury.
   J. Physiol.-London. 595 (17), 5815-5842, 2017.
   DOI: http://dx.doi.org/10.1113/JP274361
   IF: 4.739 (2016)

2. Varga, T., Mounier, R., **Patsalos, A.**, Gogolák, P., Peloquin, M., Horváth, A., Pap, A., Dániel, B., Nagy, G., Pintye, É., Póliska, S., Cuvellier, S., Ben Larbi, S., Sansbury, B. E., Spite, M., Brown, C. W., Chazaud, B., Nagy, L.: Macrophage PPAR[gamma], a Lipid Activated Transcription Factor Controls the Growth Factor GDF3 and Skeletal Muscle Regeneration.
   Immunity. 45 (5), 1038-1051, 2016.
   DOI: http://dx.doi.org/10.1016/j.immuni.2016.10.016
   IF: 22.845

Address: 1 Egyetem tér, Debrecen 4032, Hungary Postal address: Pf. 39. Debrecen 4010, Hungary
Tel.: +36 52 410 443 Fax: +36 52 512 900/63847 E-mail: publikaciok@lib.unideb.hu, ¤ Web: www.lib.unideb.hu

N. List of Other Publications

UNIVERSITY OF DEBRECEN
UNIVERSITY AND NATIONAL LIBRARY

List of other publications

3. Lyroni, K., **Patsalos, A.**, Daskalaki, M. G., Doxaki, C., Soennichsen, B., Helms, M., Liapis, I., Zacharioudaki, V., Kampranis, S. C., Tsatsanis, C.: Epigenetic and Transcriptional Regulation of IRAK-M Expression in Macrophages.
J. Immunol. 198 (3), 1297-1307, 2017.
DOI: http://dx.doi.org/10.4049/jimmunol.1600009
IF: 4.856 (2016)

Total IF of journals (all publications): 32,44
Total IF of journals (publications related to the dissertation): 27,584

The Candidate's publication data submitted to the iDEa Tudóstér have been validated by DEENK on the basis of Web of Science, Scopus and Journal Citation Report (Impact Factor) databases.

27 September, 2017

Address: 1 Egyetem tér, Debrecen 4032, Hungary Postal address: Pf. 39. Debrecen 4010, Hungary
Tel.: +36 52 410 443 Fax: +36 52 512 900/63847 E-mail: publikaciok@lib.unideb.hu, ¤ Web: www.lib.unideb.hu